Final Report

FDOT Contract No.: BDK-75-977-07
UF Contract No.: 73980/74027

Group Efficiencies of Grout-Tipped Drilled Shafts and Jet-Grouted Piles

Principal Investigators: Michael McVay
Sudheesh Thiyyakkandi
James Joiner
Viktor Adams

Department of Civil and Coastal Engineering
University of Florida
Gainesville, Florida 32611-6580

Developed for the

Peter Lai, P.E., Project Manager

August 2010

DISCLAIMER

"The opinions, findings, and conclusions expressed in this publication are those of the authors and not necessarily those of the Florida Department of Transportation or the U.S. Department of Transportation.

Prepared in cooperation with the State of Florida Department of Transportation and the U.S. Department of Transportation."

SI (MODERN METRIC) CONVERSION FACTORS (from FHWA)

APPROXIMATE CONVERSIONS TO SI UNITS

SYMBOL	WHEN YOU KNOW	MULTIPLY BY	TO FIND	SYMBOL
LENGTH				
in	inches	25.4	millimeters	mm
ft	feet	0.305	meters	m
yd	yards	0.914	meters	m
mi	miles	1.61	kilometers	km

SYMBOL	WHEN YOU KNOW	MULTIPLY BY	TO FIND	SYMBOL
AREA				
in^2	square inches	645.2	square millimeters	mm^2
ft^2	square feet	0.093	square meters	m^2
yd^2	square yard	0.836	square meters	m^2
ac	acres	0.405	hectares	ha
mi^2	square miles	2.59	square kilometers	km^2

SYMBOL	WHEN YOU KNOW	MULTIPLY BY	TO FIND	SYMBOL
VOLUME				
fl oz	fluid ounces	29.57	milliliters	mL
gal	gallons	3.785	liters	L
ft^3	cubic feet	0.028	cubic meters	m^3
yd^3	cubic yards	0.765	cubic meters	m^3
NOTE: volumes greater than 1000 L shall be shown in m^3				

SYMBOL	WHEN YOU KNOW	MULTIPLY BY	TO FIND	SYMBOL
MASS				
oz	ounces	28.35	grams	g
lb	pounds	0.454	kilograms	kg
T	short tons (2000 lb)	0.907	megagrams (or "metric ton")	Mg (or "t")

SYMBOL	WHEN YOU KNOW	MULTIPLY BY	TO FIND	SYMBOL
TEMPERATURE (exact degrees)				
°F	Fahrenheit	5 (F-32)/9 or (F-32)/1.8	Celsius	°C

SYMBOL	WHEN YOU KNOW	MULTIPLY BY	TO FIND	SYMBOL
ILLUMINATION				
fc	foot-candles	10.76	lux	lx
fl	foot-Lamberts	3.426	$candela/m^2$	cd/m^2

SYMBOL	WHEN YOU KNOW	MULTIPLY BY	TO FIND	SYMBOL
FORCE and PRESSURE or STRESS				
lbf	poundforce	4.45	newtons	N
lbf/in^2	poundforce per square inch	6.89	kilopascals	kPa

APPROXIMATE CONVERSIONS TO SI UNITS

SYMBOL	WHEN YOU KNOW	MULTIPLY BY	TO FIND	SYMBOL
LENGTH				
mm	millimeters	0.039	inches	in
m	meters	3.28	feet	ft
m	meters	1.09	yards	yd
km	kilometers	0.621	miles	mi

SYMBOL	WHEN YOU KNOW	MULTIPLY BY	TO FIND	SYMBOL
AREA				
mm^2	square millimeters	0.0016	square inches	in^2
m^2	square meters	10.764	square feet	ft^2
m^2	square meters	1.195	square yards	yd^2
ha	hectares	2.47	acres	ac
km^2	square kilometers	0.386	square miles	mi^2

SYMBOL	WHEN YOU KNOW	MULTIPLY BY	TO FIND	SYMBOL
VOLUME				
mL	milliliters	0.034	fluid ounces	fl oz
L	liters	0.264	gallons	gal
m^3	cubic meters	35.314	cubic feet	ft^3
m^3	cubic meters	1.307	cubic yards	yd^3

SYMBOL	WHEN YOU KNOW	MULTIPLY BY	TO FIND	SYMBOL
MASS				
g	grams	0.035	ounces	oz
kg	kilograms	2.202	pounds	lb
Mg (or "t")	megagrams (or "metric ton")	1.103	short tons (2000 lb)	T

SYMBOL	WHEN YOU KNOW	MULTIPLY BY	TO FIND	SYMBOL
TEMPERATURE (exact degrees)				
°C	Celsius	1.8C+32	Fahrenheit	**°F**

SYMBOL	WHEN YOU KNOW	MULTIPLY BY	TO FIND	SYMBOL
ILLUMINATION				
lx	lux	0.0929	foot-candles	fc
cd/m^2	candela/m^2	0.2919	foot-Lamberts	fl

SYMBOL	WHEN YOU KNOW	MULTIPLY BY	TO FIND	SYMBOL
FORCE and PRESSURE or STRESS				
N	newtons	0.225	poundforce	lbf
kPa	kilopascals	0.145	poundforce per square inch	lbf/in^2

*SI is the symbol for International System of Units. Appropriate rounding should be made to comply with Section 4 of ASTM E380. (Revised March 2003)

TECHNICAL REPORT DOCUMENTATION PAGE

1. Report No.	2. Government Accession No.	3. Recipient's Catalog No.

4. Title and Subtitle	5. Report Date
Group Efficiencies of Grout-Tipped Drilled Shafts and Jet-Grouted Piles	August 2010
	6. Performing Organization Code
7. Author(s)	8. Performing Organization Report No.
Michael McVay, Sudheesh Thiyyakkandi, James Joiner, and Viktor Adams	UF Project 73980/74027
9. Performing Organization Name and Address	10. Work Unit No. (TRAIS)
Department of Civil and Coastal Engineering 365 Weil Hall – P.O. Box 116580 University of Florida Gainesville, FL 32611-6580	11. Contract or Grant No. BDK-75-977-07
12. Sponsoring Agency Name and Address	13. Type of Report and Period Covered
Florida Department of Transportation 605 Suwannee Street, MS 30 Tallahassee, FL 32399	Final Report 4/30/08 - 8/28/10
	14. Sponsoring Agency Code

15. Supplementary Notes

16. Abstract

In current practice, driven piles/drilled shafts are constructed in a group at 3D center to center (c/c) spacing to minimize group interference (i.e., group efficiency factor ~ 1) as well as reduce the cost of the reinforced concrete cap. Presently, group efficiency factors for a number of new foundation types, e.g., post-grouted drilled shafts and jet-grouted piles, are unknown. This research looked into the group interaction of post-grouted drilled shafts and jet-grouted piles at typical 3D spacing. Two sets of group tests for grout-tipped drilled shafts and jet-grouted piles were performed in the Florida Department of Transportation (FDOT) test chamber in medium dense sands. The experimental top down group testing revealed that the jet-grouted piles behaved as a block at 3D spacing, whereas post-grouted drilled shafts acted independently of one another, i.e., no group interaction. A group interaction factor, as well as an analytical approach for predicting load versus displacement for single or group of jet-grouted piles, is suggested. In the case of the grout-tipped drilled shafts, the grout pressure always resulted in an upward flow of grout alongside the shaft which increased both the side and tip areas. The increased areas and grout tip preload were the three factors identified with the increased shaft and group resistance. Due to uncertainty in estimating areas, a conservative design approach for assessing single and group capacities of post-grouted drilled shafts at 5% displacement is proposed. Finally, the use of stage grouting to assess the increase in shaft capacity (skin and tip) is suggested.

17. Key Words	18. Distribution Statement
Deep Foundations, jet-grouted piles, grout-tipped drilled shafts, group behavior, axial load testing	No restrictions.

19. Security Classif. (of this report)	20. Security Classif. (of this page)	21. No. of Pages	22. Price
Unclassified	Unclassified	206	

Form DOT F 1700.7 (8-72) Reproduction of completed page authorized

TABLE OF CONTENTS

LIST OF TABLES

LIST OF FIGURES

EXECUTIVE SUMMARY

Florida Department of Transportation (FDOT) structures are supported on single or groups of pile/drilled shafts. Pile or drilled shaft caps are generally designed for maximum axial resistance for each individual pile/shaft with minimum possible spacing to reduce the cost of the reinforced concrete cap . Past research has shown that center-to-center (c/c) spacing of three times the diameter (3D) will result in a group efficiency factor [group capacity/(single pile capacity × the number of piles)] of one (1) for either driven pile or drilled shaft groups.

In the past few years, FDOT has been using post grouting technology to improve the tip resistance of drilled shafts. In addition, FDOT has recently developed a new jet-grouted pile system to improve both the side and tip resistance. Unfortunately, the efficiency factors for both post-grouted drilled shafts and jet-grouted piles in a group arrangement are unknown. This research focused on the group interaction of post-grouted drilled shafts and jet-grouted piles to establish group efficiency factors for design purposes. It was also tasked with developing analytical approaches for predicting load versus deformation response of post-grouted drilled shafts and jet-grouted pile groups.

To study the group interaction of jet-grouted piles, two small-scale group tests (four 8-inch × 8-inch × 8-ft. long piles grouped with 16-inch Ø side bulbs, and four 4.5-inch Ø × 8-ft. long pile group with 10-inch Ø side bulb at 3D spacing) were performed in the FDOT test chamber at the University of Florida's Coastal Engineering lab. Measured load-displacement response of the piles under group loading revealed that the displacements of all piles were relatively uniform irrespective of the load carried by each pile. Similarly, the soil deformation at the center of the group was almost identical to the average displacement of the piles. In addition, the vertical stress beneath the center of the group was higher than the

vertical stress increase recorded directly beneath piles due to overlapping stress bulbs from individual piles. All of these observations suggest that the piles behaved as a single block during axial loading. Finite element modeling of single jet-grouted piles (8-inch square × 8-ft. long and 6-inch square × 8-ft. long) were carried out using the two-dimensional finite element software PLAXIS-2D to investigate the soil stresses around the jet-grouted piles and the results were used to update the grouted vertical stress increase coefficient (K_g) plot proposed in a previous FDOT project (# BD545, 2009). Finally, from the experimental results, a group capacity as well as an analytical approach for predicting load-deformation response of either a single or group of jet-grouted piles was developed.

In the case of tip grouted drilled shafts, two small-scale post-grouted drilled shaft groups (four 8.5-inch Ø × 8-ft. long drilled shaft groups and four 8.5-inch Ø × 13-ft. long drilled shaft groups) at 3D spacing were tested to study the group interaction behavior of post-grouted drilled shafts. The displacement of soil at the center of the group measured during group loading was much smaller than the average displacement of the top of the shaft. Moreover, the vertical soil stresses measured beneath the shaft group during group loading showed little, if any, stress increase at the center of group versus directly under a shaft, unlike the jet-grouted pile group. Based on the measured displacements and stresses during group loading, the grout-tipped drilled shafts behaved individually with little, if any, influence on another (i.e., group efficiency factor is 1). In addition, the experimental study of post-grouted drilled shaft groups revealed that the axial capacity of post-grouted shafts at Federal Highway Administration (FHWA) failure criterion (5% diameter) increased and was a function of: (1) preloading grout tip pressures; (2) increased skin resistance due to grouting; and (3) increased tip area as a result of tip grouting. Since the increase in tip area and side resistance is subjective in nature, a conservative design approach was proposed to

estimate total capacity of post-grouted drilled shafts at 5% settlement. From the second group study, which also focused on the effectiveness of staged grouting; it was found that the staged grouting improved the capacity of drilled shafts by increasing the preloading effect and assisting with the formation of a grout bulb at the shaft tip. In addition, the effectiveness of stage grouting may be assessed by both the grout tip pressure and volumes measured.

CHAPTER 1
INTRODUCTION

1.1 Background

Deep foundations (piles/drilled shafts) are used throughout Florida to support various types of Florida Department of Transportation (FDOT) structures, e.g., bridges, signage, lighting, noise walls, etc. The piles/shafts may be placed individually or as a group when large loads are involved. Spacing of piles/shafts within a group is generally a tradeoff; at minimum spacing reduces the high cost of the concrete pile/shaft caps, but too close and axial capacity of the group is significantly reduced, that is, the axial group resistance may be significantly less than the sum of the individual pile/shaft resistance. The reduction in group capacity may be attributed to shear transfer occurring within the soil mass confined by the group. The interference of each individual member in the group is generally quantified by a group efficiency factor (group capacity/(single pile capacity × number of piles). A group efficiency factor of one (1.0) identifies that the stresses transferred to soil from each individual pile/shaft does not overlap with adjacent piles/shafts. A number of research studies have investigated group efficiencies for driven piles, as well as auger cast insitu shafts at different center-to-center (c/c) spacing. For current design, three times the diameter (3D) c/c spacing is the accepted minimum pile/shaft spacing to achieve a group efficiency factor of one (1.0). Any pile/shaft spacing less than 3D is generally accepted to have stress transfer between piles/shafts resulting in a group efficiency factor of less than one (< 1).

Unfortunately, a driven pile suffers the issue of noise and vibration associated with pile driving operation, whereas a drilled shaft suffers lowest unit skin and tip resistance of all deep foundations. To reduce noise and vibration and improve capacities, the FDOT has successively developed and implemented post grouting of drilled shaft tips. Specifically,

after the construction of a drilled shaft, the tip of the shaft has high-pressure colloidal grout pumped beneath it, which pre-mobilizes significant tip resistance and fills in all voids and anomalies in the vicinity of the shaft tip. Regrettably, drilled shafts still suffer quality control issues (i.e., the structural integrity of the shaft) and lower skin friction of all deep foundation types in typical Florida sands.

To improve total pile/shaft capacity, the FDOT developed the jet-grouted pile system, which overcomes the limitations of both driven piles and drilled shafts (both conventional and post-grouted). FDOT report BD545-31 showed that jet-grouted piles have a number of distinct advantages: (1) the reinforced precast concrete member eliminates the quality uncertainty issues inherent in cast-in-place drilled shafts; (2) jetting minimizes noise and vibration; (3) grouting maximizes the skin and tip resistance; and (4) tip grouting of the pile not only increases tip resistance, but provides a proof test, resulting in higher LRFD ϕ factors for design.

Unfortunately, the group efficiency factors for both post-grouted drilled shafts and jet-grouted piles are unknown. The objective of this research was to study the group interaction of grout-tipped drilled shafts and jet–grouted piles at typical 3D spacing from which group efficiency factors for design may be established. The research was also to validate current design methodologies for assessing single pile/shaft axial load-deformation response for grout-tipped drilled shaft and jet-grouted pile behavior from which group load-deformation was to be predicted.

1.2 Scope of Work

1.2.1 Small-Scale Testing of Jet-Grouted Pile Groups

Small-scale testing of two jet-grouted pile groups was conducted to study the soil-structure interaction between the piles within the group. Size of the piles in the group was limited by the boundary constraints of the testing chamber. The first layout chosen for study was a group of four 8-inch square × 8-ft. long jet-grouted piles (16-inch grout bulb diameters) at 24-inch (3D) center-to-center spacing. The second group was four smaller diameter jet-grouted piles (4.5-inch diameters × 8-ft. long piles and 10-inch diameter side grout bulb) at 3D spacing. The objective of the second group test was to validate the results obtained from the first group test with minimized boundary effects. Installation of each group began with the jetting of precast piles into the soil in the test chamber and then side grouting of each pile from the top down. Prior to tip grouting, top down group compression tests were conducted to estimate side resistance of the group. Subsequently, tip grouting of the individual piles was performed and then another top down load test was conducted to estimate total group capacity. The group tests involved soil/pile deformation monitoring as well as 14 soil stress measurements to study group behavior.

1.2.2 Small-Scale Testing of Grout-Tipped Drilled Shaft Groups

Two small-scale group tests of grout-tipped drilled shafts were conducted to investigate the group behavior of grout-tipped drilled shafts. The first group selected for the investigation was the group of four 8.5-inch diameter × 8-ft. long drilled shaft (L/D ~11) at 3D c/c spacing. The smaller diameter shafts were again selected to minimize chamber boundary effects. The intent of the first group test was to study the factors influencing the axial capacity of the grout-tipped drilled shaft, the grout flow pattern, and the group behavior of

the grouted shafts at typical 3D spacing. The second group studied was a group of four 8.5-inch diameter × 13-ft. long drilled shaft (L/D ~18) at 3D c/c spacing. The objective of the second test was to investigate the use of staged grouting to improve the capacity of grout-tipped shafts, as well as to validate the results of the first group tests for greater embedment depths. Again, group testing as well as individual shaft tests were performed at pre- and post- grouting. Measured axial top down testing data included soil deformation in the vicinity of shaft; load-displacement response of individual shafts; vertical and horizontal soil stresses alongside, as well as beneath individual shafts and the group. From the experimental observations, it was observed there was very little, if any, shear transfer between the shafts.

1.2.3 Numerical Modeling of Jet-Grouted Piles

Numerical modeling of single jet-grouted piles (8-inch square × 8-ft. long and 6-inch square × 8-ft. long, FDOT project # BD545, 2009) were carried out using the two-dimensional finite element package, PLAXIS-2D, to investigate the soil stresses around jet-grouted piles. The pile and soil in the test chamber were modeled with an axisymmetric model. Hardening soil (HS) model was used to model sand in the chamber. The results obtained from the numerical analysis were compared with the experimental results and used to predict the response of piles installed at other densities and strengths. The grouted vertical stress increase coefficient (K_g) plot, proposed by McVay et al. based on experimental results (FDOT project # BD545, 2009), were updated using the numerical analysis results for piles in higher strength soils.

1.2.4 Estimation of Group Efficiencies of Grouted Pile/Shaft Groups

Group efficiencies of grout-tipped drilled shafts and jet-grouted piles at typical 3D spacing were estimated using the data collected from the small-scale group testing of both

grout-tipped drilled shafts and jet-grouted piles. It was found that the group efficiency of grout-tipped drilled shaft groups at typical 3D spacing is one (1.0), as the shafts behaved individually at 3D spacing. Conversely, the jet-grouted pile group had significant group behavior at 3D spacing. Specifically, the piles failed as a block and hence had a group efficiency factor less than one.

1.2.5 Develop Appropriate Design Procedures for Grouted Pile/Shaft Groups

Load transfer methodology proposed by McVay et al. (1989, FB-Multipier) was used to develop T-Z curve and Q-Z curve for single jet-grouted pile/pile group. The proposed T-Z curve and Q-Z curve can be used to estimate the total load displacement response of both single jet-grouted piles and jet-grouted pile groups with reasonable accuracy.

The study also proposes a simple approach to estimate the minimum ultimate design capacity of post-grouted shafts at a displacement of 5% diameter (FHWA 1999), which could be used with great confidence for design purposes. The latter does not consider the increase in tip area and side resistance as result of tip grouting, which was observed in the experimental study. Thus, the group capacity could be estimated by multiplying the minimum ultimate design capacity of single post-grouted shafts with the number of shafts in the group (group efficiency equal to 1).

CHAPTER 2
LITERATURE REVIEW

2.1 Soil-Structure Interaction of Cast Insitu Piles/Shaft

Most deep foundations consist of a group of piles/shafts. The piles/shafts are placed at the minimum possible spacing to reduce the cost of the concrete pile/shaft cap. Failure of the group may occur either by failure of the individual piles or failure as an overall block . The load capacity of a group of vertically loaded piles/shafts can, in many cases, be considerably less than the sum of the capacities of the individual piles/shafts comprising the group as there will be shear transfer occurring through the soil from one pile/shaft to another. Generally, a group efficiency factor of one (1) means that the shear stress transfer from one pile/shaft is not overlapped with that of an adjacent pile/shaft. Past research has shown that a group efficiency factor of one (1) is achieved at a minimum center-to-center spacing of three times the diameter of the pile/shaft. The pile/shaft soil-pile/shaft interaction may be characterized as in Figure 2-1.

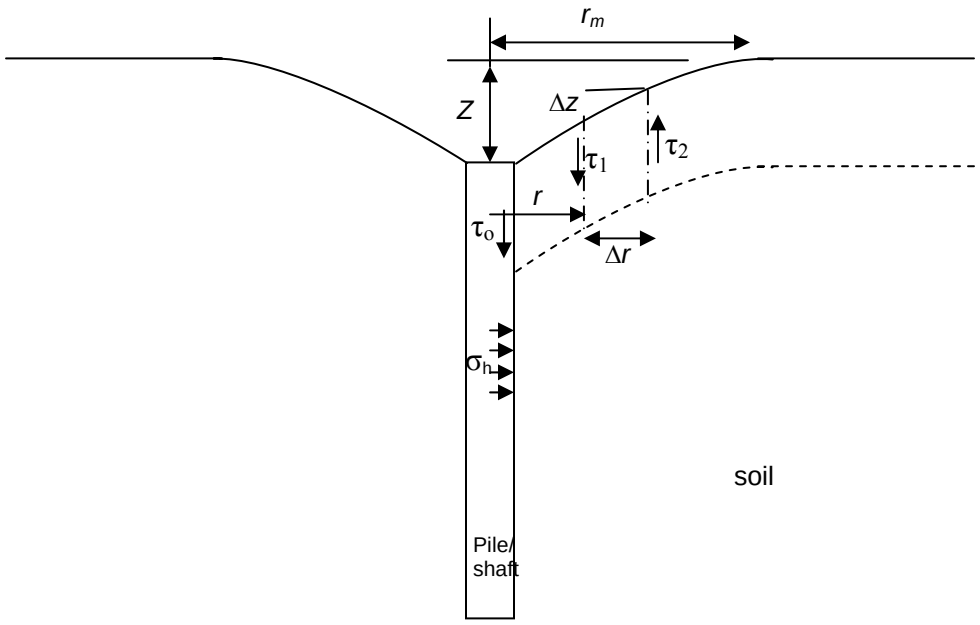

Figure 2-1 Pile/shaft soil-pile/shaft interaction.

If one considers the case of ultimate pile/shaft capacity, maximum side shear stress (τ_o) is mobilized along the surface of the pile/shaft. For any vertical slice (Figure 2-1), the shear stress (τ_1, τ_2) must always diminish with radius r, and is negligible at a radial distance r_m (radius of influence). Hence, it is evident that any pile/shaft placed within the distance r_m of an adjoining pile/shaft, undergoes shear transfer and settlement from the loaded adjoining pile/shaft, without any load being applied to the pile/shaft.

In the case of a side grouted pile, pressure grouting increases both horizontal stress (σ_h) and shear strength of the soil around the pile. Besides increasing the soil's shear strength, the shear modulus (G) also increases. Consequently, for any applied load, the soil shear strain γ ($\Delta z/\Delta r$) must be smaller. Hence, in the case of ultimate capacity, much larger side shear stresses are expected alongside the grouted pile/shaft perimeter. At the radial distance r_m, the shear stress is much greater for grouted pile/shafts compared to conventional cast insitu piles/ shafts. Consequently, the vertical pile/shaft deformation Z ($\Sigma\Delta z_i$) is larger (summing to the distance r_m), but shearing strain γ is smaller due to high shear modulus for any radial distance 'r' compared to a non-grouted cast insitu pile/shaft. This suggests that a group of grouted piles/shaft could have greatly reduced efficiency factors (i.e., grout capacity/number of pile/shafts × individual capacity) for typical spacing, e.g., 3D. A low shear strain is expected within the footprint of the group due to the increased confining stress and shear modulus, and much higher shear strain is expected outside the footprint where shear modulus is greatly diminished. Consequently, the grouted pile group may fail through block failure at the vertical slip boundaries as shown in Figure 2-2(a). The vertical side capacity of the shaft is equal to the shear stress on the vertical slip surface times the surface area of the outside block (Figure 2-2(b)). Since the shear stress may decrease linearly from pile/shaft to the vertical slip surfaces and the surface area of the block linearly increases, it is realistic to calculate the

group capacity by multiplying the single grouted pile/shaft shear stress by the footprint perimeter (Figure 2-2(b)) of the group itself.

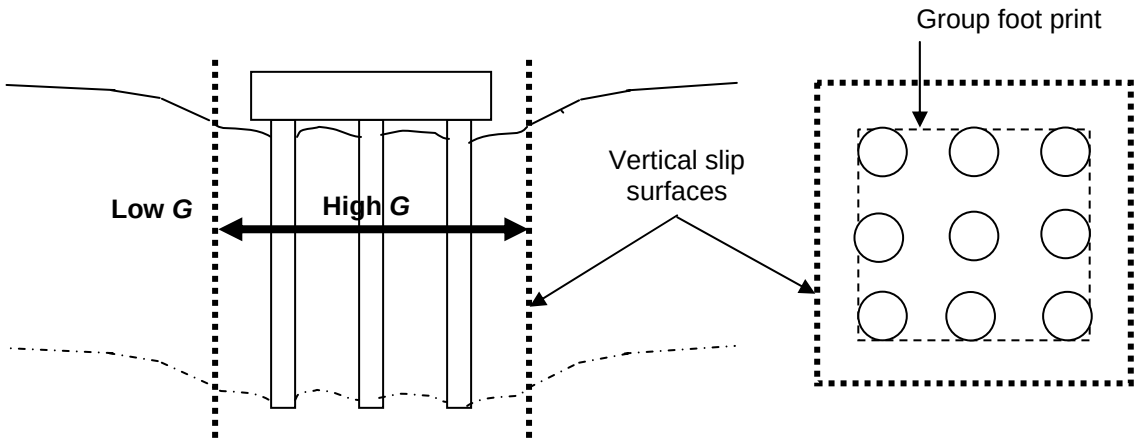

(a) Hypothesized vertical grouted pile/shaft displacement (b) Plan view of pile/shaft group

Figure 2-2 Pile/shaft views.

Hence, group efficiencies of the pile/shaft group are expected to be less than 1.0 at typical spacing of 3D. But for a tip grouted shaft (no side grouting) group, a combined conventional single shaft summation for side shear is expected, however, the tip resistance may exhibit a group footprint.

2.2 Cavity Expansion Theory

Cavity expansion analysis offers useful solutions for a variety of geotechnical engineering problems, including pressure meter testing, cone penetration testing, pile driving, pile loading to failure, tunnel deformation, and finally, the process of grouting a pile insitu. Cavity expansion processes are of two basic types: (1) expansion from a finite radius and (2) expansion from zero initial radius (i.e., cavity creation problem). Initially, cavity expansion theory focused on solving metal indentation problems (Bishop et al. 1945; Hill 1950). The cavity expansion theory was first applied in the geotechnical engineering field by

Gibson and Anderson (1961) for the interpretation of pressure meter tests. The theory has been progressively refined and applied to various geotechnical problems in the last four decades (Palmer 1972; Vesic 1972; Hughes et al. 1977; Carter et al. 1986; Yu and Houlsby 1991; Salgado and Randolph 2001; Salgado and Prezzi 2007). In the case of a jet-grouted pile, side grouting resembles the expansion of a cylindrical cavity from a finite radius and tip grouting resembles the expansion of a spherical cavity. Hence, classical cavity expansion theory can be used to predict the expected grout pressure during the installation of jet-grouted pile. In this work, elastic perfectly plastic closed form solutions of Yu and Houlsby (1991) and limit pressure charts given by Salgado and Randolph (2001) are used to predict the expected grout pressure. Yu and Houlsby's closed form solution are based on an elastic perfectly plastic soil with Mohr-Coulomb failure criterion and a constant rate of dilatation (ψ). The straightforward procedure for constructing a pressure expansion curve and calculating limit pressure presented by Yu and Houlsby (1991) is given below:

(a) Choose input parameters for the soil, i.e., E (Young' modulus), ν (Poisson's ratio), c (cohesion), ϕ (friction angle), ψ (dilation angle), p_0 (insitu mean effective stress) and parameter 'm', which is equal to 1 for cylindrical analysis and 2 for spherical analysis. Use of the parameter 'm' allows use of generic equations for both types of cavity and is obtained from the generic equilibrium equation for cylindrical/spherical cavity, $r\left(d\sigma_r/d_r\right)+m.\left(\sigma_r-\sigma_\theta\right)$ where σ_r and σ_θ are radial stress and hoop stress, respectively.

(b) Calculate the following terms from the input parameters:

$$G=\frac{E}{2.\left(1+\nu\right)} \tag{2.1}$$

$$M=\frac{E}{1-\nu^2\left(2-m\right)} \tag{2.2}$$

$$Y = \frac{2c\cos\phi}{1-\sin\phi} \tag{2.3}$$

$$\alpha = \frac{1+\sin\phi}{1-\sin\phi} \tag{2.4}$$

$$\beta = \frac{1+\sin\psi}{1-\sin\psi} \tag{2.5}$$

$$\gamma = \frac{\alpha(\beta+m)}{m(\alpha-1)\beta} \tag{2.6}$$

$$\delta = \frac{Y+(\alpha-1)p_0}{2(m+\alpha)G} \tag{2.7}$$

$$\eta = \exp\left\{\frac{(\beta+m)(2-m)[Y+(\alpha-1)p_0][1+(2-m)\nu]}{E(\alpha-1)\beta}\right\} \tag{2.8}$$

$$\xi = \frac{[1-\nu^2(2-m)](1+m)\delta}{(1+\nu)(\alpha-1)\beta} \times \left[\alpha\beta + m(1-2\nu) + 2\nu - \frac{m\nu(\alpha+\beta)}{1-\nu(2-m)}\right] \tag{2.9}$$

(c) Calculate the cavity radius from the small strain elastic expression $(a\text{-}a_0)/a_0 = (p - p_0)/2mG$; for pressure '$p$' less than the pressure 'p_1', which is required to initiate plasticity, $p_1 = 2mG\delta + p_0$.

(d) Calculate the cavity pressure ratio 'R' from the following equation, for a given value of 'p' (greater than p_1 and less than the limit pressure p_{lim}):

$$R = \frac{(m+\alpha)[Y+(\alpha-1)p]}{\alpha(1+m)[Y+(\alpha-1)p]} \tag{2.10}$$

(e) Evaluate a/a_0 from the following equation and the radial displacement 'u' ($u = a - a_0$):

$$\frac{a}{a_0} = \left\{\frac{R^{-\gamma}}{(1-\delta)^{(\beta+1)/\beta} - (\gamma/\eta)\Lambda_1(R,\xi)}\right\}^{\beta/(\beta+m)} \tag{2.11}$$

Evaluate sufficient terms in the infinite series to obtain an accurate value of Λ_1:

$$\Lambda_1(x,y) = \sum_{n=0}^{\infty} A_n^1 \tag{2.12}$$

$$A_n^1 = y^n \ln x / n! \quad \text{if } n = \gamma\,; \quad \text{otherwise} \quad A_n^1 = \frac{y^n}{n!(n-\gamma)}\left[x^{n-\gamma} - 1\right] \tag{2.13}$$

The procedure from (d) to (e) above can be repeated to construct the complete cavity pressure expansion relationship. By setting (a/a_0) to approach ∞ in Equation 2.11, the limit pressure p_{lim} can then be obtained.

Salgado and Randolph (2001) presented a numerical method for solution of cavity expansion problems taking into account stress-equilibrium and strength and flow assumptions, which resulted in charts for cylindrical/spherical cavity expansion limit pressures (p_{lim}) as a function of soil strength (ϕ_c = critical state friction angle), relative density (D_r), and depth or initial lateral/mean insitu stress for sands. Figure 2-3 shows Salgado's cylindrical cavity limit pressure chart for $\phi_c = 30°$ (for other charts refer to Appendix A).

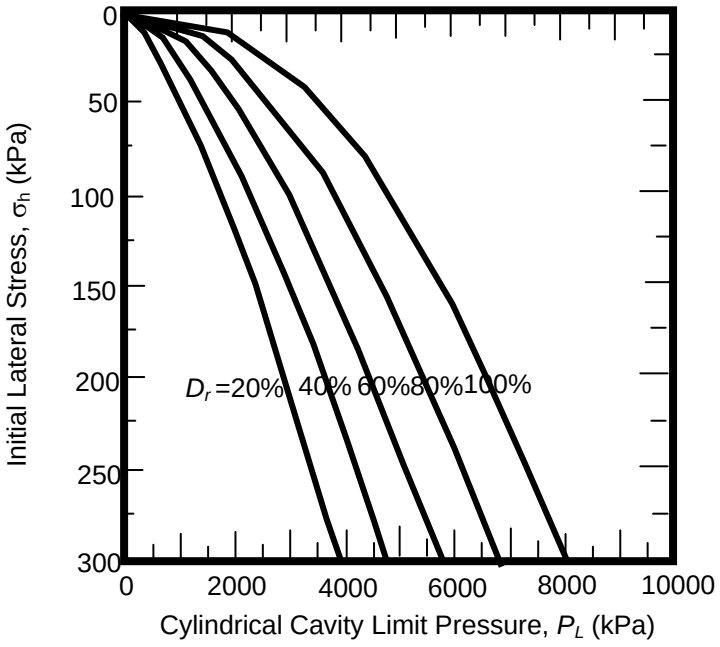

Figure 2-3 Cylindrical limit pressure as a function of lateral stress, D_r, and $\phi_c = 30°$ (Salgado and Randolph 2001).

2.3 Past Research on Post-Grouted Drilled Shafts

Significant end bearing resistance of a drilled shaft is unusable due to the required displacement for mobilization. For instance, at AASHTO and FDOT permissible service displacements (< 2 inches), the axial load applied to large diameter drilled shafts is mainly resisted by skin friction. The skin resistance of drilled shaft is fully mobilized at a displacement of about 1/4-inch (i.e., 0.5 to 1% of shaft diameter in the normal case). But, displacements of about 10-15% of shaft diameter are required to fully mobilize the end bearing (Bruce 1986; Mullins and Dapp 2006). To regain some of the unusable capacity, post grouting the drilled shafts has been successfully used worldwide for the last four decades. The post grouting process consists of: (1) casting a drilled shaft with a grout delivery system integrated to the rebar cage; and (2) injecting high pressure grout beneath the tip of the shaft after sufficient curing of the shaft, which preloads the insitu soil and compresses any debris left by the drilling process.

The effort to improve the end bearing of the drilled shaft by pressure grouting began in Asia and Europe in the early 1960s. The first known published test results of using shaft grouting was by Gouvenot and Gabix (1975). The results of the testing indicated an increase of 2.5 times in shaft capacity. A review of published works on pile construction and the benefit of post grouting between 1975 and 1985 was presented by Bruce (1986). More recently, tip and shaft grouting were used for piles/drilled shafts in sands (Plumbridge and Hill 2001).

There are mainly three types of grout distribution systems commonly used in practice, namely: stem type; sleeve port type; and flat jack type. The stem type is the simplest form of grout distribution system and consists of a pipe end at the shaft tip. This is not an efficient grout distribution system, and hence, it is only utilized in the remediation of substandard

shafts with inadequate capacity. The sleeve port type, also known as a tube-a-manchette, primarily consists of a pipe network at shaft tip with pre-drilled holes and the pipe network is connected to grout tubes at the top of the shaft. The grout system has both grout entry and exit pipes, which allow the flushing of the grout system and regrouting of the shaft, if necessary. The pipe network at the shaft tip is wrapped with a rubber membrane at the location of the holes to prevent blockage at the hole during the casting of the shaft and allows the grout to flow out during the grouting stage. This also prevents the return of pumped grout to the pipe network. Sometimes a gravel plug is placed in the excavated hole before lowering the sleeve-port with a steel plate above it (Sliwinski and Fleming 1984). This arrangement is shown in Figure 2-4. The steel plate isolates the sleeve-port from the concrete, and the gravel pack provides more soil interface for the grout to flow into. Flat jack types have a confined grout mass contained within an impermeable membrane/plate system. The grout lines cannot be flushed, unlike the sleeve-port type. Figure 2-5 shows the flat jack type grouting system used by Mullins et al. (2001).

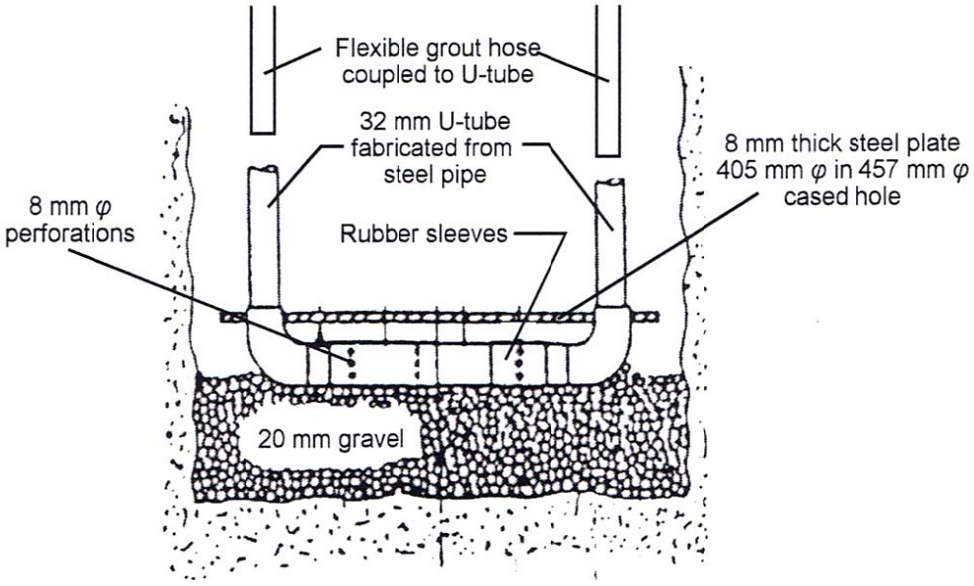

Figure 2-4 Sleeve-port type (Sliwinski and Fleming 1984).

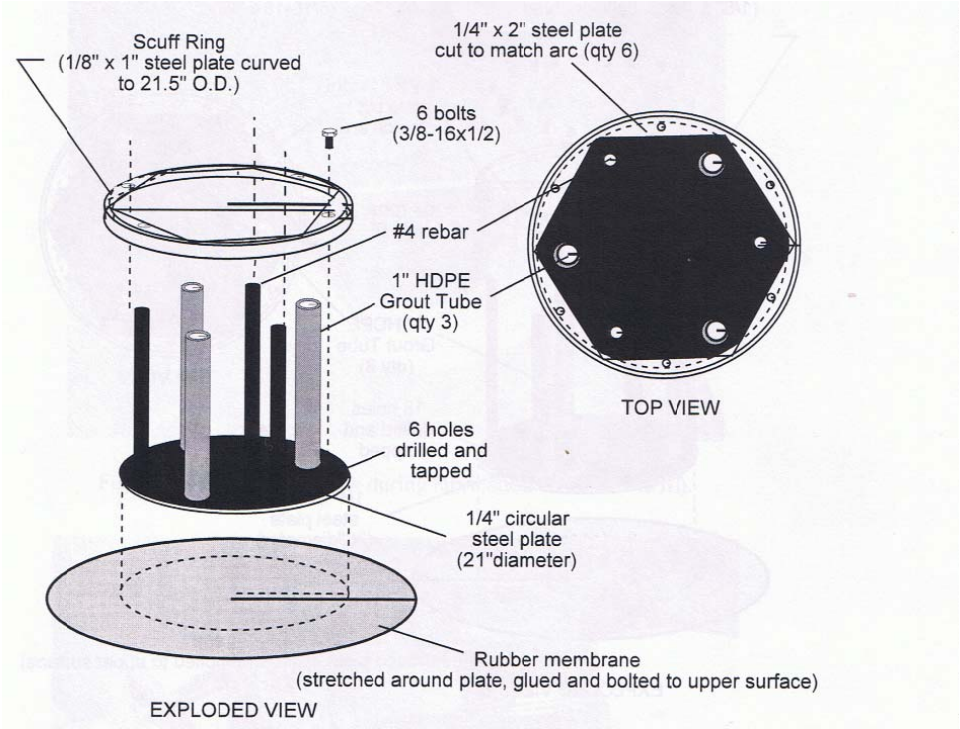

Figure 2-5 Flat jack type (Mullins et al. 2001).

Unfortunately, the use of post-grout drilled shafts was not widely accepted in the United States due to the absence of a rational design methodology. Recently, Mullins and Dapp (2006) presented a design methodology to estimate the end bearing of post-grouted shafts based on field test results, and a number of contractors have entered the market of post grouting drilled shafts. In the past 5 to 10 years, post grouting of drilled shafts has become quite common in the United States. Following are steps involved in the design procedure presented by Mullins and Dapp (2006):

(1) Calculate the end bearing capacity (q_b) at a displacement of 5% of diameter of shaft using Reese and O'Neill (1988) method (Equation 2.14):

$$q_b = 0.057N \tag{2.14}$$

where N is the uncorrected SPT blow count.

(2) Calculate the total ultimate side resistance (F_s) of the shaft.

(3) Divide the total ultimate side resistance by cross-sectional area A of the shaft to estimate the maximum anticipated grout pressure ($GP_{\max}$):

$$GP_{\max} = \frac{F_s}{A} \tag{2.15}$$

(4) Calculate the Grout Pressure Index (GPI) as the ratio of GP_{max} to q_b:

$$\text{GPI} = \frac{GP_{\max}}{q_b} \tag{2.16}$$

(5) Establish the maximum permissible service displacement as the ratio of the shaft diameter($\%D$).

(6) Determine the Tip Capacity Multipier (TCM) using Equation 2.17 or Figure 2-6:

$$\text{TCM} = 0.713.\text{GPI}.(\%D)^{0.364} + \frac{\%D}{(0.4(\%D)+3.0)} \tag{2.17}$$

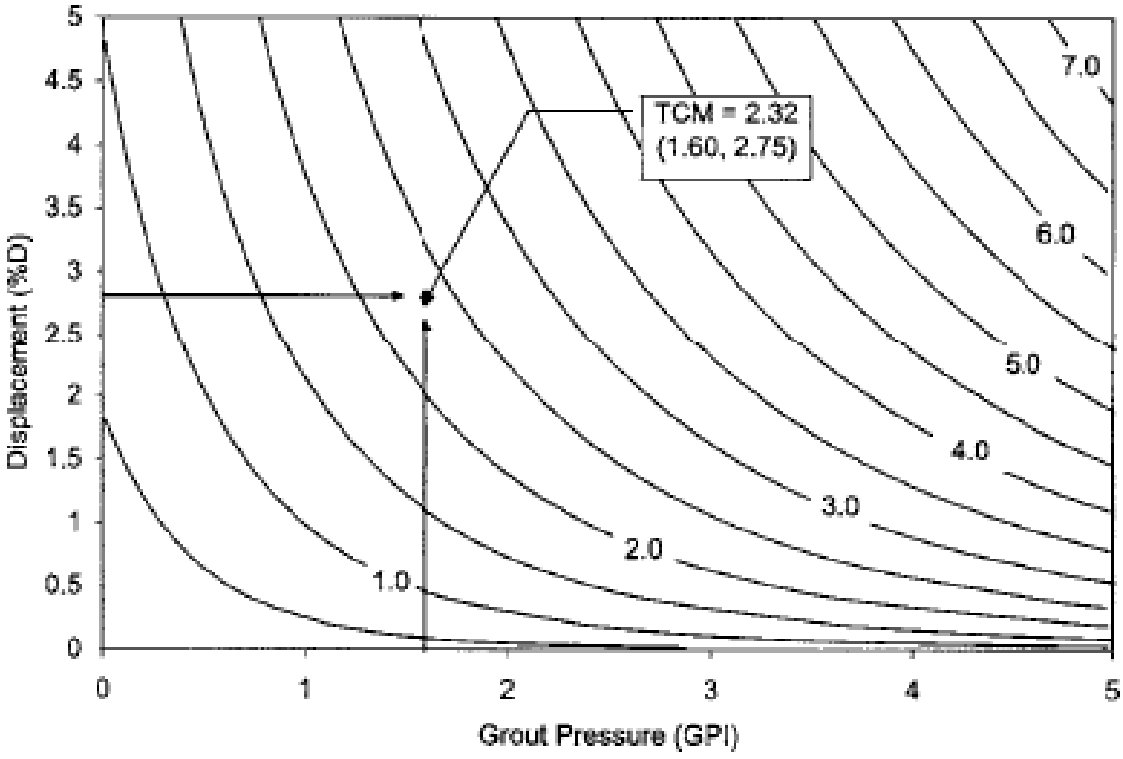

Figure 2-6 TCM contour (Mullins and Dapp 2006).

(7) Estimate the grouted unit tip resistance as the product of TCM (step 6) and the ultimate ungrouted end bearing capacity (step 1):

$$q_{grouted} = \text{TCM}.q_b \tag{2.18}$$

2.4 Past Research on Jet-Grouted Piles

One of the major drawbacks of driven piles is the associated noise and vibration. Pile jetting has been widely used to aid pile penetration into dense to very dense sand layers to minimize pile damage during driving and/or diminish the associated vibrations as the jetting pressure loosens (erodes) the soil at the tip of the pile and the flow of the jetting fluid reduces the shaft friction along the pile by about 30%. Recently, Giken, Inc., has developed pushed/jetted pile installation equipment for steel sheet and pipe piles. In soft soils, the pile is pushed, whereas in dense, stiff or hard soils, a disposable jet tip is attached to assist in the pile installation by jetting. Tsinker (1988) published the following flow rate equation to estimate water requirements for jetting:

$$\frac{Q}{D} = \left[530\left(d_{50}\right)^{1.3} l^{0.5}\right] + 0.017\pi l k \tag{2.19}$$

where Q = flow rate (m^3/hr);
D = pile diameter or width (m);
d_{50} = average size of sand particles (mm);
l = desired submerged length of pile (m); and
k = $(\Sigma k_n l_n) / l$ = avg. filtration coefficient (m/day).

The first known published test results of using shaft grouting was by Gouvenot and Gabix (1975). The results of the testing indicated an increase in shaft friction by 2.5 times. A review of published works on pile construction and the benefit of post grouting between 1975 and 1985 were presented by Bruce (1986). More recently, tip and shaft grouting were used for piles/drilled shafts in sands (Plumbridge and Hill 2001). A number of different apparatus for injecting grouts along the pile-soil interface have been developed; mostly

appear as in Figure 2-7 from the University of West Australia (Joer et al. 1998). Typical grout mixes used for grouting drilled shaft tips are combinations of cement, sand, and water. Micro fine materials (e.g., fly ash, bentonite, etc.) are also used to replace cement partially and to improve pumpability. Generally, grout mixes with aggregate materials greater than 3/8 inches are called compaction grouts which are generally used to prevent hydro fracturing of the soil.

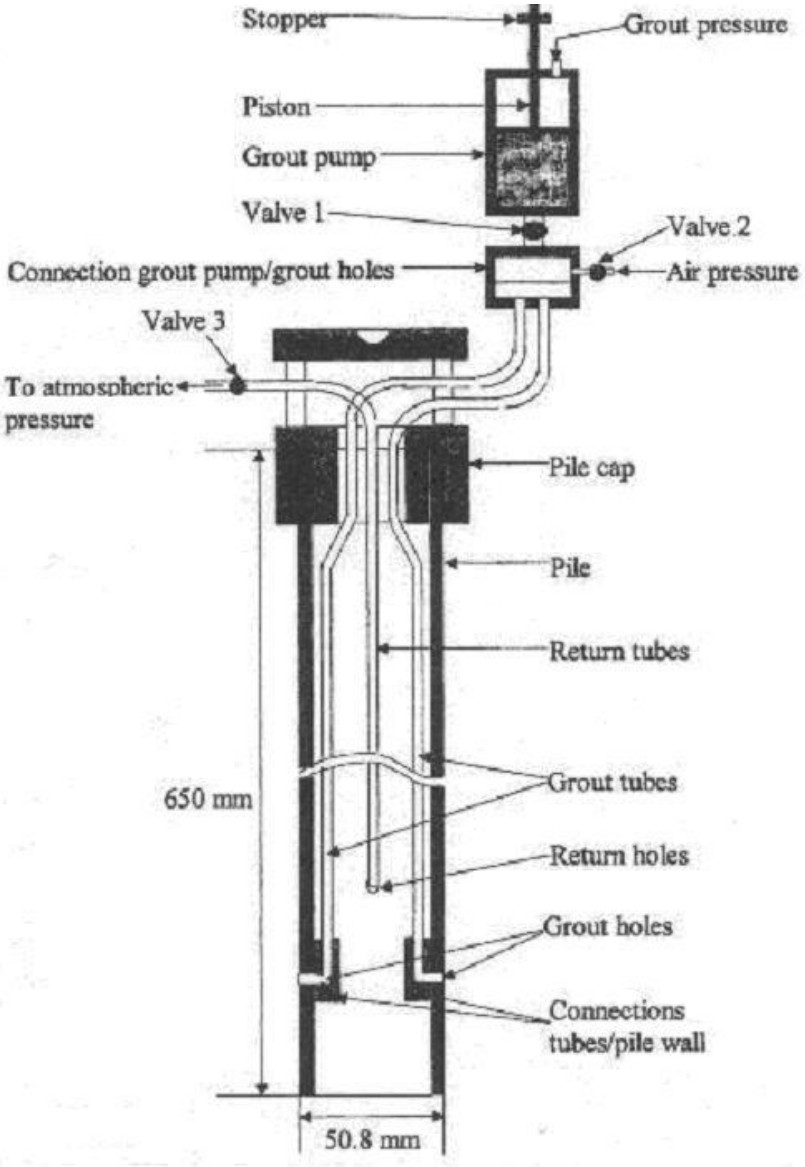

Figure 2-7 Side grouting system for precast pile (Joer et al. 1998).

However, side grouting of pile with the use of the grouting system developed by Joer et al. (1998) and compaction grout has the following drawbacks: 1) the pile grout lines could only be used once (i.e., no re-grouting was possible); 2) compaction grout is prone to sand locking; and 3) very poor bonding between the delivered grout and the pile which is attributed to grout type (compaction) and the path of grout expansion.

McVay et al. in the previous Florida Department of Transportation (FDOT) project BD545 (2009) developed a new jet-grouted pre-cast concrete pile with a new grout delivery system, which overcame the drawbacks of the grout system developed by Joer et al. (1998). Installation of the jet-grouted pre-cast pile was comprised of three distinct phases: jetting a pre-cast pile; side grouting the pile; and finally, tip grouting. The jet-grouted pile consisted of separate grout delivery systems for side grouting and tip grouting. The side grouting had top and bottom grouting zones, and each had its own grout delivery system. Figure 2-8 shows the final schematic of the pre-cast pile with grout delivery systems before jetting. The side grout system consisted of inlet and outlet pipes which made regrouting possible. Each of the side grout pipes (entry and exit) had a series of holes drilled into the grout tubes in pairs with gum rubber (1/4-inch thick) membrane covering each pair of holes. The gum rubber membrane allowed the grout to exit the grout pipe under high pressure, but prevented the ingress of grout and the egress of water when cleaning the pipes. The center jet pipe was used later for tip grouting. The jet tip was covered with a nozzle which prevented sand/fines ingress from the surrounding soil mass into the grout lines. In order to eliminate "sand locking" in the grout pipes, a grout mix consisting of cement, micro-fine fly ash, and water was used. To prevent flow of grout along the weakest path during side grouting, expandable membranes were wrapped around the pile at each grout zone into which the grout was pumped. These membranes both confined the grout zones as well as helped radial expansion

of the zones during grouting, which resulted in high radial soil stress around the pile. The membranes also prevented the mixing of grout with soil and improved bonding between grout and pile.

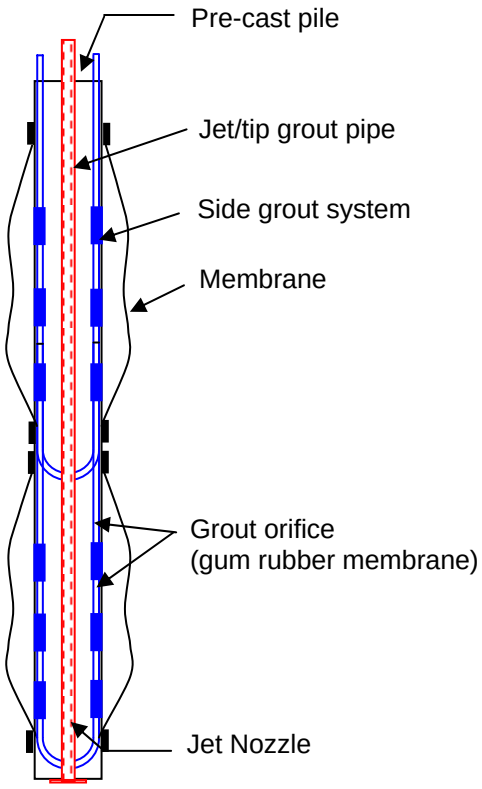

Figure 2-8 Schematic of pre-cast pile with grout delivery systems and membrane.

McVay et al. (2009) also presented a methodology for the design of jet-grouted piles. The expected side grout pressure and grout tip pressure was equal to the cylindrical cavity expansion limit pressure and the spherical cavity expansion limit pressure at corresponding depths, respectively. The limit pressure at various depths could be determined using one of the cavity expansion solutions available in the literature (e.g., Yu and Houlsby 1991; Salgado and Randolph 2001, etc.). Another alternative for determining the cylindrical cavity limit pressure at various depths would be performing the pressure meter tests. McVay et al.

proposed the following equation to estimate unit skin friction of jet-grouted pile based on the stress state around pile after installation:

$$f_s = \sigma_{vg}\left[\frac{\sin\phi_c}{1-\sin\phi_c}\right]\sin(90-\phi_c) \tag{2.20}$$

where f_s = unit skin friction;
ϕ_c = critical state friction angle;
σ_{vg} = vertical stress after grouting weight, $\left(\sigma'_{vg} = K_g\sigma'_{v0} = K_g\ \gamma' h\right)$;
h = depth;
γ' = buoyant unit weight; and
K_g = grout vertical stress increase coefficient (K_g) as given in the chart in Figure 2-9:

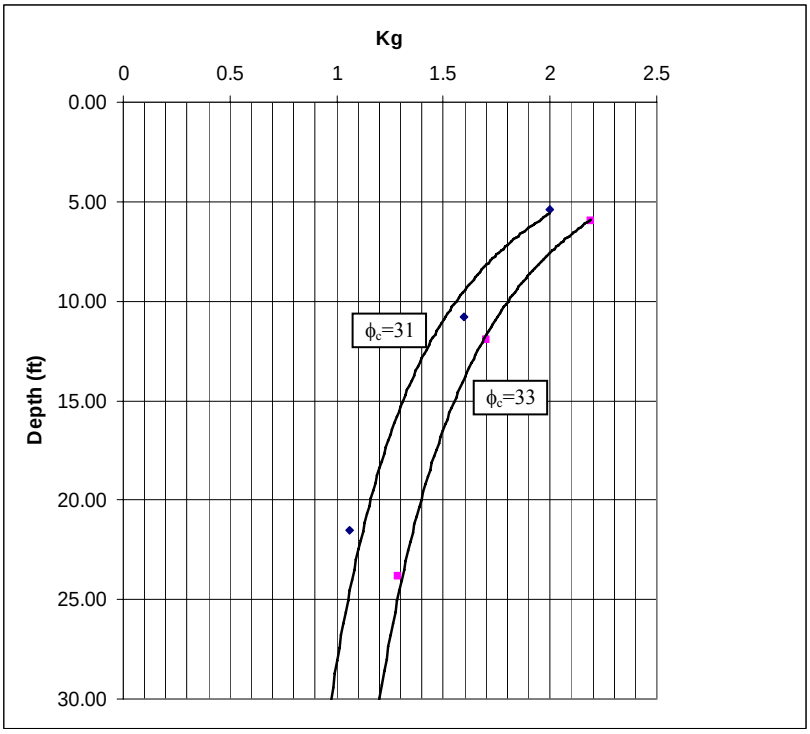

Figure 2-9 Estimate of grout vertical stress coefficient, K_g.

CHAPTER 3
TEST CHAMBER, SOIL PROPERTIES, INSITU TESTING, INSTRUMENTATION, TEST FRAME, AND SUPPORT SYSTEM FOR REACTION BEAM

3.1 Test Chamber and Reaction Shafts

The FDOT test chamber constructed in the Coastal Engineering lab at the University of Florida was used for all group testings of jet-grouted piles/grout-tipped drilled shafts. The test chamber (see Figure 3-1) has a clear depth of 35 ft. and diameter of 12 ft. Two 6-inch diameter slotted PVC pipes wrapped in filter fabric and placed along the walls of the chamber were used to control water levels within the test chamber. The benefits of conducting the testing in chamber include: 1) ensuring the replication of the pile-soil stresses; 2) permitting soil excavation to expose pile/soil grout zones; and 3) allowing for repetitive testing or parametric investigation. There are two drilled shafts (4 ft. in diameter and 45 ft. long) installed collinearly with the center of the test chamber to carry the reaction load during the top down testing. Each of the shafts can resist a maximum tensional load of 300 kips.

Figure 3-1 Test chamber and reaction shaft.

3.2 Soil Properties

Soil used in the test chamber was typical Florida silty sand (A-2-4). Shown in Figure 3-2 is the grain size distribution of the soil. Minimum and maximum dry densities of the silty sand were 92 pcf and 115 pcf, respectively. Direct shear tests on the soil at minimum and maximum dry densities showed angles of internal friction of 30° and 36°, respectively.

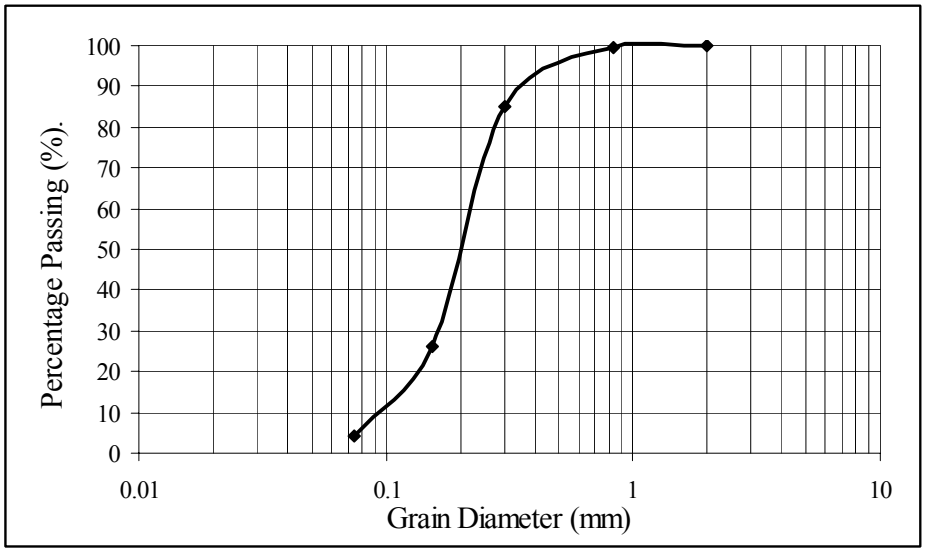

Figure 3-2 Grain size distribution of soil.

3.3 Geokon 4800 Stress Gages and Calibration

To measure both the lateral and vertical stress within the test chamber, Geokon model 4800 earth pressures cells were used (see Figure 3-3). The gages are capable of being installed in dry or fully saturated conditions. The gages were calibrated by submersion into a 40-ft. deep water tank in the Coastal Engineering lab. Gage readings were taken using a GK-401 readout box. Readings were taken at every 5-ft. interval up to a depth of 35 ft. in the water column. Figure 3-4 shows the (calibration) plot of measured pressure versus actual pressure. The gage placement in the test chamber for each group test was different, which will be depicted along with the description of each group testing.

Figure 3-3 Geokon stress gage.

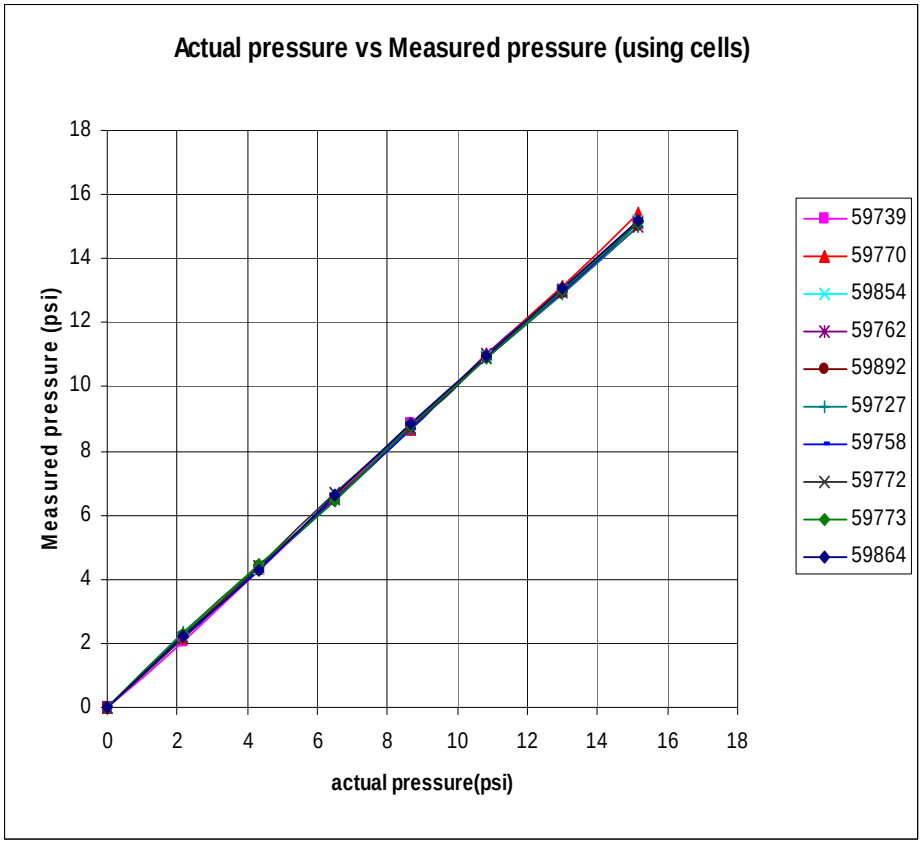

Figure 3-4 Calibration of stress gages.

3.4 Insitu Testing in the Test Chamber – PMT and SPT

Pressure meter testing (PMT) was conducted in the test chamber at three different depths (3 ft., 6 ft. and 11 ft.) to estimate the expected maximum grout pressures (limit pressure) during the side grouting of jet-grouted pile. The 3-ft. and 6-ft. depths corresponded to the middle of the top side grout bag and bottom side grout bag, respectively. Tests were conducted at two different locations for comparison purposes. The PMT data was also used to estimate shear modulus/Young's modulus of soil, which was used as an input parameter in the finite element modeling of jet-grouted piles. The tests were performed by personnel from the FDOT State Materials Office (SMO) (see Figure 3-5) based on the request of the researchers. Shown in Figure 3-6 to Figure 3-8 are the PMT results at various depths. From Figure 3-6, it can be seen that the average limit pressure at 3-ft. depth was about 60 psi. However, the pressure-expansion curves at 6 ft. and 11 ft. showed that the steady state of expansion was not reached during the tests, and hence, the limit pressures at 6 ft. and 11 ft. were more than 75 psi and 100 psi, respectively. Standard Penetration Tests (SPT) were performed in the test chamber at a depth of 8 ft. (corresponding to the tip of the 8-ft. jet-grouted piles/shafts) and the average SPT blow count was about 6.

Figure 3-5 Pressure meter testing.

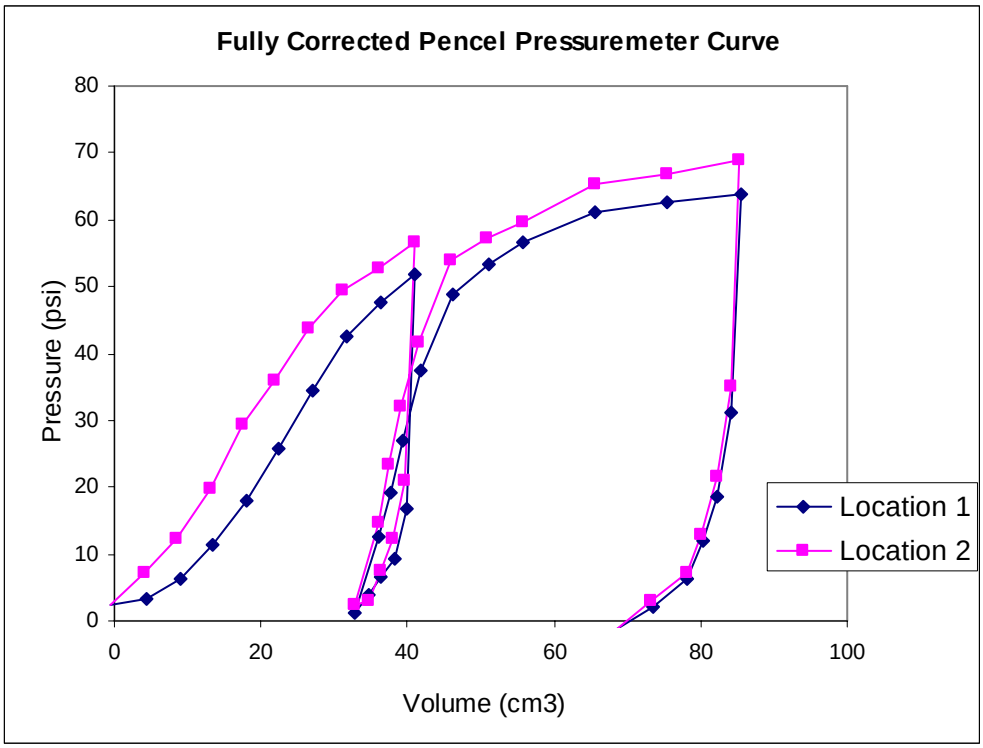

Figure 3-6 PMT results at 3-ft. depth.

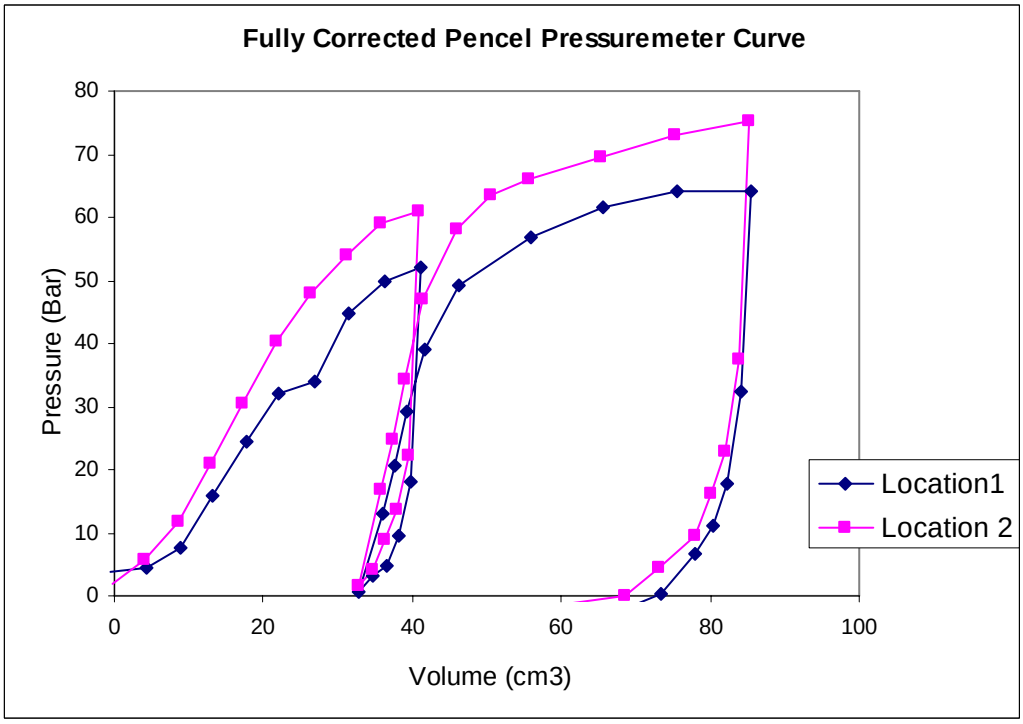

Figure 3-7 PMT results at 6-ft. depth.

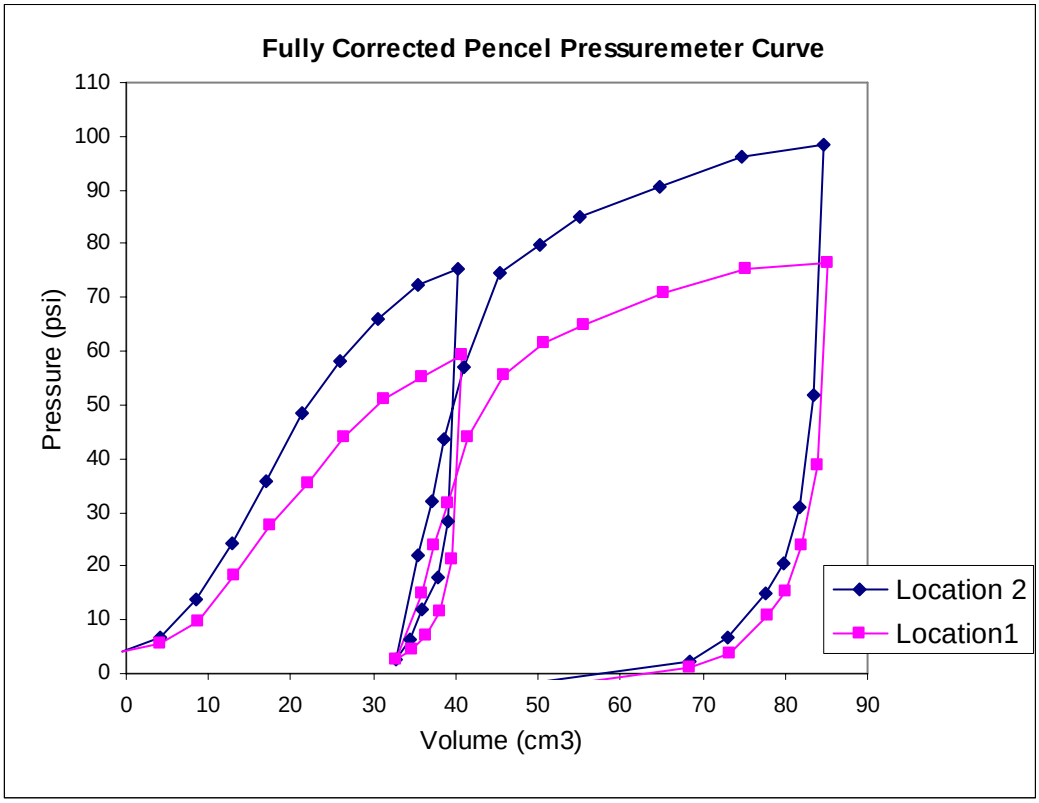

Figure 3-8 PMT results at 11-ft. depth.

3.5 Design and Construction of Group Test Frame

A test frame for all the group tests was designed according to 13th edition of AISC (ASD). The frame was adjustable to allow group testing of different size piles/shafts. Figure 3-9 shows the group test frame constructed for top down testing. The frame primarily consisted of three 42-inch long I-beams -W16 × 57. Side plates and sufficient number of stiffeners (1/4-inch thickness) were welded to I-beams to increase shear and moment capacity. The frame was able to transfer a maximum load of 600 kips to the pile/shaft group. Note, the frame ensured that uniform load would be applied to each pile within the group. The load was measured at the top of each pile with a 200-kip load cell.

Figure 3-9 Grout test frame.

3.6 Construction of Support System for Reaction Beam

Shown in Figure 3-10 is a support system positioned on one of the reaction shafts. This provided enough clearance (about 7.5 ft.) between the pile top and the bottom of the reaction beam for the jack, load cells, and instrumentation. The support system was basically a three-dimensional frame fabricated using different steel sections (tube, channel, pipe, etc.). The support systems rested on the top of each reaction shaft and were fastened to Dywidag bars, which transferred load from the reaction beam to the reaction shaft. The frame provided sufficient lateral stability to the reaction beam during pile loading, unlike the steel cribbing and stack of I-beams, which were used to support the reaction beam in previous load testing. Figure 3-11 shows the reaction beam with the support system.

Figure 3-10 Support system for one end of the reaction beam.

Figure 3-11 Reaction beam with support system.

CHAPTER 4
EXPERIMENTAL BEHAVIOR OF JET-GROUTED PILE GROUPS

4.1 Introduction

This chapter reports on the experimental testing carried out to investigate the group behavior of jet-grouted piles. Size of the piles within the group was limited by boundary constraints of the testing chamber. Specifically, past cavity expansion research in sands (especially dense and medium dense sand) has shown significant chamber boundary influences in case of penetrating objects (e.g., cones). Similarly, limit pressure during grouting, as well as frictional resistance of an individual pile, may be influenced by the immediacy of the chamber boundary. Fahey et al. (1986) suggested that a flexible chamber boundary should be at least 10 diameters away to minimize the influence of boundary. Unfortunately, due to the need to remove both the piles and the soil from the chamber in the present study, the chamber boundary had to be rigid (not flexible). Since it was expected that the as-built jet-grouted piles would be larger, e.g., 30 inches, it was decided to model both a larger and a smaller group in the test chamber. The first layout chosen for study was a group of four 8-inch square × 8-ft. long jet-grouted piles (16-inch grout bulb diameter) at 24-inch (3D) center-to-center spacing. For this layout, the chamber boundary was only 7 diameters away from the pile, and hence, the group capacity might be influenced by the boundary. The second group was four smaller diameter jet-grouted piles which minimized the influence of boundary effects. The second group had four 4.5-inch diameter × 8-ft. long piles (10-inch diameter side grout bulb). For the smaller diameter piles, the chamber boundary was more than 13 diameters away from the pile. A description of design, construction, and testing of both groups is presented followed by an analysis of the results.

4.2 Testing of 8-inch Square × 8-ft. Long Jet-Grouted Pile (16-inch Diameter Side Grout Bulb) Group

4.2.1 Design of 8-inch Square × 8-ft. Long Jet-Grouted Pile Group

As mentioned, four 8-inch square by 8-ft. long piles in a square group layout were selected for the first group test. Typical pile spacing of three diameters (i.e., 3D) would limit the grout volume that might be placed alongside each jet/grouted pile. Earlier research, FDOT BD 545 RPWO # 31, entitled "Prestressed Concrete Pile Installation Utilizing Jetting and Pressure Grouting," has shown a scalable relationship between the pile perimeter and side grouting membrane perimeter of 1:2 (validated from 4-inch micro-piles to 16-inch full-scale test). The latter was postulated from the two-way shear equation for concrete members (i.e., $Vu = 4b_o((f_c')^{1/2})$, where b_o is the perimeter of the precast pile and $4b_o$ may be approximated as πD (i.e., perimeter of grout volume where D = the diameter of grout membrane) with safety factor of 2. Accordingly, 8-inch precast piles should be capable of supporting a grout membrane diameter of approximately 20 inches, which at 3D spacing would result in only 4-inch spacing between adjacent grout bulbs, if they are ended prismatic, but if the grouting resulted in barrel shapes, then the piles could possibly touch. In addition, due to lateral confinement (i.e., grouting of nearby piles), it was believed that extremely large grout pressures would be required to place the grout. Consequently, it was decided to limit the diameter of the grout bulb to 16 inches (perimeter ratio of 1.5), which would result in 8-inch spacing between grout bulbs (i.e., 1D clear spacing). Even with the smaller grout membrane diameters, it was not known if significantly higher grout pressures would be required to install the piles. Evident from the discussion, the behavior of grouted in place pile/shaft groups are expected to be quite different than non-grouted pile/shaft groups.

Plumbing fittings for jetting and grouting phases were selected in conformity with a previous FDOT report BD 545 RPWO # 31. Due to the limited space available inside the

pile, 1-inch PVC pipe was considered for use in the grout delivery system and 1.5-inch steel pipe was selected for jetting. Again, the jetting pipe was also used for tip grouting during the grouting phase. Two separate grout delivery systems were designed for the top and bottom halves of the piles. Each system had its own grout entry and exit pipe. Each of the grout pipes (entry and exit) has a series of 3/8-inch and 1/2-inch holes drilled into the 1-inch PVC pipes in pairs at 4-inch intervals. The larger diameter holes (1/2-inch) were located at the bottom of the grout pipes and the smaller holes located at the top. A 1-inch diameter gum rubber membrane (1/4-inch thick) covered each pair of holes. The gum rubber membrane allowed the grout to exit the grout pipe under high pressure, but prevented the exit of water when cleaning the pipes.

Area of steel reinforcement was calculated according to building code requirements for structural concrete (ACI 318-02 2002). Area of reinforcement was determined for a maximum anticipated load of 150 kips (i.e., one-fourth of 600 kips, which is the total load carrying capacity of reaction shafts). The following equation (ACI Equation 10-2) was used to calculate A_{st}:

$$P_u = 0.8\Phi \left[0.85 f_c' (A_g - A_{st}) + f_y A_{st}\right] \quad (4.1)$$

where Φ = 0.65, strength reduction factor for concrete in compression (ACI 9.3);
f_c' = 4,000 psi, concrete compressive strength;
A_g = gross cross-sectional area of pile; and
f_y = 60,000 psi, yield strength of longitudinal reinforcement.

In solving the above equation, it was found that an area of steel reinforcement of 1.23 in^2 was required for the section, and hence, four #5 bars were selected, having a total cross-sectional area of 1.23 in^2. According to ACI 7.10.5, #3 size lateral ties with 6-inch c/c spacing were selected. A cross section of the pile at top, center, and bottom are given in Figure 4-1, and the final schematic of the pre-cast pile with grout delivery systems is shown in Figure 4-2.

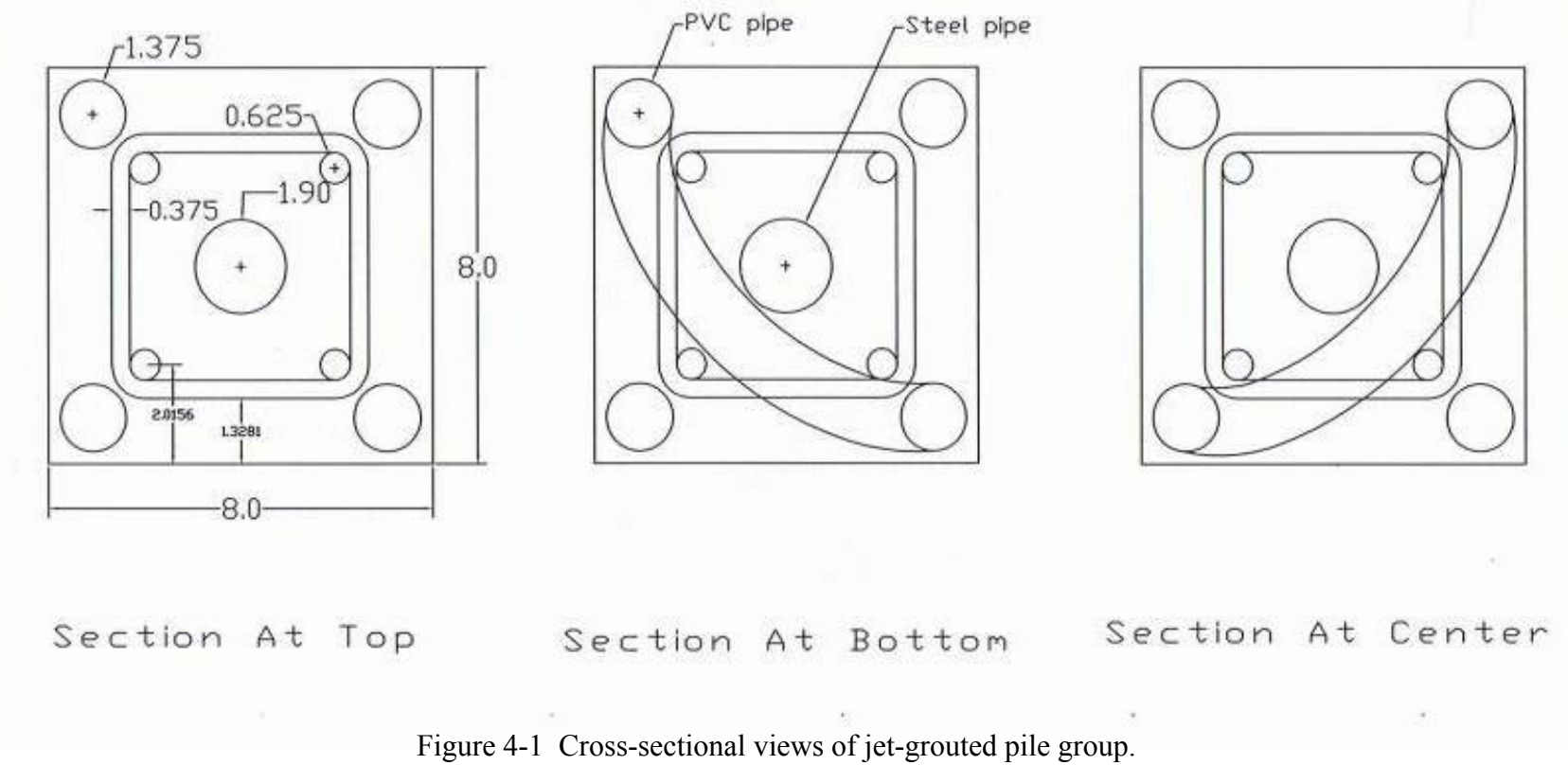

Figure 4-1 Cross-sectional views of jet-grouted pile group.

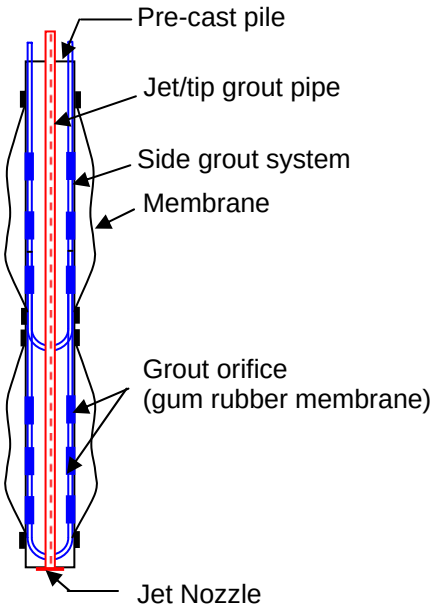

Figure 4-2 Schematic of pre-cast pile with grout delivery systems and membrane.

4.2.2 Construction of 8-inch Square × 8-ft. Long Jet-Grouted Piles

Formworks for casting piles were assembled using plywood sheets and were coated with a chemical to ensure the forms would easily release from the cured concrete. Figure 4-3 shows the formworks made for casting piles. The steel rebar cages were formed according to the design discussed earlier. Grout delivery systems were assembled using 1-inch PVC pipes and gum rubber as shown in Figure 4-4. Steel pipes, 1-inch in diameter and 1 ft. long, were attached to the top of each PVC pipe in the grout delivery system. The rebar cage, jetting pipe, and grouting systems were then positioned in the formwork according to the design as shown in Figure 4-5. The top of each grouting pipe and jetting pipe were extended outside the piles and to be used later to attach fittings and hoses during jetting and grouting. The concrete mix used for the piles was designed for a specified compressive strength of 4000 psi at 28 days using the absolute volume method. A summary of the mix ingredients for the concrete follows.

Figure 4-3 Formwork for casting piles.

Figure 4-4 Grout delivery pipes.

Figure 4-5 Rebar cage, jetting pipe, and grouting systems positioned in the formwork.

The mix used for the one cubic yard of concrete consisted of water (280 lb), cement (685 lb), coarse aggregate (1735 lb), and fine aggregate (1135 lb). The piles were cast in the formwork (see Figure 4-6) and covered with plastic to protect them from weather during the curing process. Concrete cylinders were also cast in order to monitor the strength of the concrete while curing.

Figure 4-6 Piles with formwork (after pouring concrete).

4.2.3 Preparation of 8-inch Square × 8-ft. Long Piles for Testing

Water under pressure was flushed through the grout system of each 8-inch × 8-inch × 8 ft. pile to ensure that the grout systems (i.e., top and bottom) were working properly. After that, semi-rigid membranes were attached to the upper and lower portions of each pile as shown in Figure 4-7. The membrane prevented the flow of grout along the weakest path during side grouting and helped radial expansion of the grout zones during grouting, which resulted in high radial soil stress around the pile. In addition, no mixing occurred between grout and soil, ensuring proper bonding between the grout bulb and the side of the pile.

Rubber nozzles (see Figure 4-8) were next attached to the bottom of each jet pipe to reduce the cross sectional area of the pipe for proper jetting and grouting processes.

Figure 4-7 Attachment of semi-rigid membrane to pile.

Figure 4-8 Rubber nozzle used for jetting and tip grouting.

4.2.4 Filling the Test Chamber and Pressure Gage Placement

It was expected to have the task of filling the test chamber completed by December 2008. Unfortunately, load testing of a previous project delayed use of the test chamber. After load testing, the FDOT conducted pressure meter testing in the test chamber. Consequently, the existing pile and soil were removed from the test chamber only in the second week of February 2009. The soil was removed by use of a truck mounted auger. During this process, the steel frame supporting the stress gages near the chamber boundary was damaged. This also delayed progress of the project. Moreover, a new pipe system had to be installed for the new stress gage layout. This pipe system (Figure 4-9) protects the wiring of instrumentation during jetting/grouting, as well as soil removal after load testing. The stress gage wiring was routed to a small room near the test chamber for computer monitoring to avoid exposure to rain. Figure 4-10 shows the layout of the stress gages in the test chamber. The soil was placed through free fall from the top of the chamber using a Bobcat loader. The moisture content of the soil was in the range of 5 to 7%. The filling process is shown in Figure 4-11. In order to reduce the influence of chamber boundary, it was decided to conduct tests at a relative density (D_r) of around 40% (i.e., dry density of 101 pcf). Soil was placed in a 1.5-ft. lift and compacted using a vibratory plate compactor (see Figure 4-12).

While filling the test chamber, a number of hand cone penetrometer tests were also performed on each compacted soil layer. Cone tip resistances varied from 25 kg/cm^2 to 40 kg/cm^2 for all the lifts. Based on typical relationships of relative density with SPT N values (Figure 4-13), the N values ranged from 6 to 9. Using the CPT data, similar SPT N values (6 to 9) were found.

Figure 4-9 Pipe system for routing stress gage wiring to monitor facility.

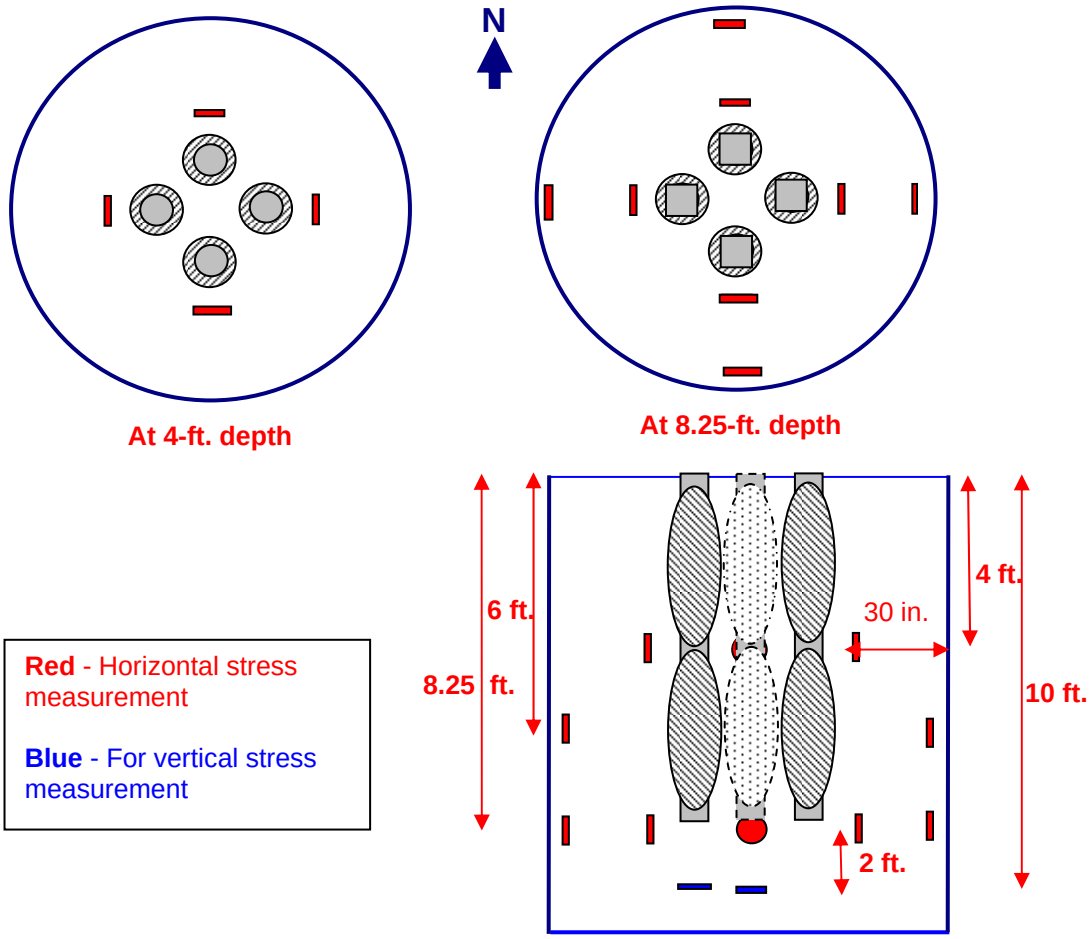

Figure 4-10 Stress gage layout.

Figure 4-11 Filling test chamber with loose silty sand.

Figure 4-12 Soil compaction using vibratory plate compactor.

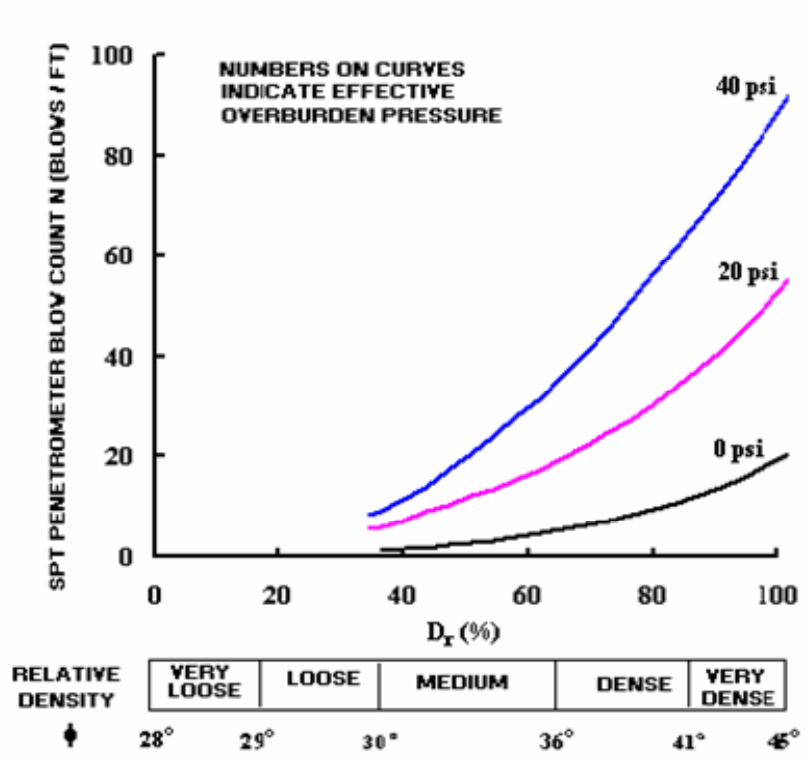

Figure 4-13 SPT *N* values versus relative density.

Once the chamber had been filled to a depth of 10 ft., two stress gages were placed horizontally as shown in Figure 4-14 to measure vertical stress. Again, soil was placed in layers and at a depth of 8-ft., and two sets of stress gages (as shown in Figure 4-10) were placed vertically to measure horizontal stress (see Figure 4-15). After placement of the stress gages at a depth of 8 ft., soil was added to the test chamber until the sand surface was 4 ft. from the top. Subsequently, four more stress gages were placed at 30 inches away from the chamber boundary. Figure 4-16 shows the test chamber after filling was completed.

Figure 4-14 Stress gages placed horizontally at 10-ft. depth.

Figure 4-15 Stress gages placed vertically at 8-ft. depth.

Figure 4-16 Test chamber in fully filled state.

4.2.5 Jetting the Piles into Test Chamber and Side Grouting

Jetting of the piles into the test chamber was done one-by-one at a time interval of 24 hours. The one-day time break between each jetting process was needed to allow water to percolate to a greater depth, and thus, to eliminate the quick condition created in the chamber due to the previous jetting. Pile jetting began by positioning a pile over the test chamber with the help of a forklift. Figure 4-17 shows a test pile prior to jetting. Then, a 2-inch flexible hose connected to the city water supply at a constant pressure of 60 psi, was attached to the top of the pile. Jetting initiated with the flow of water from the city water supply to the test

Figure 4-17 Pile prior to jetting.

pile (see Figure 4-18), and subsequently, the test pile was lowered with the forklift as penetration occurred. After approximately 4 to 5 minutes of jetting, the test pile had penetrated up to the required depth. Then, water that had accumulated at the top of chamber was pumped out. Shown in Figure 4-19 is the test chamber with piles after the jetting of all four of the piles. From the stress gage data collected before, during, and after jetting, it was found that there was no considerable change in the soil stresses in the test chamber due to the jetting process. Since the water was percolating slowly, the water level in the test chamber was continuously monitored and pumped out. A sufficient time gap (around 10 days) was given between jetting and grouting to ensure that the water level in the chamber was at significant depth before grouting was started.

Figure 4-18 Pile during jetting.

Figure 4-19. Piles jetted into the ground.

Grouting of piles commenced with the top membrane of the south pile. The grout mix consisted of cement, 10% micro-fine fly ash, and water at a water/cement ratio of 0.45. The grout was mixed in the mortar mixer shown in Figure 4-20. Then, the grout was transferred manually to the holding tank of the grout pump shown in Figure 4-21. The grout was then pumped from the holding tank through a 1.5-inch high pressure line to the pile (Figure 4-22). There were two pressure gages at the pile head to measure both the inlet and outlet grout pressures. After placement of approximately 15 gallons of grout at an inlet and exit pressure of approximately 60 psi, grout began to flow upward through the ground surface near the pile (Figure 4-23). This is probably due to the tearing of the membrane near the top pleating, and it was decided to stop grouting the bag. The grout delivery lines were flushed with water and plans were made to regrout the bag later.

Figure 4-20 Grout mixing using mortar mixer.

Figure 4-21 Grout pump with holding tank.

Figure 4-22 The 1.5-inch high pressure line connected from the grout pump to the pile.

Figure 4-23 Upward grout flow through the ground surface near the pile.

Grouting of the top membrane of the diagonally opposite pile (north pile) began on the same day afternoon. As in the case of the south pile, grout started to flow up to the ground surface at a grout volume of approximately 15 gallons and pressure of 60 psi. The grout delivery lines were flushed with water, and it was decided to regrout the membrane later. The next day, grouting of the other two membranes was carried out. Like the first two membranes, the grout came to the ground surface at a pressure of about 50-60 psi and a volume of around 14-15 gallons. The grout delivery lines were cleaned in preparation for regrouting the membranes following grouting of the bottom membranes.

Next, the bottom membrane of the south pile was grouted with 25 gallons of mixed grout. The maximum recorded grout pressure was 140 psi on the pump and 120 psi on the return line from the pile. After lunch, the process was repeated for the bottom membrane of the north pile. Again, 25 gallons of grout was mixed and pumped into the semi-rigid membrane. Grout pressures on the order of 140 psi were observed at the pump and 100 psi on the return line from the pile. The next day, 25 gallons of grout were pumped to the remaining two bottom membranes. The maximum recorded grout pressure was 150 psi on the pump and 120 psi on the return line for the west pile, while 145 psi was recorded on the pump and 130 psi on the return line for the east pile. No grout was observed coming up through the ground or at the bottom of the jet tubes.

After finishing the grouting of the bottom membrane, regrouting of the top membranes was done. The final grout volume in each of the top membranes was about 23 to 24 gallons. The maximum grout pressure observed during the regrouting of all the top membranes was in the range of 80 to 100 psi.

4.2.6 Top Down Testing of Side Grouted Pile

In order to separately determine the distribution of skin and tip resistance of jet-grout pile groups, it was decided to conduct two top down tests: one after side grouting to assess skin resistance; and another after tip grouting to find out total axial capacity. Tip resistance could then be estimated by deducting skin resistance from the total capacity.

Accordingly, after waiting approximately three weeks following side grouting of the test piles, the load frame for the vertical top down testing was set up (Figure 4-24). The test setup consisted of spacer tubes on each pile to cover grout pipe for tip grouting, load cells of 200-kip capacity on each pile to measure load distribution, a test frame, a hydraulic jack, another load cell of 600-kip capacity to measure total load, a reaction beam with a support system, and the displacement monitoring instrumentation. Vertical displacement of individual piles during the load test was monitored by four digital levels (Figure 4-25) borrowed from LOADTEST of Gainesville, Florida. Shown in Figure 4-26 is an example of the barcode strips positioned on each pile for vertical displacement monitoring. Soil deformation was measured using three 0.0001 digital dial gages (Figure 4-27) placed in a row; one at the center of the chamber, one at 29 inches from center and the third one at 6 inches from the chamber boundary. In June 2009, load testing of the side grouted pile group was performed with the help of personnel from the LOADTEST group. LOADTEST personnel were kind enough to be present at the test site to monitor the pile displacement despite their busy schedule. The top down test was performed in seven load steps with a five-minute interval between increments, followed by an unloading phase. Since the test was intended to estimate skin resistance of the jet-grouted pile group, loading ceased when a displacement of about 0.15 inch was observed at the top of the pile group.

Figure 4-24 Vertical top down test setup.

Figure 4-25 Digital levels for pile displacement monitoring.

Figure 4-26 Example of barcode strips positioned on each pile for displacement monitoring.

Figure 4-27 Digital dial gages for soil deformation monitoring.

4.2.7 Tip Grouting of Piles

After the completion of the top down test on the side grouted pile group, it was decided to grout the tip of each pile individually. Tip grouting started with the south pile. Grout mix design was the same as that for side grouting. Displacements of each pile and soil deformation (at the center of the pile group) were measured using digital dial gages as shown in Figure 4-28. Grouting of the pile was stopped when the top of the pile and surrounding soil started to move upward significantly. The maximum grout pressure observed was 220 psi at a grout volume of 21 gallons (refer to Table 4-1).

When tip grouting of the west pile began on the following morning, the grout pressure was immediately increased to more than 600 psi and no grout was pumped to the pile. Initially, it was thought that this might be due to blockage in the hose that carries the grout

Figure 4-28 Tip grouting of pile.

Table 4-1 Tip Grouting Data

Pile	**Maximum Grout Pressure** (psi)	**Grout Volume** (gal)
South	220	21
North	250	17
East	260	19
West	240	21

from the holding tank to the pile. An examination of the hose revealed there was no blockage inside the hose. Subsequently, grouting was attempted on the north pile, but the result was the same as the west pile. Based on the initial results from the north and west piles, it was realized that the soil around the piles had become densified as well as possibly plugging the grout pipe outlets. It was decided to jet water through the grout pipe to create a cavity below the pile tips prior to the grouting process. It was also decided to increase the water-cement ratio of grout mix from 0.45 to 0.50. Accordingly, the tip grouting of the north, east, and west piles were carried out successfully using the new grout mix after creating a small cavity below the pile tip prior to grouting. Tip grouting data of each pile is shown in Table 4-1.

4.2.8 Top Down Testing after Tip Grouting

After waiting approximately three weeks following the tip grouting of the test piles, top down testing was performed to assess the increase in total axial capacity of the group as a result of tip grouting. As identified in Section 4.2.7, top down testing of the group had been carried out after side grouting of the piles to assess the skin resistance of the group. Shown in Figure 4-29 is the test setup for the vertical top down testing. The setup included 200-kip capacity load cells placed on each pile to measure individual load distribution, a

Figure 4-29 Vertical top down test setup.

simply supported test frame, hydraulic jack, another load cell of 600-kip capacity to measure total load, a reaction beam with support system, and displacement monitoring instrumentations. Vertical displacements of each individual piles during the load test were monitored by four digital levels lent by LOADTEST, Gainesville, Florida. Soil deformation was measured using four 0.0001 digital dial gages (see Figure 4-30) placed in a row; one at the center of the chamber, a second one at 20 inches from center, a third one at 40 inches from center and the fourth one at 6 inches from the chamber boundary. The top down test was performed in 13 load steps (20-kip load increments for the first 12 load steps and 10 kips for the last load step) with a five-minute wait time between load increments, followed by an unloading phase. The test continued until a displacement of about 2 inches was observed at the top of the pile group.

Figure 4-30 Digital dial gages for soil deformation monitoring.

4.2.9 Excavation of 8-inch × 8-inch × 8-ft. Jet-Grouted Pile Group

After completion of the top down load testing of the pile group, excavation of the test chamber was initiated to study the jet/grout pile group. Piles were excavated manually to ensure no breakage and accurate membrane perimeter measurements. Shown in Figure 4-31 is the hand excavation of the top of the pile group. A mini excavator (Figure 4-32) was used to remove the rest of the soil from the test chamber.

Figure 4-31 Hand excavation of the top of the pile group.

Figure 4-32 Mini excavator.

Figure 4-33 shows the exposed pile group in the chamber and Figure 4-34 shows the lifting of the whole pile group using fork lift. It took about one week to excavate the pile group from the test chamber. Shown in Figure 4-35 is the pile group set near the test chamber for examining both the side and tip grout bulbs. Each pile in the group appears to possess good quality grout zones, the diameter of the upper side grout bulb varied from 11 to 19 inches along the pile, and the diameter of the lower side grout bulb varied from 12 to 18 inches along the pile. In Figure 4-36, which shows one of the tip grouted bulbs, it can be seen that the bulb is nearly symmetric with a diameter in the range of 15 to 19 inches.

Figure 4-33 Exposed pile group.

Figure 4-34 Lifting of the pile group using fork lift.

Figure 4-35 Pile group resting on ground.

Figure 4-36 Views of a grout bulb.

Shown in Figure 4-37 are piles in the test prior to their removal. Evident from the picture, there was some overlapping of tip grout bulbs, i.e., some part of a bulb occupying space above another one, but without physical contact. This was attributed to the grouting sequence and the fact that the tip grouting of the piles was not done simultaneously. During tip grouting of a pile, grout flowed in radial directions from the tip. But existing grout bulbs (if any) of adjacent piles exerted resistance to lateral flow of the grout, and hence, the fresh grout was displaced to the zone above an existing bulb.

Figure 4-37 Overlapping of tip bulbs.

4.2.10 Measured Soil Stresses in the Vicinity of the Group

Variation of soil stresses in the vicinity of the pile group was measured using the stress gages placed within the test chamber (Figure 4-10). Figures 4-38 through 4-42 show the variation of stress observed at different locations during the various stages of the research, i.e., grouting and load testing. It can be seen from the figure that stresses around the pile increase during grouting and decrease immediately after grouting due to unloading. The side resistance of a single pile/group depended on the residual stress state around the pile/group. Stress variation during load testing is discussed in detail in the next section.

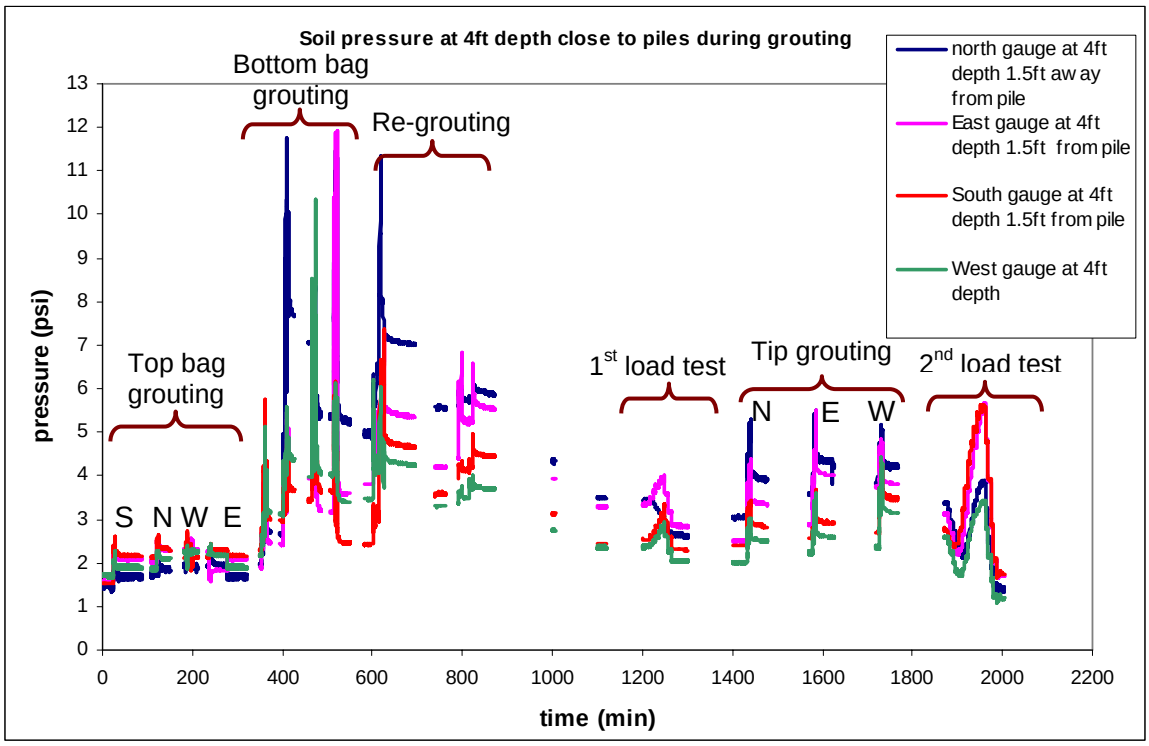

Figure 4-38 Variation of horizontal stress at 4-ft. depth close to pile.

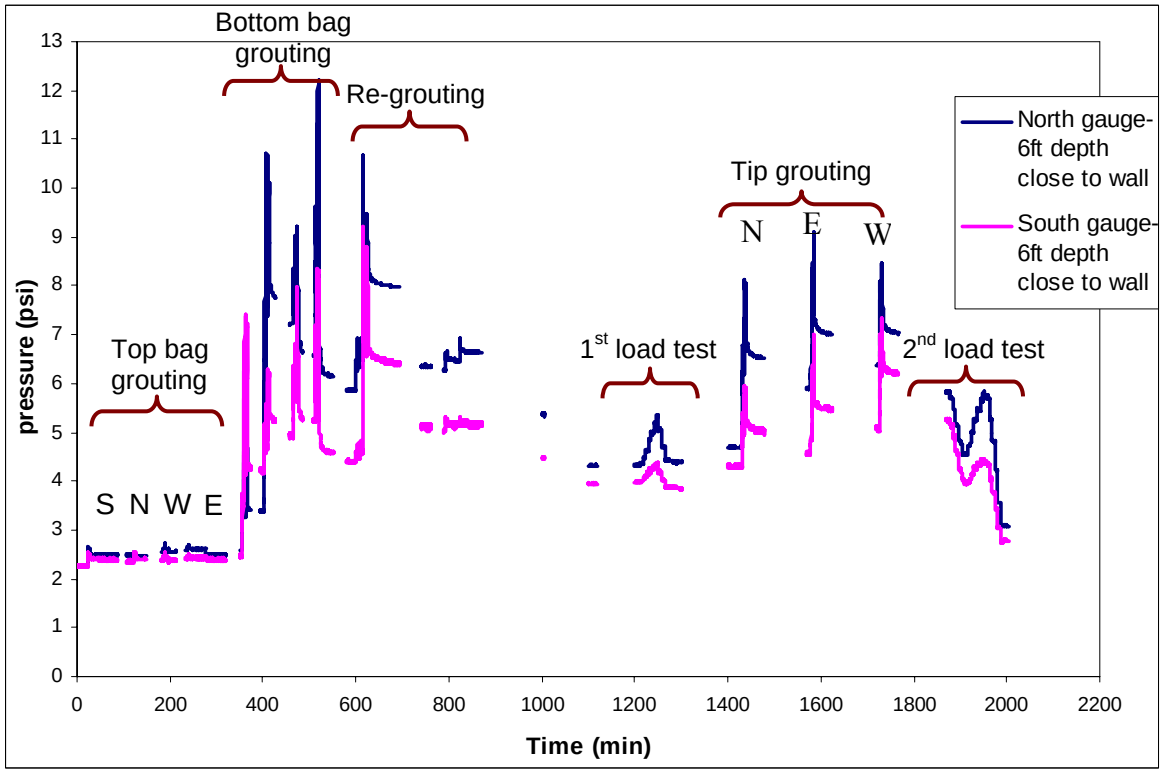

Figure 4-39 Variation of horizontal stress at 6-ft. depth close to chamber boundary.

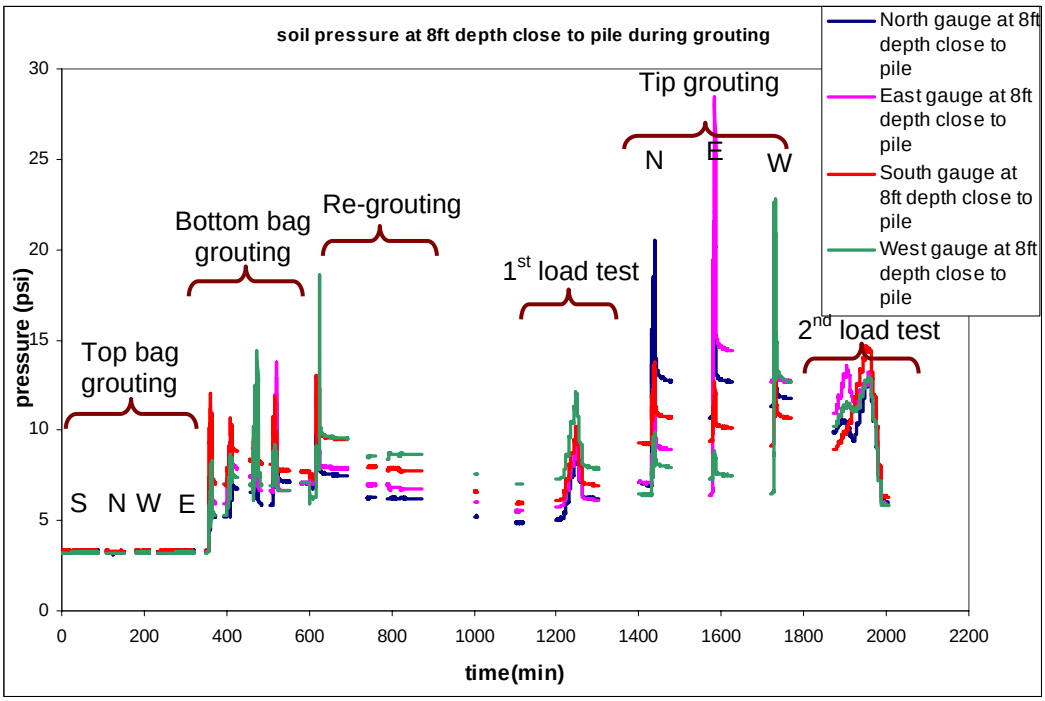

Figure 4-40 Variation of horizontal stress at 8-ft. depth close to pile.

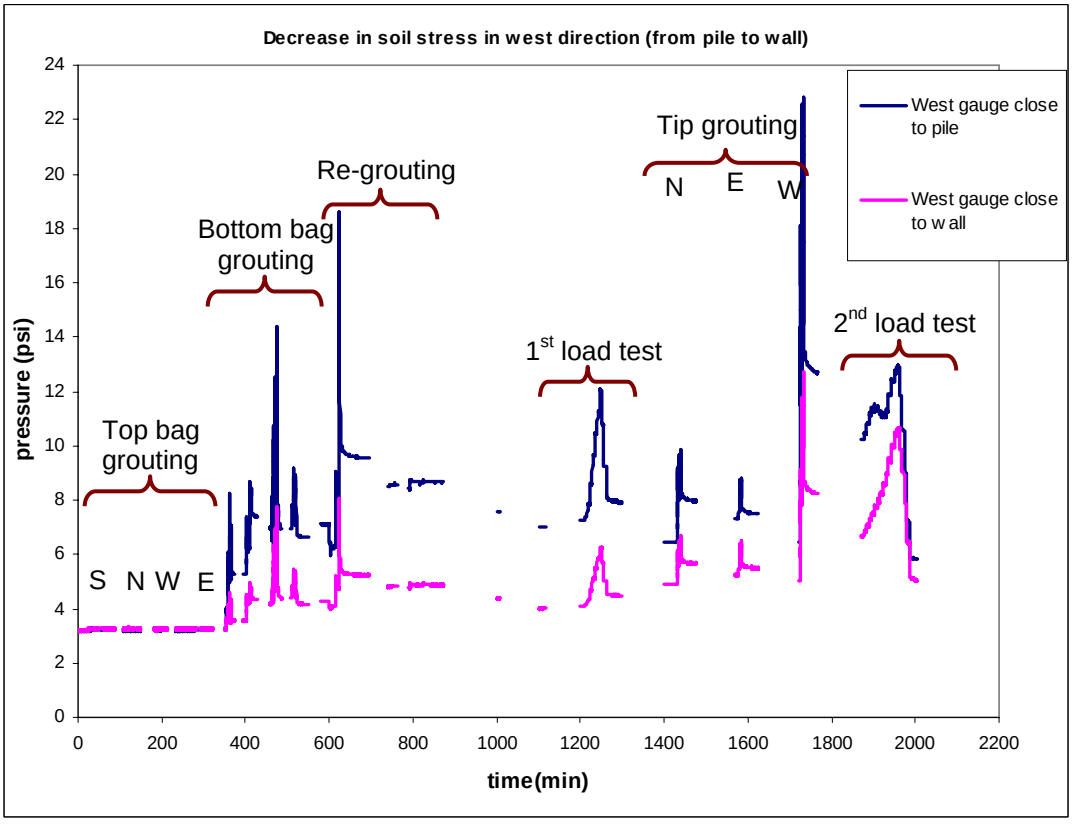

Figure 4-41 Comparison of horizontal stress variation–close to pile and away from pile at 8 ft.

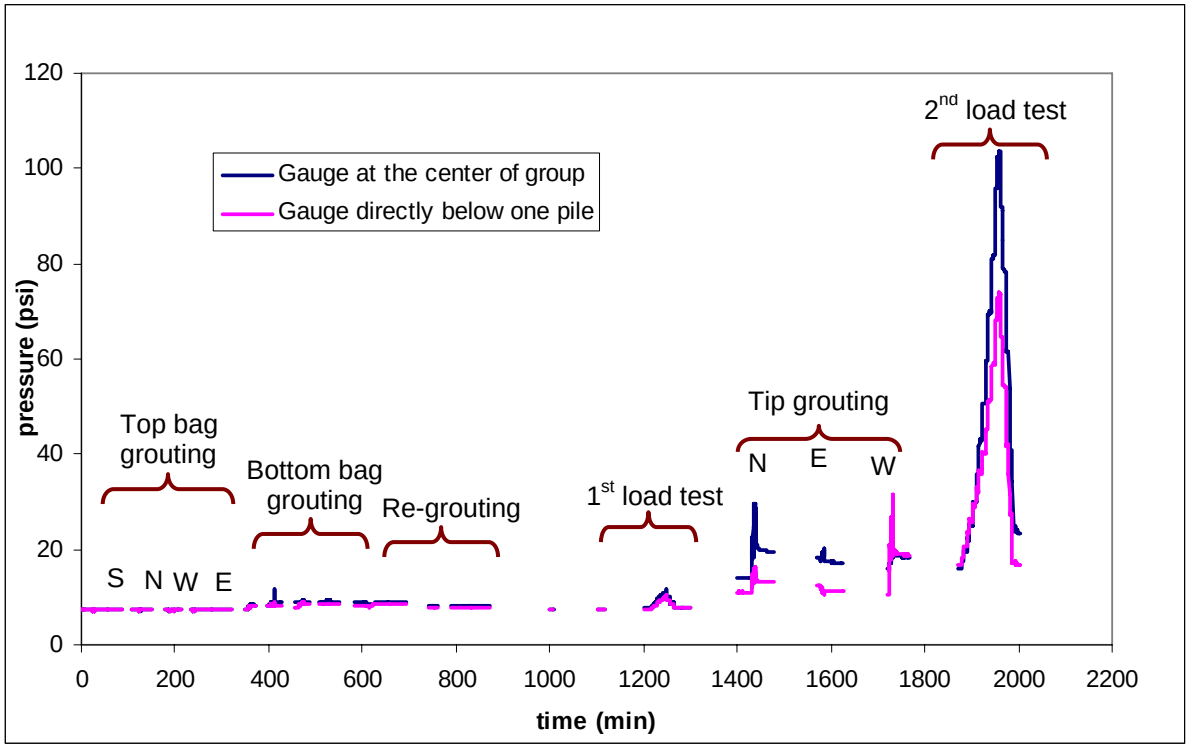

Figure 4-42 Variation of vertical stress at 10-ft. depth.

4.2.11 Analysis of Experimental Jet-Grout Group Behavior

This section analyzes the results obtained from the experimental study of the 8-inch × 8-inch × 8-ft. jet-grouted pile group and discusses the group behavior of the piles. Shown in Figure 4-43 is the load versus vertical displacement at the top of each pile. Evident was the non uniform distribution of applied load; the south pile had the smallest resistance, whereas the east pile carried the highest load. Interestingly, the vertical displacements of piles were relatively uniform irrespective of the difference in load distribution. This suggests that load is being transferred (i.e., shear stress) among piles and that the group behaves as a block during loading. It can be seen from Figure 4-44 that the average displacement at the pile heads and the soil within the boundary of the pile group is the same. Also shown in Figure 4-45 is the soil deformation profile at various applied loads. Note, the quadratic variation of soil deformation from the periphery of the pile group towards the chamber boundary

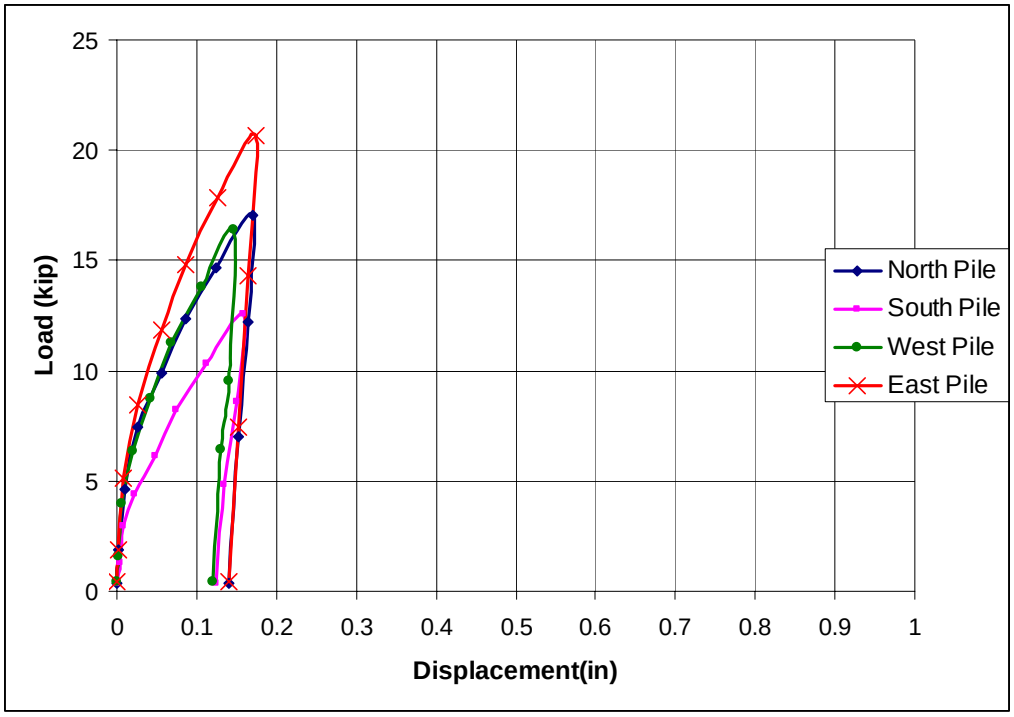

Figure 4-43 Load versus displacement of piles.

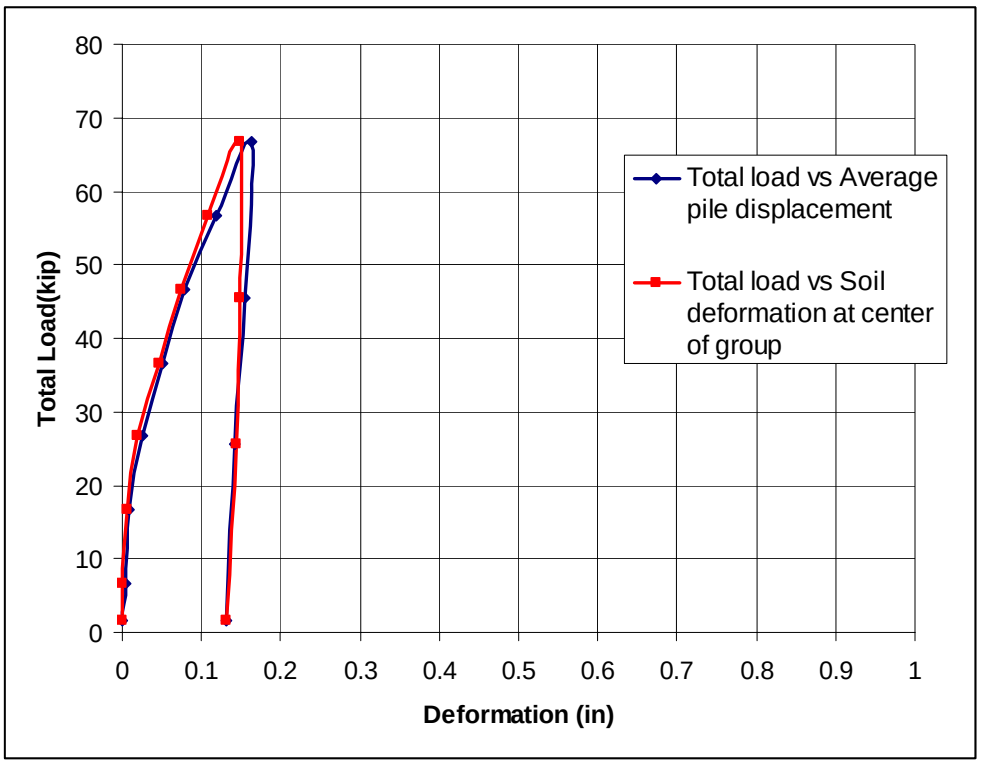

Figure 4-44 Total load versus average displacement of pile group and soil deformation.

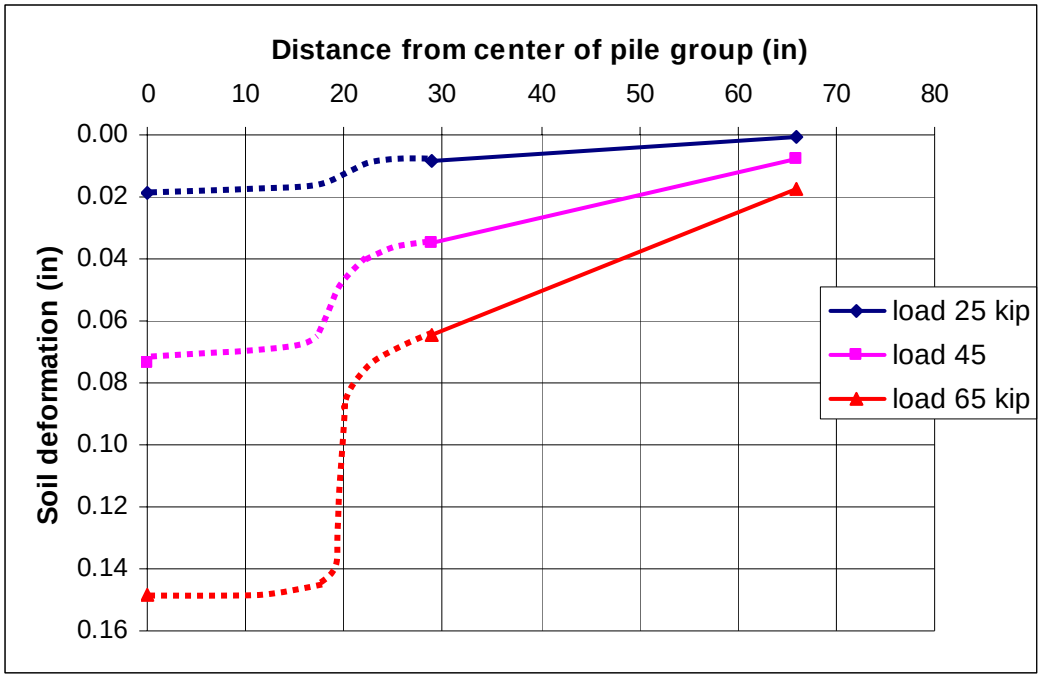

Figure 4-45 Soil deformation profile.

(dotted lines in Figure 4-45 are the approximation of soil deformation based on pile displacements and soil deformation at the center of the group).

Figure 4-46 shows DeBeer's log-log plot of total load versus average displacement of the pile group. It can be seen in the plot that there is no change in slope of the curve, which demonstrates that skin resistance may not have been fully mobilized. Moreover, it can be seen from the Figure 4-42 that the stress gages below the pile group show little increase in vertical stress during the first load test, and suggest that the entire applied load was carried by skin resistance. Hence, it can be concluded that skin resistance of the pile group was at least 65 kips.

Side resistance of the 8-inch standard driven pile group and the 8-inch diameter drilled shaft group were determined using FDOT's FB-Deep software to compare with that of jet-grouted piles in similar soil conditions. Using an SPT value of $N = 6$, the software gave skin resistance for a driven group as 23 kips and in the case of a drilled shaft group of 19.5 kips.

Comparison with the jet-grouted pile group suggests an increase of side friction by a factor of 2.8 for driven piles and a factor of 3.3 for drilled shafts.

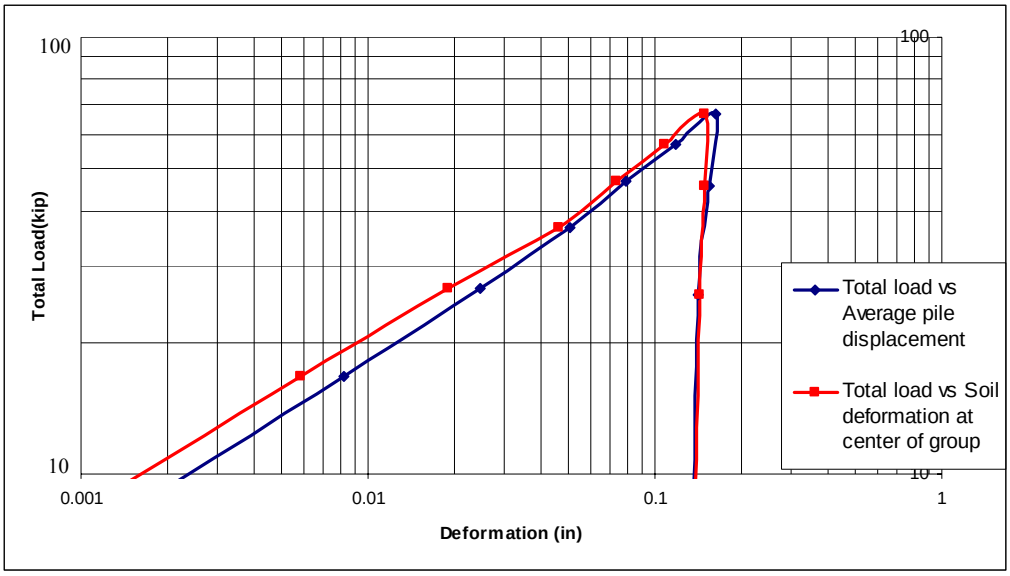

Figure 4-46 Log-log plot of total load versus average displacement (DeBeer's method).

Shown in Figure 4-47 is the individual load versus vertical pile displacements from top down group testing after tip grouting. Evident from the shape of the curves, significant end bearing is mobilized for the group response. Also, since displacements of piles are relatively uniform during loading, block behavior of the pile group for both side and tip of the group is suggested. Further justification is suggested from Figure 4-48 which shows that the average displacement of the pile group was almost the same as the soil deformation at the center of the group. Shown in Figure 4-49 is the soil deformation profile at various loads, which displayed a quadratic variation of soil deformation from the boundary of pile group towards the chamber wall similar to the observation during side shear mobilization.

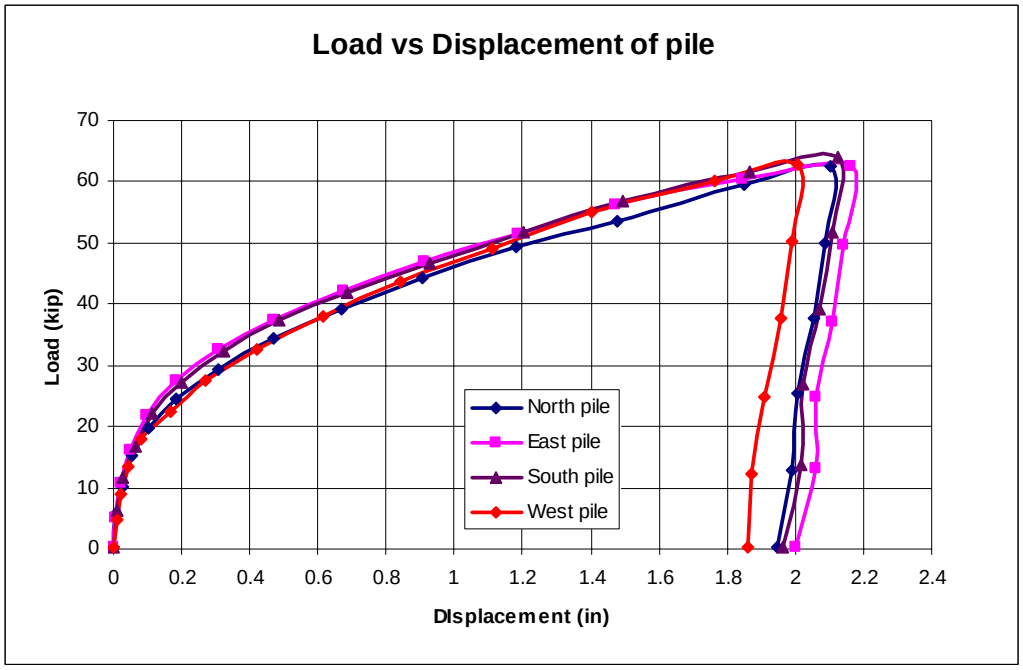

Figure 4-47 Load versus vertical displacement of piles.

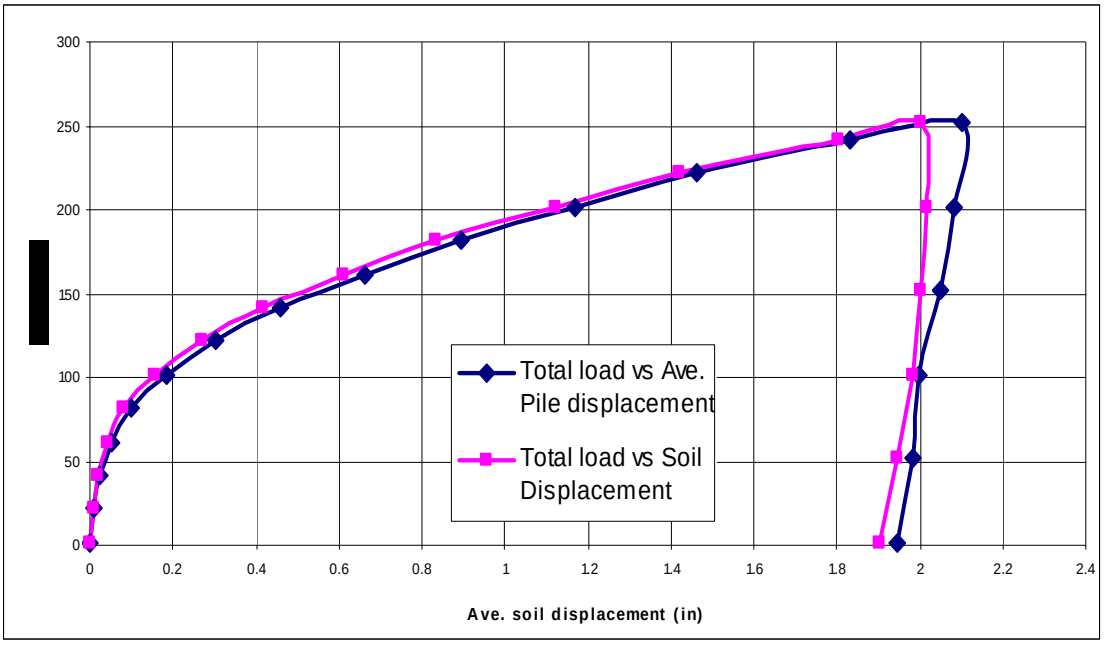

Figure 4-48 Total load versus average displacement of pile group and soil deformation.

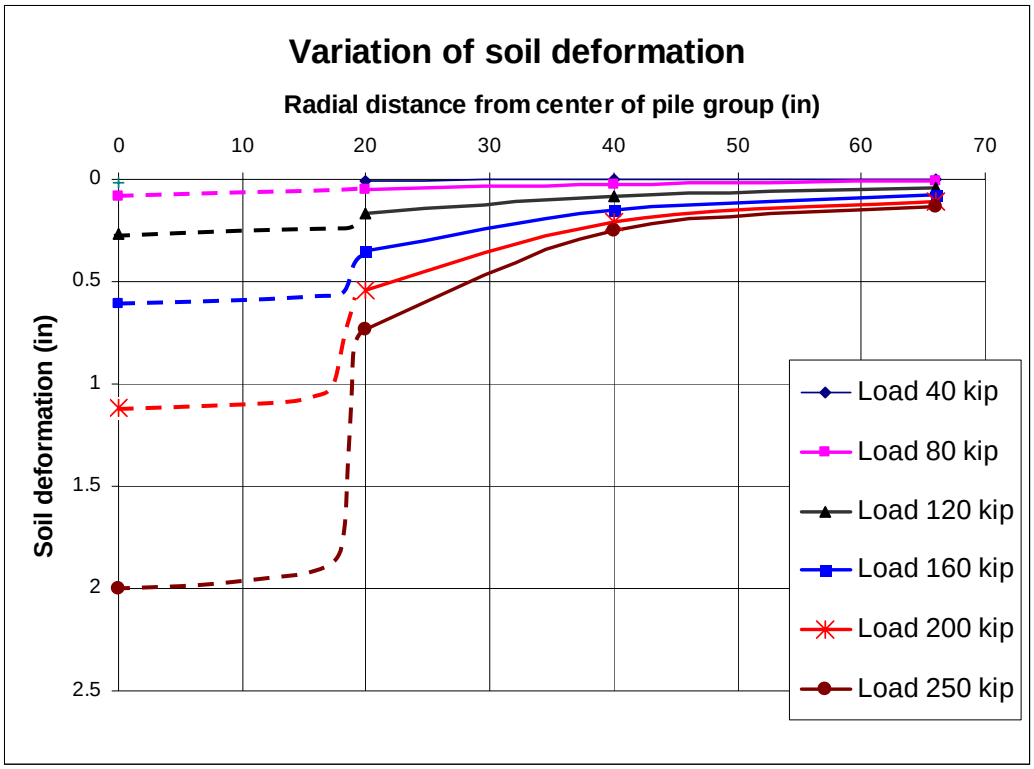

Figure 4-49 Soil deformation profile.

Horizontal stress measurement in the test chamber during the axial load test (Figures 4-50 and 4-51) indicated that the lateral stress decreased with an increasing axial load until the full mobilization of skin resistance (5 load steps), and then, increased with an increase in applied load. During the unloading phase (Figure 4-50 and 4-51), the lateral stress always decreased. It is believed that the decrease in lateral stress during skin resistance mobilization was due to the rotation of the origin of planes or pole such that the failure plane aligns in the vertical direction (FDOT BD 545-31).

Shown in Figure 4-52 is the variation of vertical stress at depth of 10 ft. during top down testing at the center of the group and below the west pile. Of interest is the increase in stress at the center of the pile group versus the edge supporting superposition of stresses and elastic theory.

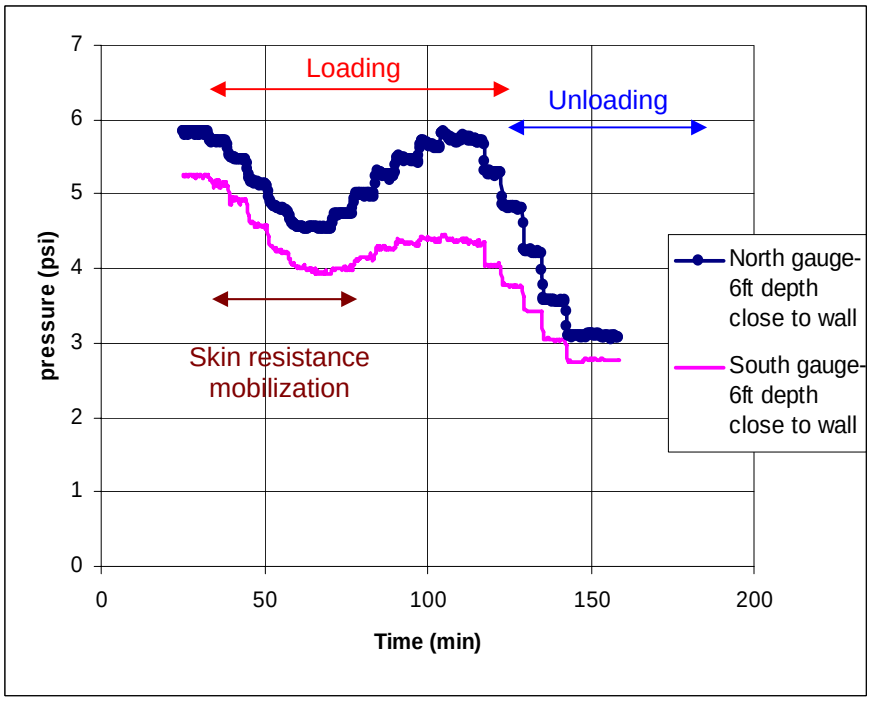

Figure 4-50 Variation of lateral stress during load test at 6-ft. depth, 6 inches off from the boundary.

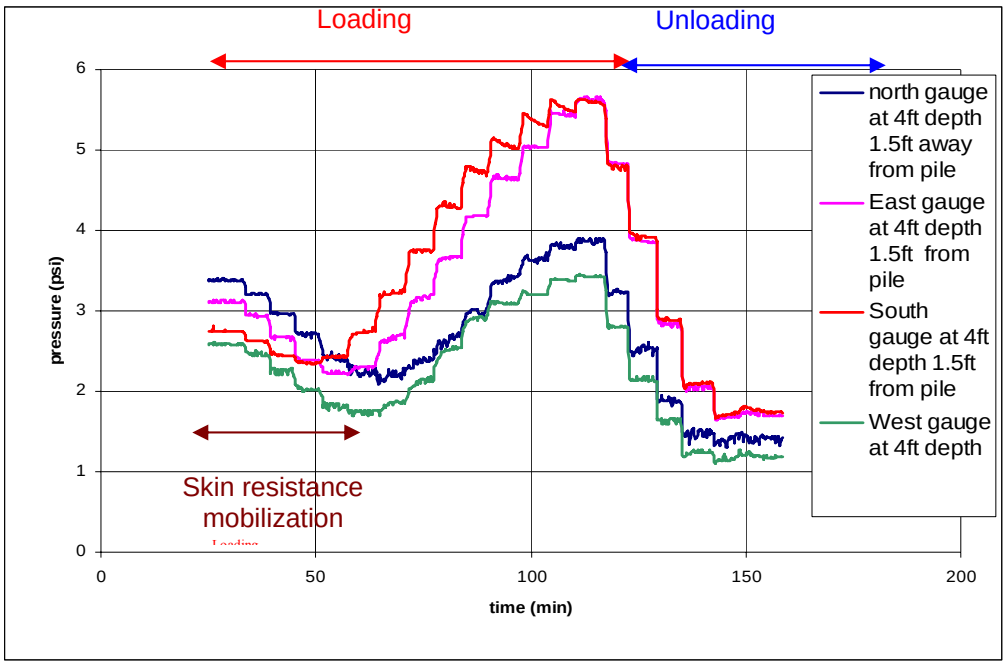

Figure 4-51 Variation of lateral stress during load test at 4-ft. depth, 24 inches away from center of pile.

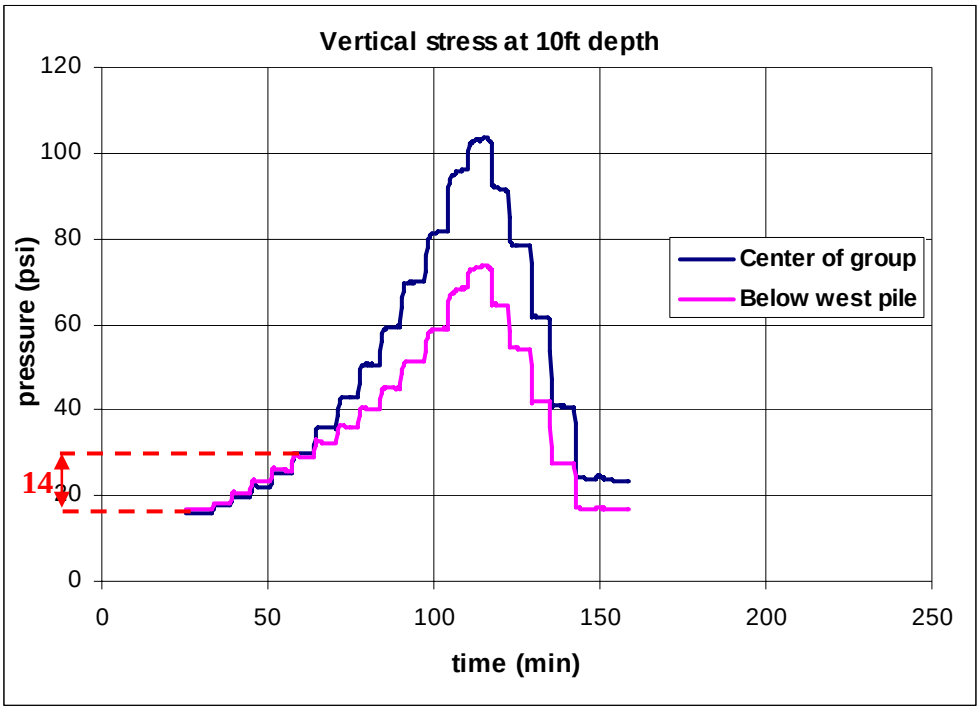

Figure 4-52 Vertical stress gage data at 10-ft. depth during top down testing.

As shown in Figures 4-50 and 4-51, the skin resistance of the pile group was fully mobilized when five equal load steps were applied to the group head (i.e., at a total axial load of about 100 kips, Figure 4-49). The corresponding increase in vertical stress at a depth of 10 ft. (center of the group) was 14 psi (Figure 4-52). Assuming a uniform stress distribution at the group base, as shown in Figure 4-53, the vertical stress at the base of the group may be back calculated from the vertical stress at the 10-ft. depth using Boussinesq's theory (15 psi). For the applied top load of 100 kips, the tip force may be calculated from Boussinesq stress (15 psi) times block area of group equal to 25 kips (the vertical stress at base × the effective base area = 15 psi × 1600 in^2/1000 = 25 kips). Hence, skin resistance of the pile group would be equal to 75 kips (100 kips – 25 kips = 75 kips), which is the measured value indicated in Table 4-2.

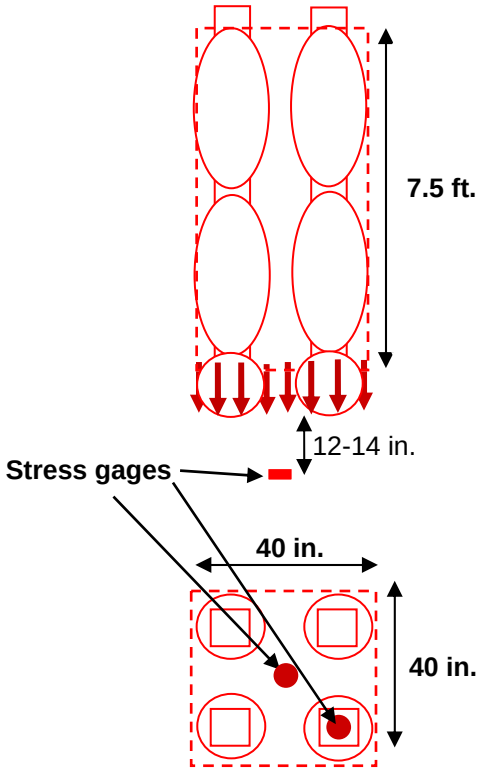

Figure 4-53 Effective area of block.

Table 4-2 Measured and Predicted Skin Resistance of a Single Pile and the Pile Group

	Pile Group (kips)	**Single Pile** (kips)
Using tip grout data	70	22
McVay's equation	76.6	24
Measured (Total – Tip)	75	

Since the piles act as a block during loading, total side resistance of the group can be estimated by multiplying the unit skin friction with the surface area of block. Unit skin resistance of single jet-grouted pile may be estimated using the equations proposed by McVay et al. (FDOT project BD 545 RPWO #31 2009) as follows:

$$f_s = \sigma_{vg}\left[\frac{\sin\phi_c}{(1-\sin\phi_c)}\right]\sin(90-\phi_c) \qquad (4.2)$$

where $\sigma'_{vg} = K_g.\,\gamma'.h$ and K_g from the chart shown Figure 4-54.

The piles were embedded approximately 8.5 ft. in the ground with an average at-rest vertical stress of 935 psf (γ: 110 pcf × 8.5 ft.) at the bottom of the pile. Grout vertical stress coefficient, K_g, of 1.7 was obtained for a depth of 8.5 ft. and a critical state failure angle of ϕ_c ~ 31° from Figure 4-54. Multiplying the at-rest vertical effective stress σ'_{vo} = 935 psf by K_g gave σ'_{vg} = 1590 psf, and then, f_s of 1447 psf (1.447 ksf) was estimated from Equation 4.2. If a linear variation of unit skin friction is assumed along the pile, an average unit skin friction along the pile would be equal to 0.766 ksf. Then, side resistance of a block may be computed as f_s (0.766 ksf) × surface area of block (100 ft^2) = 76.6 kips (Table 4-2). Similarly, skin resistance of an individual pile may be estimated as f_s (0.766 ksf) × the surface area of the pile (31.41 ft^2) = 24 kips (Table 4-2).

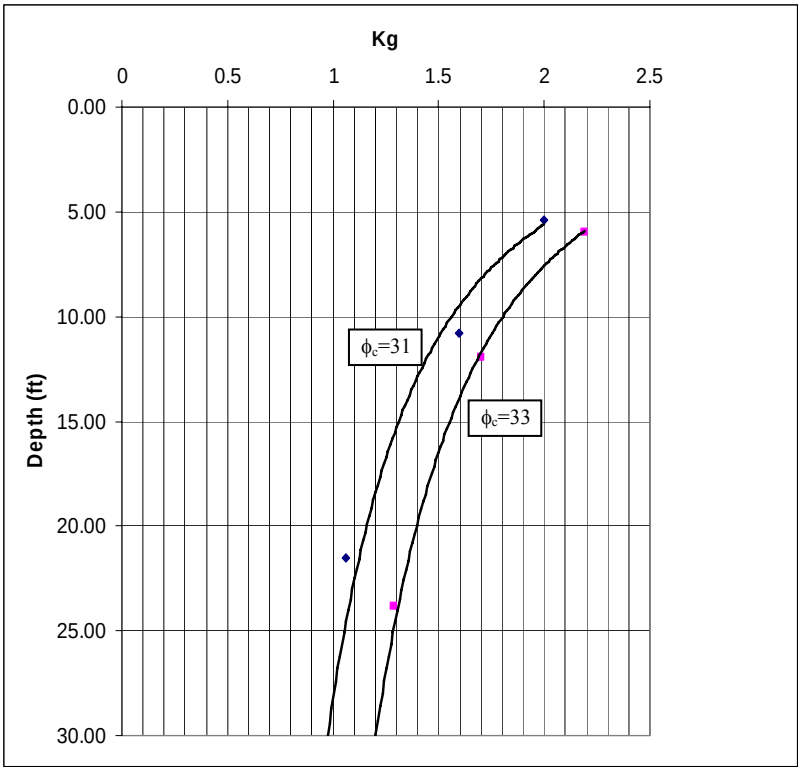

Figure 4-54 Grout vertical stress coefficient, K_g.

Tip grouting data can also be used to estimate skin resistance of individual piles. The ultimate axial skin friction of a pile should be equal to the tip grout pressure of 180-220 psi

times an effective tip area. An effective area is assumed as the area of circle (100.5 in^2) with diameter equal to diagonal distance (11.3 inches) of pre-cast pile. Consequently, skin resistance of a pile can be estimated as 18 to 22 kips (180 to 220 psi × 100.5 in^2 = 18 kips to 22 kips), which is comparable with the value obtained using McVay's equation (Equation 4.2). The unit skin resistance of pile can then be determined as 0.7 ksf [22 kips/surface area of side grouted pile (π × (16/12) ft. × effective length (7.5 ft) = 31.41 ft^2) = 0.7 ksf] and the side resistance of the block would be 70 kips (0.7 × effective surface area of block (100 ft^2), Figure 4-51).

Table 4-2 shows the measured and predicted skin resistances of a single pile and the pile group. It can be seen that the group shear resistance is less than the sum of individual pile resistances, which is attributed to the reduced block area of the group versus the sum of the individual pile surface areas.

Figure 4-55 depicts the comparison of group response before and after tip grouting. A higher initial slope of curve in load test 2 (grouped pile tips) versus test 1 (grouted pile sides only) is due to initial mobilization of the end bearing during the mobilization of skin resistance.

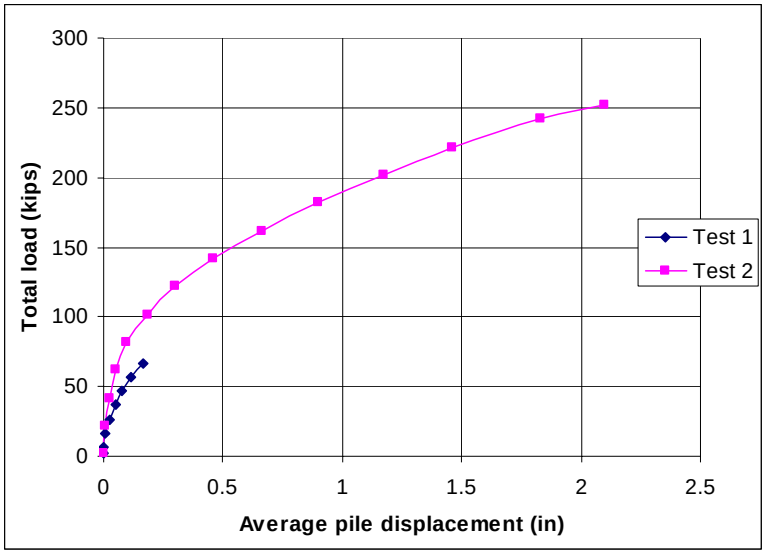

Figure 4-55 Comparison of load tests.

4.3 Testing of 4.5-inch Diameter × 8-ft. Long Jet-Grouted Pile (10-inch Ø side grout bulb) Group

4.3.1 Design and Construction of Pre-cast 4.5-inch Diameter × 8-ft. Long Jet-Grouted Piles

As mentioned in Section 4.1, four piles of 4.5-inch diameter by 8-ft. long (L/D ratio-21) composed the second group test for jet-grouted piles. The diameter of the side grout bulbs for each pile was limited to 10 inches to ensure 1D clear spacing between grout bulbs of adjacent piles as tested with the first group. Figure 4-56 shows a schematic of the cross section of a jet-grout pile system. The structural reinforced section of the pile was a 4.5-inch steel pipe with a 1/4-inch wall filled with concrete. One-inch steel pipes were used for both the grout delivery system and tip jetting system. Again, two separate grout delivery systems were designed for side grouting of the top and bottom half of the piles. The delivery systems were positioned outside the pile (welded to the outer surface of the pipe), since the space available inside the 4.5-inch steel pipe was not adequate to contain both the top and bottom side grout systems. Both the top and bottom grout systems had their own grout entry and exit pipes. Each of the grout pipes (entry and exit) had a pair of 3/8-inch holes drilled at multiple

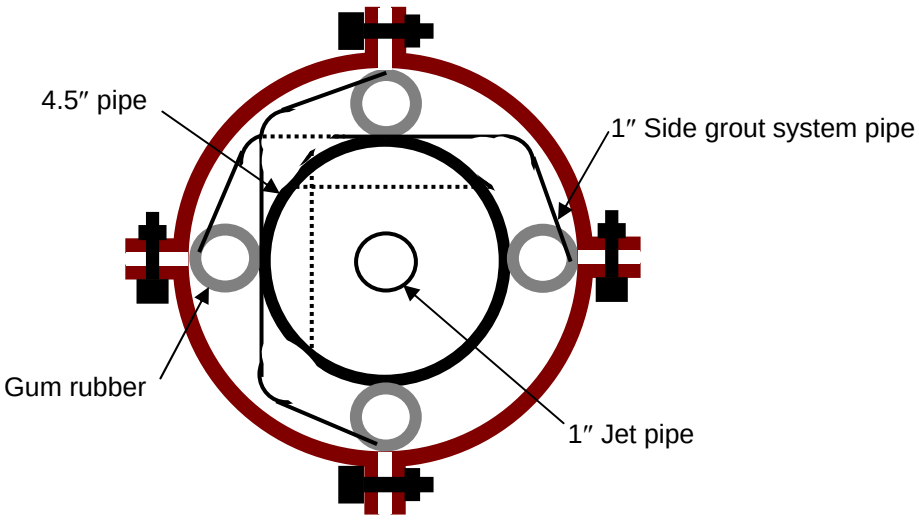

Figure 4-56 Cross section of pile with grouting/jetting system.

locations in the 1-inch pipes at 4-inch intervals along the bottom half of the grout system. A 1-inch diameter gum rubber (1/4-inch thick) membrane covered each pair of holes. The gum rubber membrane allowed the grout to exit the grout pipe under high pressure, but prevented the exit of water when cleaning the pipes.

Shown in Figure 4-57 is the side grout delivery system assembled for the 4.5-inch diameter jet-grouted pile, and in Figure 4-58 is the 4.5-inch steel pipe with side grout delivery systems, jet pipe, and steel ring for membrane attachment. After welding the grout pipe systems, jet pipe, and membrane holding system to the 4.5-inch steel pipe, concrete was placed within the annular space between the 4.5-inch steel pipe and jet pipe (Figure 4-59). Following sufficient time for curing of the concrete, water under pressure was flushed through each grout system to ensure that the grout systems (i.e., top and bottom) were working properly. Subsequently, the semi-rigid membranes were attached to the upper and lower portions of each pile as shown in Figure 4-60. The jetting nozzles (PVC caps with a number of holes as seen in Figure 4-61) were then attached to the bottom of each jet pipe to complete construction of each pile.

Figure 4-57 Side grout delivery system.

Figure 4-58 Pile with grout delivery systems.

Figure 4-59 Piles after pouring concrete.

Figure 4-60 Attachment of semi-rigid membrane to pile.

Figure 4-61 Nozzle jetting.

4.3.2 Filling the Test Chamber with Soil and Stress Gage Placement

The test chamber was filled with uniform silty sand at relative density between 40 and 45%, with a moisture content in the range of 7 to 9%. The soil was placed in 1.5-ft. lifts and compacted using multiple passes of vibratory plate compactor. Again, multiple levels of stress gages were placed in the compacted fill to measure both horizontal and vertical stresses. Figure 4-62 shows the layout of stress gages used for soil stress measurement during the installation and testing of the jet-grouted pile group. Four gages (Figure 4-62), were placed below the pile group to monitor vertical stress variations (two directly below the center of the pile group, one below the east pile and another one below the west pile) to measure individual pile and group behavior during top down loading. Four gages were placed beneath the pile group at a depth of 8.75 ft. (Figure 4-62) to measure horizontal stress measurement mainly during tip grouting. Other sets of gages were placed at depths of 6.25 ft. (corresponding to the middle of the bottom side bag) and 2.75 ft. (corresponding to the middle of the top side bag) as presented in Figure 4-62 to measure stresses during grouting

and load testing. In total, 16 stress gages were used in the test chamber for soil stress measurement.

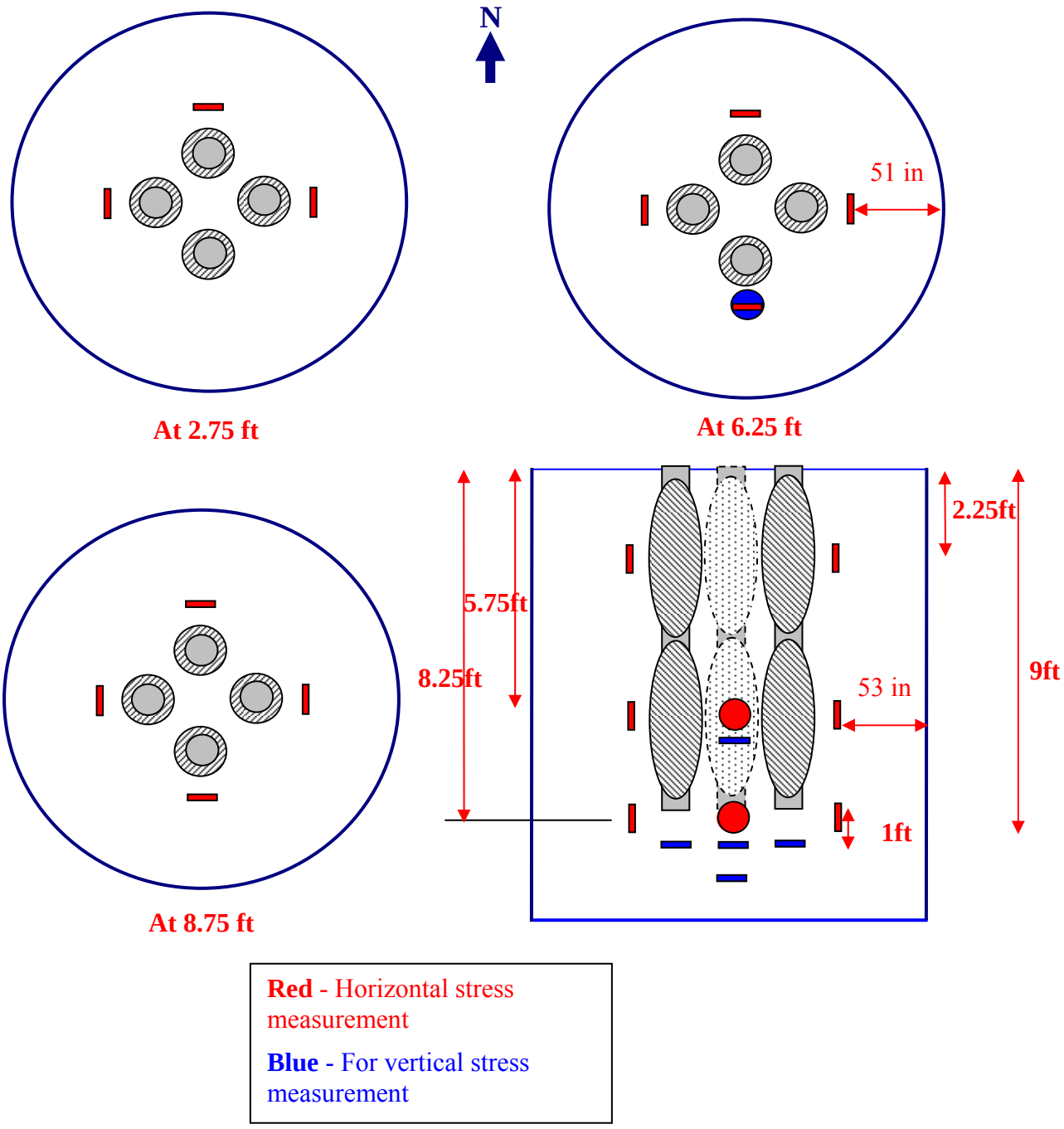

Figure 4-62 Stress gage layout.

4.3.3 Jetting the Piles into Test Chamber and Side Grouting

After filling the test chamber with the silty-sand, the piles were jetted into the test chamber one at a time. A sufficient time interval was used between pile jetting to allow water to migrate within the test chamber and eliminate the quick condition created near any pile due to previous jetting. Jetting was accomplished with a 2-inch hose connected to the city water supply (60 psi) and to the top swivel connector at the top of the jet grout pile (Figure 4-63). The pile, initially held up with a forklift, usually penetrated the soil under its own weight, but was guided to its final group position by hand. Approximately 4 to 5 minutes of jetting was required to install the 8-ft. pile to the required depth. Any water accumulated at the top of the chamber was pumped out. Figure 4-63 shows different stages of pile jetting. From the stress gages (Figure 4-62), data were collected before, during, and after jetting. It was found that there were only minimal changes in the soil stresses within the test chamber due to the jetting process.

Figure 4-63 Pile jetting.

After installation of all the piles and ensuring that the water level in the test chamber was at the planned location, side grouting of the piles was initiated. The grout mix consisted of cement, 10% micro-fine fly ash and water at a water/cement ratio of 0.45. About 11.5 gallons of grout which corresponds to the volume of grout needed to fill the annular space between the pile and the grout bag was pumped into each grout bag (Figure 4-64). During grouting of each pile's top membranes, radial cracks were observed in the ground surface; however, no grout was observed at the ground surface, suggesting no tearing of the membrane due to grout pressure. After sufficient curing of grout in the top membranes, grouting of the bottom side membranes was carried out. Similar to the top bags, approximately 11.5 gallons of grout was pumped into the bottom bags in agreement with the estimated volume to fill the annular space between the 4.5-inch pile and the grout bag. Maximum sustained grout pressure measured during the grouting of both the top and bottom bags are given in Table 4-3. The grouting started with the west pile, followed by the east, then south piles and ended with the north pile for both top and bottom grouting. As expected, the grout pressure increased with successive grouting at each elevation. The increase in grout pressure was due to both the densification and increase of soil stresses around the piles.

Table 4-3 Grout Pressure During Side Grouting

Pile	**Grout Pressure** (psi)	
	Top Bag	**Bottom Bag**
West	50	120
East	50	110
South	52	150
North	57	150

Figure 4-64 Side grouting.

4.3.4 Top Down Testing of Side Grouted Piles

As with the first group of jet-grouted piles, a top down test was performed on the side grouted piles (prior to tip grouting) to separate skin resistance of pile group from the total axial capacity.

Accordingly, after sufficient time for curing the side grouted test piles, the load frame for the vertical top down testing was set up. The test setup was similar to the previous group

test with the exception of the displacement of the piles and soil deformation being monitored using digital dial gages. Again, soil deformation at the center of group, group boundary, and outside the group boundary were monitored to investigate group effect. The top down test was performed in eleven load steps with a five-minute interval between increments, followed by an unloading phase with four load decrements. Since the test was intended to estimate skin resistance of the jet-grouted pile group, loading ceased when a displacement of approximately 1/4-inch was observed at the top of the pile group.

4.3.5 Tip Grouting of Piles

After the completion of the top down compression test of the group, tip grouting of each pile was carried out. The grout mix design was the same as that used for side grouting. Based on the first grout test (8-inch square pile group), it was observed that the tip grouting of the first pile (south pile) caused the densification of soil beneath the other piles which, in turn, hindered the grouting of the other group piles. Consequently, as with the first group, a small cavity was created beneath each pile tip by jetting with water prior to tip grouting of each pile. This small cavity assisted with the formation of the grout bulb beneath each pile, and the effect was negated by the grout volume and pressure pumped into the cavity. Grouting of each pile was stopped when the top of each pile moved upward by about 1/4-inch (i.e., full mobilization of side resistance). Tip grouting data of each pile is shown in Table 4-4 by order of grouting. As shown in the table, an increase in tip grout pressure was observed during subsequent grouting and it was attributed to the densification of soil due to the grouting of adjacent piles, as well as the resistance (stress increase) offered by the adjacent grout bulbs.

Table 4-4 Tip Grouting Data

Pile	**Maximum Grout Pressure** (psi)	**Grout Volume** (gal)
West	245	5
East	250	5
South	270	6
North	310	7

4.3.6 Top Down Testing after Tip Grouting

Top down load testing was conducted on the jet-grouted pile group following tip grouting to estimate the total axial capacity of the group. Pile displacements and soil deformations during group loading were measured using 0.0001 digital dial gages. The axial test was carried out in 10 load steps with a five-minute interval between load increments, followed by an unloading phase with four equal load decrements. The testing was stopped when an average displacement of 1.2 inches was observed at the top of the pile group. Results of the group test are discussed in Section 4.3.9.

4.3.7 Excavation of 4.5-inch Diameter × 8-ft. Long Jet-Grouted Pile Group

Excavation of the jet-grouted pile group was carried out following the top down load testing to characterize the side and tip grout zones of each pile. The pile group was excavated carefully to ensure no breakage of grout bulbs alongside or at the tip of the piles. Soil from the test chamber was removed using a mini excavator. Shown in Figure 4-65 is the exposed jet-grouted pile group in the test chamber and in Figure 4-66 is the pile group positioned near the test chamber after being lifted from the test chamber for inspection of both the side and tip grout bulbs. As evident in the photograph, each pile in the group possesses good quality grout zones. The diameter of all side grout bulbs was in the range of

9.5 to 10.5 inches as expected. The tip bulbs (see Figure 4-67) were nearly symmetrical with a diameter in the range of 11 to 12 inches.

Figure 4-65 Jet-grouted pile group in the test chamber.

Figure 4-66 Pile group resting on ground.

Figure 4-67 View of tip grout bulbs.

4.3.8 Measured Soil Stresses in the Vicinity of the Group

Variation of soil stresses in the vicinity of the pile group was measured during various stages of jetting, grouting, load testing, etc. Figures 4-68 through 4-72 show the measured vertical and horizontal stresses observed at different locations at various stages of the research, i.e., grouting and load testing.

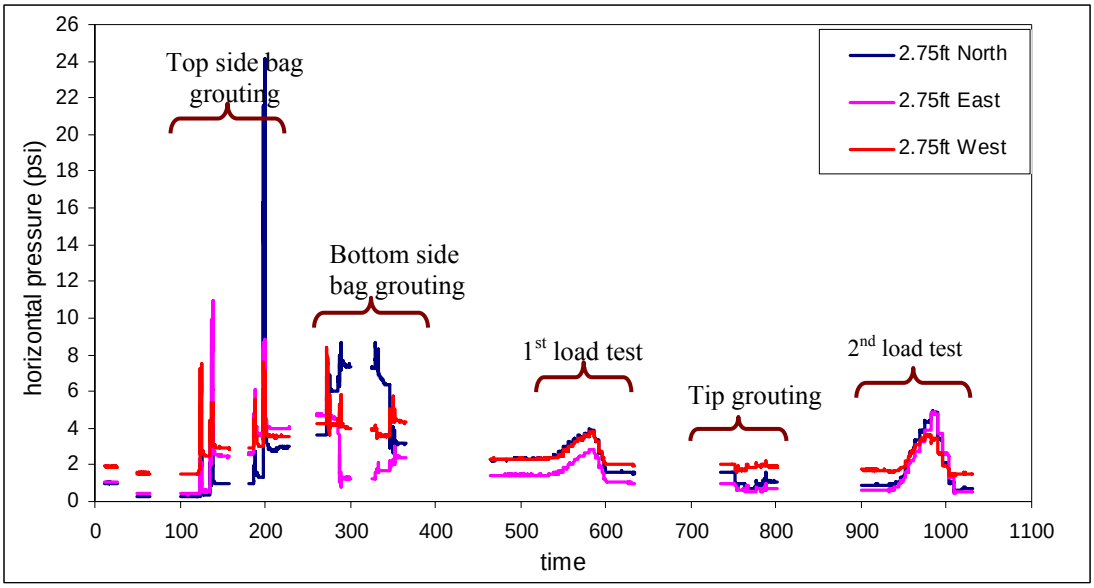

Figure 4-68 Variation of horizontal stress at 2.75-ft. depth close to pile.

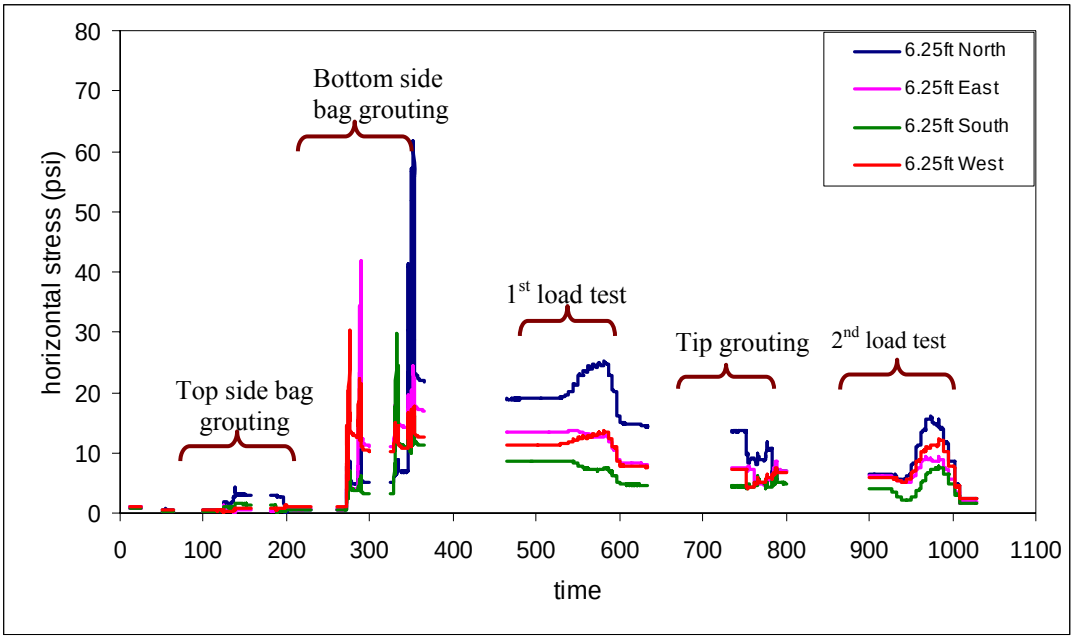

Figure 4-69 Variation of horizontal stress at 6.25-ft. depth close to pile.

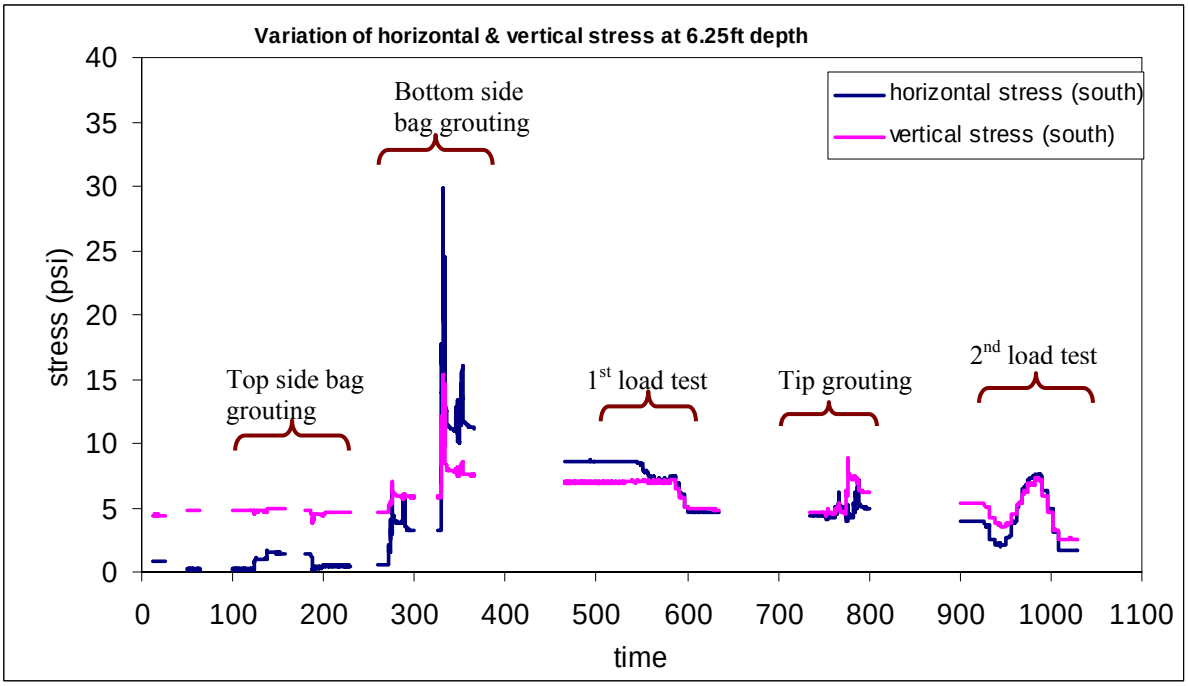

Figure 4-70 Comparison of horizontal and vertical stress changes at 8-ft. depth.

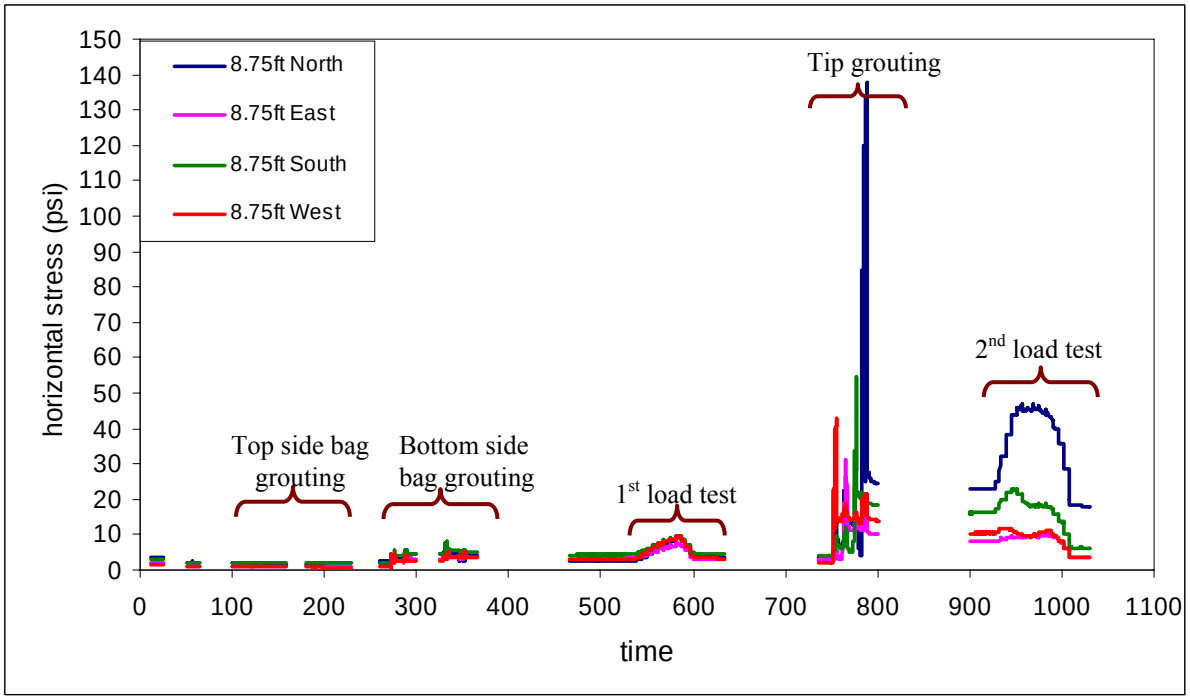

Figure 4-71 Variation of horizontal stress at 8.75-ft. depth close to pile.

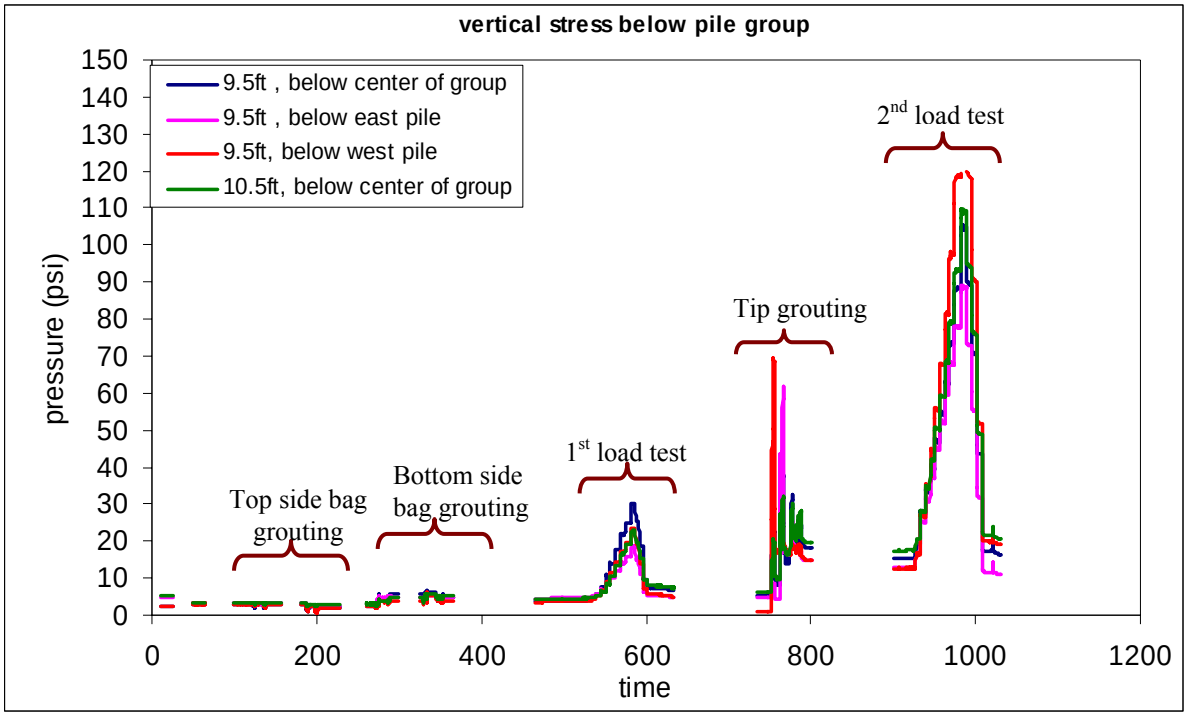

Figure 4-72 Changes in vertical stress beneath pile group.

4.3.9 Analysis of Experimental Jet-Grout Group Behavior

This section analyzes the results obtained from the experimental study of the 4.5-inch diameter × 8-ft. long jet-grouted pile group and discusses the group behavior of the piles. Shown in the Figure 4-73 is the load versus vertical displacement at the top of each pile observed during the group test conducted prior to tip grouting. Even though the distribution of applied load was non uniform as shown in Figure 4-73, the vertical displacements of piles were relatively uniform at each load increments similar to the observations from the first group study. This implies that load is being transferred through shear within the group and the group is acting as a single block during loading. Shown in Figure 4-74 is the total load versus average displacement of pile group with a maximum group load of 63 kips at an average top displacement of 0.3 inch.

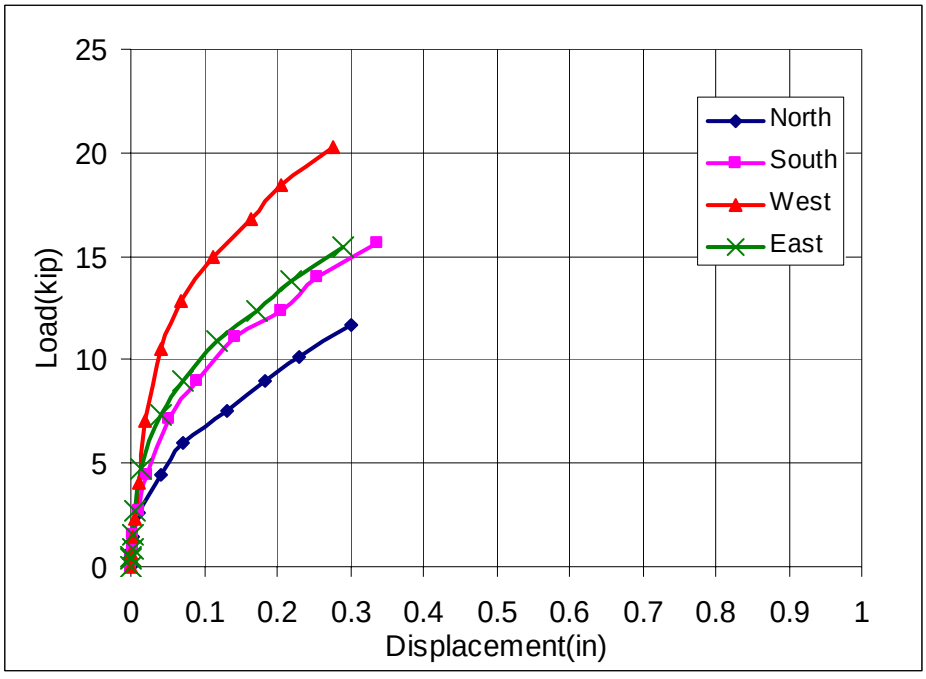

Figure 4-73 Load versus displacement of piles.

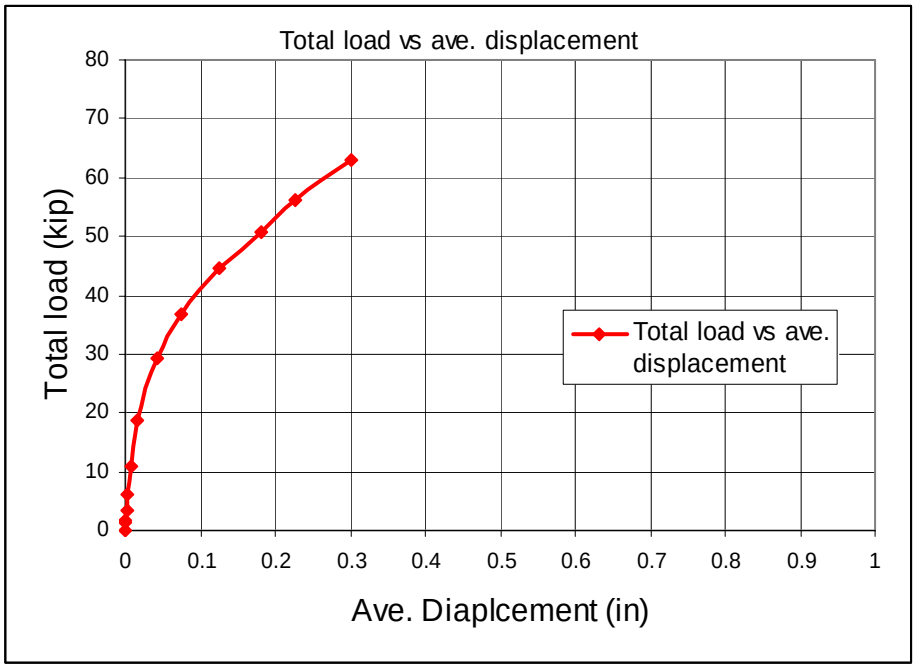

Figure 4-74 Total load versus average displacement of pile group.

Figure 4-75 shows the increase in vertical stress beneath pile group during the first load test. Evident from the figure, the increase in vertical stress at the center of the pile group was more than the stress increase beneath a pile, suggesting the block behavior of pile group (superposition of stresses from piles). It can be seen from the Figure 4-75 that the increase in vertical stress below center of group at 9.5 ft. (i.e., 1 ft. below group tip) was 25 psi. The vertical stress at the base of the group was back calculated from the vertical stress at 9.5-ft. depth using Boussinesq's theory as 35 psi. Then the tip force may be calculated from Boussinesq stress (35 psi) times block area of group (the vertical stress at base x the effective base area = 35 psi × 552 in^2/1000) equal to 19.3 kips. Knowing the top and tip force, the side resistance of the pile group was computed as (applied load – tip force = 63 kips -19.3 kips) 43.7 kips.

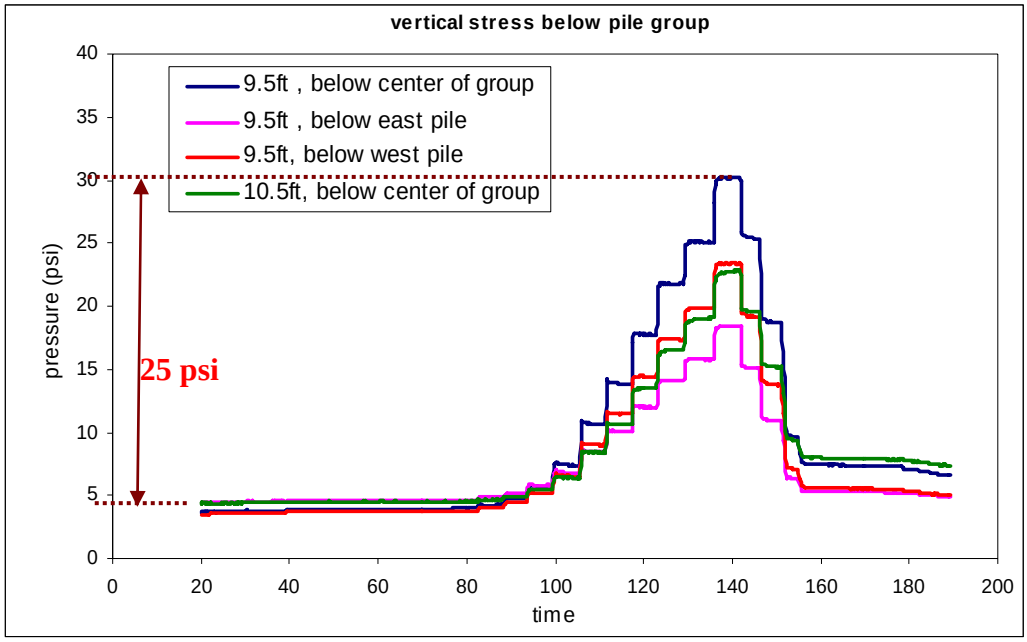

Figure 4-75 Variation of vertical stress below pile group during load test prior to tip grouting.

As in the first group analysis, the total side resistance of the group was predicted by multiplying the surface area of block with unit skin friction (0.766 ksf, calculated in the first group analysis) estimated using Equation 4.2 with K_g from Figure 4-54 proposed by McVay et al. (FDOT project BD 545 RPWO # 31). The side resistance of block may be computed as f_s (0.766 ksf) × surface area of block [4× length of one side of block (23.5 inch) × effective length of pile (7.5 ft.) = 58.75 ft^2] = 45 kips, which is quite close to the measured value of 43.7 kips. Similarly skin resistance of individual pile may be estimated as f_s (0.766ksf) × surface area of pile (π × diameter of bulb (10 inch) × effective length pile (7.5 ft) =19.625 ft^2) = 15 kips. Using tip grout pressure, the skin resistance of individual pile can be estimated as 14.2 kips (skin resistance = grout pressure × effective tip area = 250 psi × 56.745 in^2 = 14.2 kips) which is comparable with the value predicted using McVay's equation (Equation 4.2). The effective tip area used in the calculation was the area of the bottom plate (Figure 4-76)

used to hold bottom end of side grout membrane. Next, the unit skin resistance of an individual pile using tip grout pressure was estimated as 0.723 ksf [14.2 kips/surface area of side grouted pile ($\pi \times$ (10/12) ft. $\times$ effective length (7.5 ft) =19.635 ft^2) = 0.723 ksf] and using block area, the side resistance of the group was computed as 42.48 kips (0.723 $\times$ effective surface area of block: 58.75 ft^2).

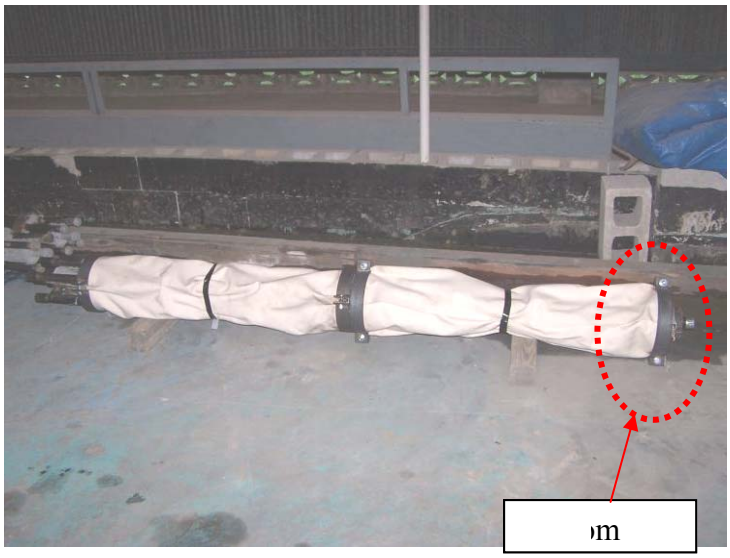

Figure 4-76 Precast pile with plate and ring system holding the membrane.

Table 4-5 shows the measured and predicted skin resistance of a single pile and the pile group using different approaches. Evident from the table, the ultimate shear resistance of group is less than the sum of individual pile resistances which is attributed to the smaller block area of the group compared to the sum of the individual pile surface areas.

Table 4-5 Measured and Predicted Skin Resistance of a Single Pile and the Pile Group

	Pile Group (kips)	**Single Pile** (kips)
Using tip grout data	42.48	14.2
McVay's equation	45	15
Measured (Total – Tip)	43.7	

Shown in Figure 4-77 is the individual load versus vertical pile displacements from the top down group testing after tip grouting. Evident from the shape of the curves, significant end bearing is mobilized during the group loading. Displacements of piles were relatively uniform during the load application of each increment, suggesting the pile group behaved as block during loading. Further justification is evident from a comparison of average pile movements vs. soil deformation at the center of the group in Figure 4-78. Shown in Figure 4-79 is the soil deformation profile of the ground surface which displays a quadratic variation from the boundary of pile group towards the chamber wall like the observation during the first group study. Note, if the piles did not act as a block but individually, the settlement at the center of the group would be less than at the pile locations (see grout-tipped shaft response, Chapter 5).

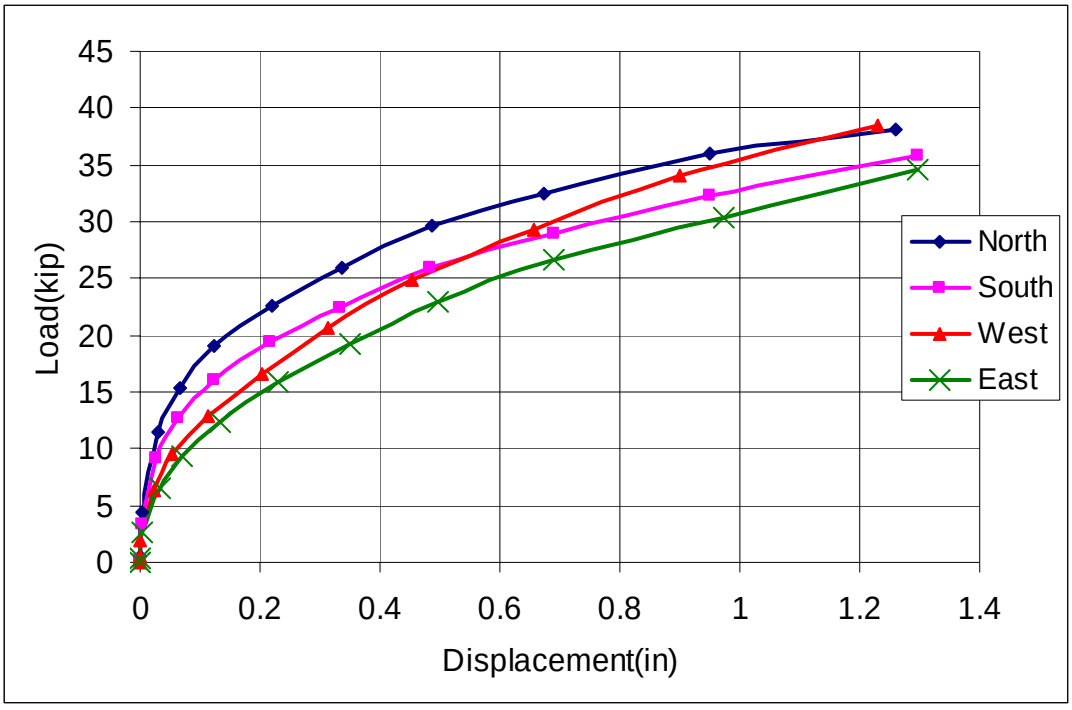

Figure 4-77 Load versus displacement of piles.

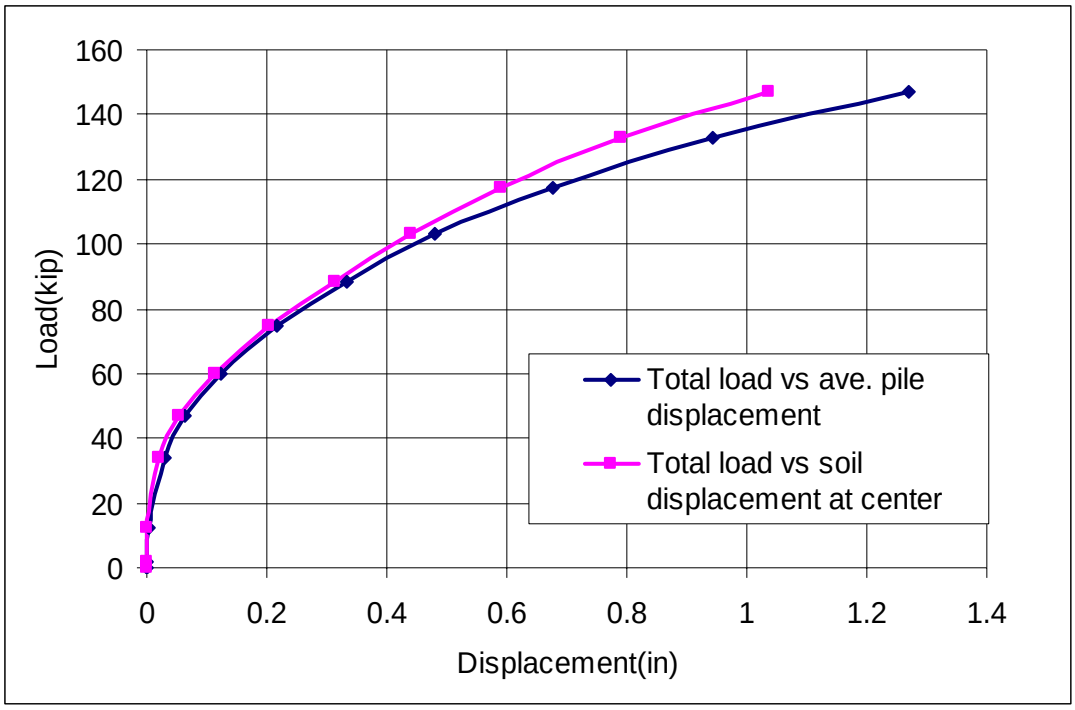

Figure 4-78 Total load versus average displacement of pile group and soil deformation.

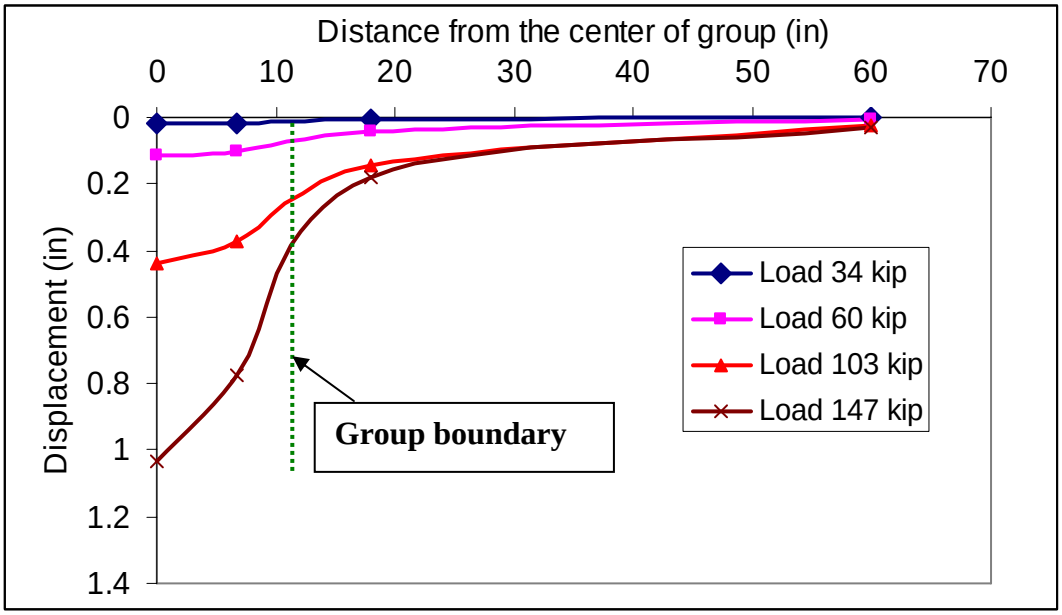

Figure 4-79 Soil deformation profile.

CHAPTER 5
EXPERIMENTAL BEHAVIOR OF GROUT-TPPED DRILLED SHAFT GROUP

5.1 Introduction

This chapter focuses on the experimental investigation of group behavior of grout-tipped drilled shaft groups. The first group considered for study was the group of four 8.5-inch diameter × 8-ft. long drilled shaft (L/D ~11) at 3D c/c spacing. The small diameter shafts were chosen to minimize the influence of chamber boundary on the results. The objective of the first group test was to study the influence of preloading, and tip bulb area on the axial capacity of grout-tipped drilled shaft as well as study the grout flow pattern, and estimate the axial group efficiency of tip grouted shafts at 3D spacing.

The second group chosen for the study was the four 8.5-inch diameter × 13-ft. long drilled shaft (L/D ~18) group at 3D c/c spacing. The intent of the latter test was to investigate the effectiveness of staged grouting in increasing the capacity of grout-tipped shafts and to validate the results obtained from the first group test at greater embedment depths. A description of various stages of the experimental investigation, the data measured, as well as analysis of the results, is also presented.

5.2 Testing of 8.5-inch Diameter × 8-ft. Drilled Shaft Group

5.2.1 Fabricating the Rebar Cage and Tip Grout System for Drilled Shafts

Area of steel reinforcement for the 8.5-inch diameter × 8-ft. drilled shaft was calculated according to building code requirements for structural concrete (ACI 318-02). The area of reinforcement was determined for a maximum anticipated load of 150 kips. The rebar cage consisted of five #5 rebars as longitudinal reinforcement and #3 rebars at 12-inch spacing for shear reinforcement. Tip grout delivery systems were assembled from 1-inch steel pipes,

fittings and gum rubber. There were three pairs of 1/2-inch diameter holes (at 90° to each other) at the bottom of each shaft which were covered by gum rubber for grout delivery, Figure 5-1. The gum rubber membrane allowed the grout to exit the grout pipe under high pressure, but prevented the exit of water when cleaning the pipes. A steel plate of 1/2-inch thickness and a steel ring of 4-inches long and 1/4-inch thick was welded to the bottom of the rebar cage. The bottom of the steel ring was covered with an Ultra-Soft polyurethane membrane (1/8-inch thick with tensile strength of 150 psi and a stretch limit of 500%). The steel plate-ring-membrane system protected the bottom of the shaft where the grout exits the shafts. Figure 5-1 shows the rebar cage and grout system for the drilled shafts.

Figure 5-1. Rebar cage and grout system.

5.2.2 Filling the Test Chamber with Soil and Stress Gage Placement

In order to eliminate the drilling and difficulties associated with installing the shaft, it was decided to position four 8.5-inch (outer diameter equal to the diameter of shaft) PVC casing at 3D spacing before filling the test chamber (Figure 5-2). This ensured the verticality of the hole and prevented caving and necking of the shafts. This approach also allowed the placement of stress gages for soil stress measurement in close proximity to the shafts. Figure 5-3 shows the layout of stress gages for the group test. It was decided to place two sets of stress gages horizontally (one directly below the center of the pile group and another one below one of the shafts) at a depth of 9 ft. and 11 ft. below the ground surface, i.e., 1 ft. and 3 ft. below the bottom of the shaft group to measure changes in soil stresses during grouting as well as top down static load testing. At 8.3 ft. from the ground surface, there were seven stress gages for horizontal stress measurement and one for vertical stress measurement as

Figure 5-2 PVC casing positioned before filling the test chamber.

shown in Figure 5-3. Gages were placed in a row (east-west direction) to measure the variation of stresses in the radial direction during grouting as well as loading. At a depth of 4-ft., three gages were placed for horizontal stress measurement (two outside the shaft group and one at the center of group), and one gage was placed for vertical stress measurement at the center of the group. In total, 16 stress gages were used for measuring soil stresses.

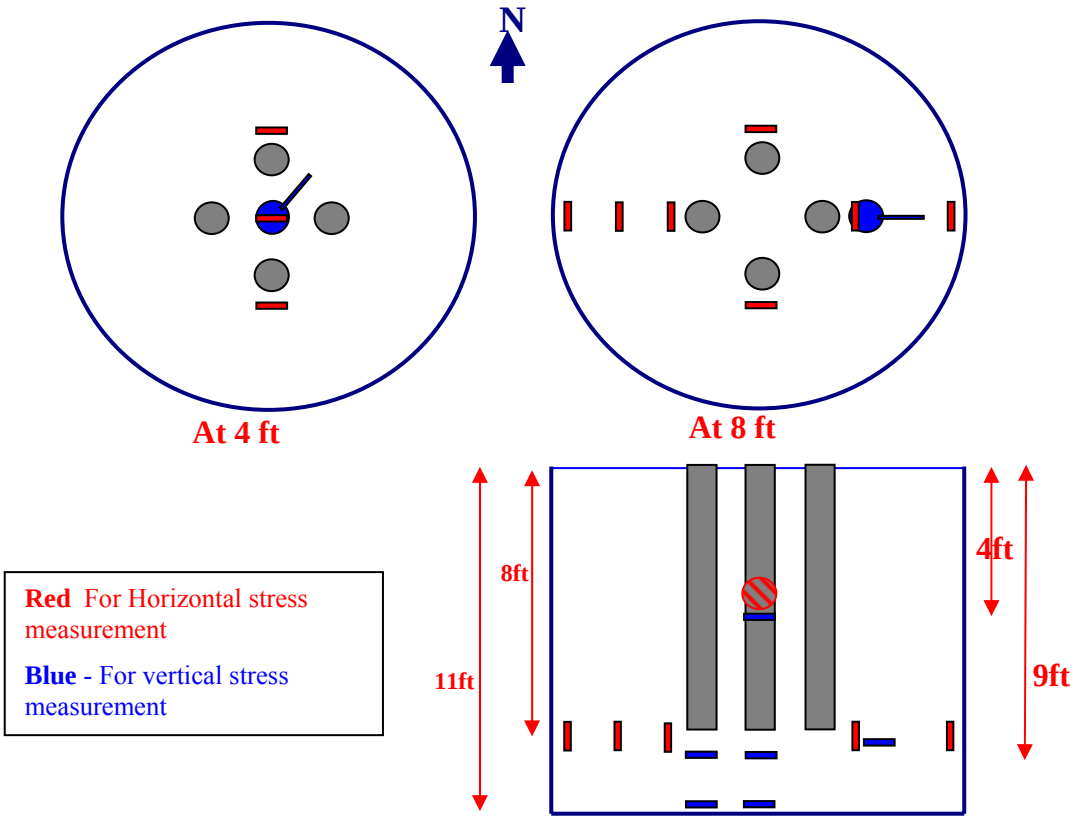

Figure 5-3 Stress gage layout.

The soil placed within the test chamber was uniform silty-sand. The moisture content of the soil was in the range of 6-8%. The soil was placed through free fall from the top of the chamber using a Bobcat loader. Shown in Figure 5-4 is the filling process.

In order to reduce the influence of chamber boundary, it was decided to conduct tests at a D_r of around 40-45% (i.e., dry density = 101 pcf). Soil was placed in 1.5-ft. lifts and compacted using a vibratory plate compactor with the exception of the area near the shafts

where a hand rammer was used. Figure 5-5 shows the test chamber fully filled. While filling the test chamber, a number of hand cone penetrometer tests and density tests were performed on each compacted soil lift. Soil dry densities for any lift was in the range of 99-102 pcf.

Figure 5-4 Filling the test chamber.

Figure 5-5 Test chamber in fully filled state.

Cone tip resistances varied from 25 kg/cm^2 to 40 kg/cm^2 for all the lifts. Based on typical relationships of relative density with SPT *N* values, the *N* values ranged from 6 to 9 for D_r of 40%. Using the CPT data, similar SPT *N* values (6 to 9) were found.

5.2.3 Insitu Casting of Drilled Shafts

The drilled shaft concrete mix was designed for a compressive strength of 4000 psi at 28 days using the absolute volume method. The mix used for one cubic yard of concrete consisted of a water/cement ratio of 0.46, water (280 lb), cement (685 lb), coarse aggregate (1735 lb), and fine aggregate (1135 lb) and a slump of 4 inches.

Shaft construction began with the placement of the reinforcement cage (Figure 5-1) with attached grout tip system. Next, the concrete was placed in the casing and vibrated (Figure 5-6) with a wand. Subsequently, the casing was pulled out using a fork lift as shown in Figure 5-7. Finally, the top of the shaft was leveled and concrete cylinders were cast to assess concrete strength at one and two weeks. Figure 5-8 shows the drilled shaft group after concreting.

Figure 5-6 Concrete vibrated with a wand.

Figure 5-7 Pulling the casing out.

Figure 5-8 Drilled shafts.

5.2.4 Top Down Testing of Drilled Shaft Group Prior to Tip Grouting (Group Test 1)

After waiting two weeks for concrete strength gain following casting, top down group testing was conducted to estimate individual shaft skin resistance as well as drilled shaft group behavior. Figure 5-9 shows the test setup which consisted of spacer disks on each shaft span grout delivery pipe, 200-kip capacity load cells placed on the top of each

Figure 5-9 Load test setup.

shaft to measure load distribution, a test frame, hydraulic jack, another 600-kip capacity load cell to measure total load, a reaction beam and support system, and displacement monitoring instrumentation. Shaft and soil displacement were measured using 0.0001 digital dial gages. The top down test was performed in ten load steps with a five-minute interval between increments, followed by an unloading phase. Since the test was intended to estimate only the skin resistance of the group, loading stopped when an average displacement of about 0.25 inch was observed at the top of shafts.

5.2.5 Tip Grouting of Drilled Shafts

After the completion of top down shaft group test, the tip of each shaft was grouted individually. The grout mix consisted of cement, 10% micro-fine fly ash and water at a

water/cement ratio of 0.50. Displacements of each shaft and soil deformation (at the center of shaft group) were measured using digital dial gages as shown in Figure 5-10. It was decided to stop grouting when the top of the shaft had an upward displacement of at least 0.25 inch, which is approximately equal to the downward displacement of the prior load test to mobilize unit side resistance.

Figure 5-10 Tip grouting.

Tip grouting started with the south shaft and the displacement of the shaft was negligible up to a grout volume of 14 gallons. The shaft reached an upward displacement of 0.25 inch when 17 gallons were pumped to the tip of the shaft. The maximum grout pressure observed during the grouting was 85 psi. When the tip grouting of the north shaft started, the shaft moved immediately upward and the volume of the grout pumped was about 0.5 gallon at a maximum grout pressure of 85 psi. The response of other shafts (west and east) to tip grouting was similar to the north shaft. Tip grouting data of each shaft is given in Table 5-1.

Table 5-1 Grouting Data (8.5-inch Diameter × 8-ft. Drilled Shafts)

Shaft	Grout Pressure (psi)	Grout Volume (gallon)
South	85	17
North	85	0.5
West	85	0.5
East	85	3

Since the volume of void (empty space inside the bottom ring, Figure 5-1) at shaft tip is less than 0.5 gallon, a grout volume of 0.5 gallon is sufficient to fill the void space within the ring at the shaft bottom and compress the soil below the shaft tip. Due to the large volume of grout pumped in the south shaft tip, it was thought initially that a massive grout bulb was formed beneath the south shaft tip.

5.2.6 Top Down Testing on Tip Grouted Drilled Shaft Group

In order to assess the total load capacity of the group, the group interaction and influence of the larger grout volume beneath the south shaft, it was decided to conduct load tests in the following sequence:

1) Top down testing of the group (same load is expected to act on all shafts);
2) Top down testing of the group with more load on the south shaft (one with large grout volume);
3) Loading on the south shaft alone; and
4) Loading on the west shaft alone.

Details of each load test follow.

5.2.6.1 Top down testing of the group (Group test 2a)

After waiting approximately three weeks following tip grouting of the test shafts, top down testing on the group was conducted. The test setup was exactly the same as the pre tip grouted load test. A schematic view of the loading system is given below (Figure 5-11).

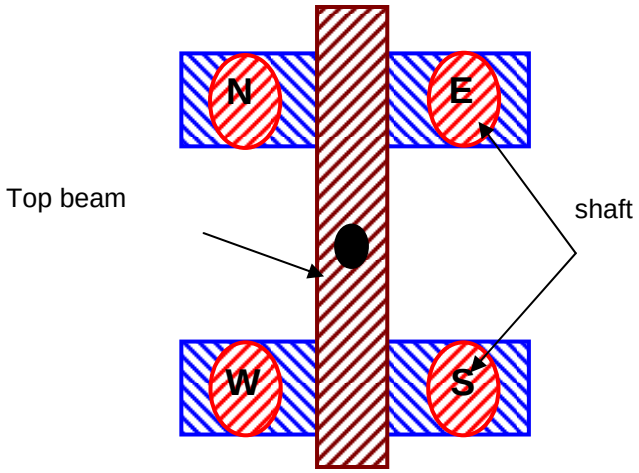

Figure 5-11 Load system–Group test 2a.

The test was performed in nine load steps with a five-minute interval between increments, followed by an unloading phase. The test continued until a maximum displacement of about 0.8-inch was observed at the top of the shaft group. The maximum displacement of soil at the center of the group was 0.278 inch, which was much less than the average displacement of shaft (0.68 inch). The displacement of the south shaft (0.45 inch) was less than the displacement of other shafts and this is attributed to the larger volume of grout pumped into the south shaft tip.

5.2.6.2 Top down testing of the group with more load on the south shaft (Group test 2b)

Since the maximum observed displacement of the south shaft observed was only 0.45, which suggests not fully mobilized group resistance, it was decided to conduct another group

test with more loads on the south shaft versus the other shafts. A schematic view of the loading system is given below (Figure 5-12).

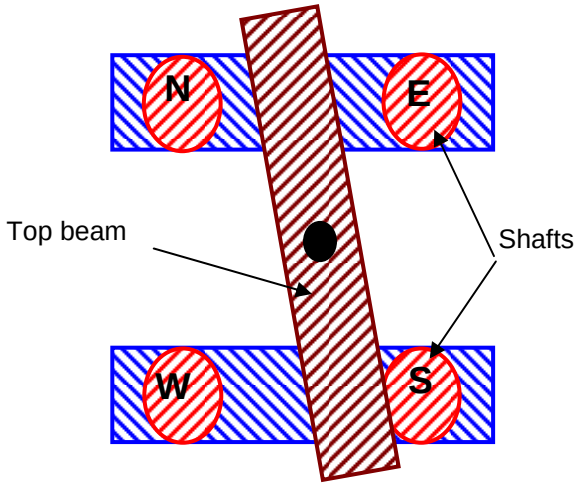

Figure 5-12 Load system–Group test 2b.

The test was performed in ten load steps with a five-minute interval between increments, followed by an unloading phase. The test continued until a maximum displacement of about 1.5-inch was observed at the top of the pile group. For this scenario, failure deformations were observed for all shafts.

5.2.6.3 Loading on the south shaft alone

In order to estimate the influence of a large grout volume pumped into the south shaft on group interaction, loading on just the south shaft was conducted. Figure 5-13 shows the test setup for the load test. Note, digital dial gages were used to measure the displacement of all shafts, and soil stresses in the vicinity of the shaft group were measured throughout the load test sequence.

Figure 5-13 Load test setup–South shaft.

5.2.6.4 Loading on the west shaft alone

Load testing on the west shaft was conducted to compare to the results obtained from the single south shaft test. It was believed that the west shaft was more representative of the other tip grouted shafts within the group. Of interest was the comparison between individual and group response of the shafts. The results of the test are discussed in more detail in Section 5.2.9.

5.2.7 Excavation of 8.5-inch Diameter × 8-ft. Tip-Grouted Drilled Shafts

After completion of the various top down single and group tests, the drilled shafts were pulled out using a forklift (Figure 5-14). Shown in Figure 5-15 is the south shaft after pull

out. Evident from the figure, there was no grout bulb formed at the shaft tip, instead, a grout zone formed alongside the shaft. Specifically, during tip grouting, the void space at the shaft tip (Figure 5-1) is first filled and then grout flowed upside along the shaft-soil interface, which was due to the minimum principal stress. Similar results were observed for all the shafts (Figures 5-16, 5-17, 5-18). Controlling the size of the grout zone along the shaft depended on the volume of grout pumped.

Figure 5-14 Pulling out drilled shaft.

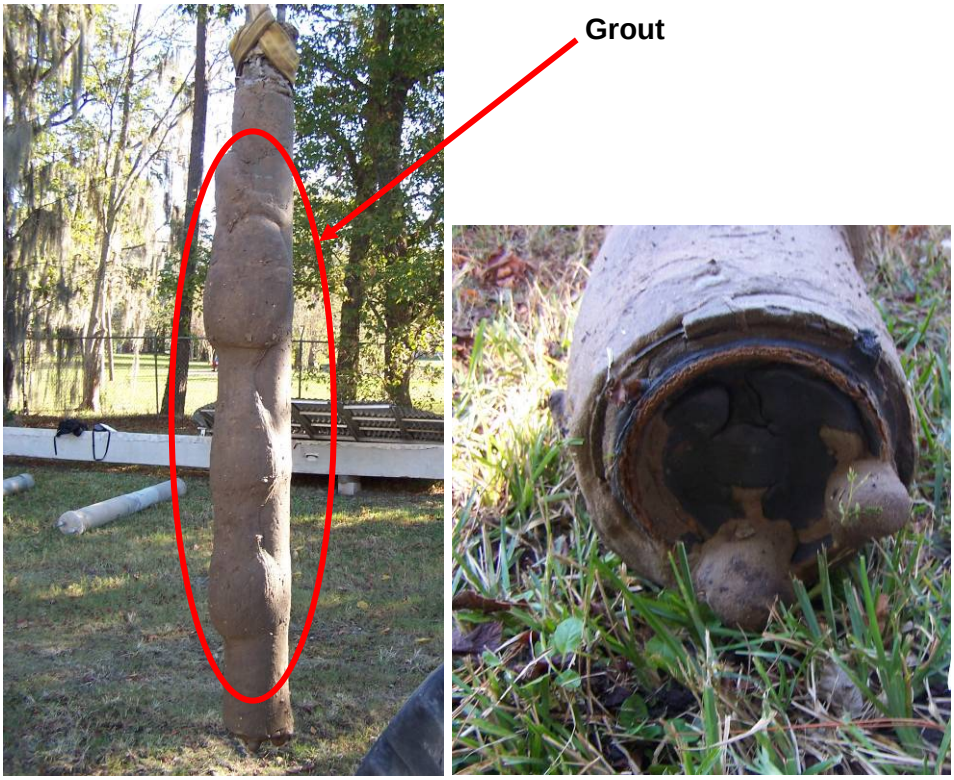

Figure 5-15 South shaft.

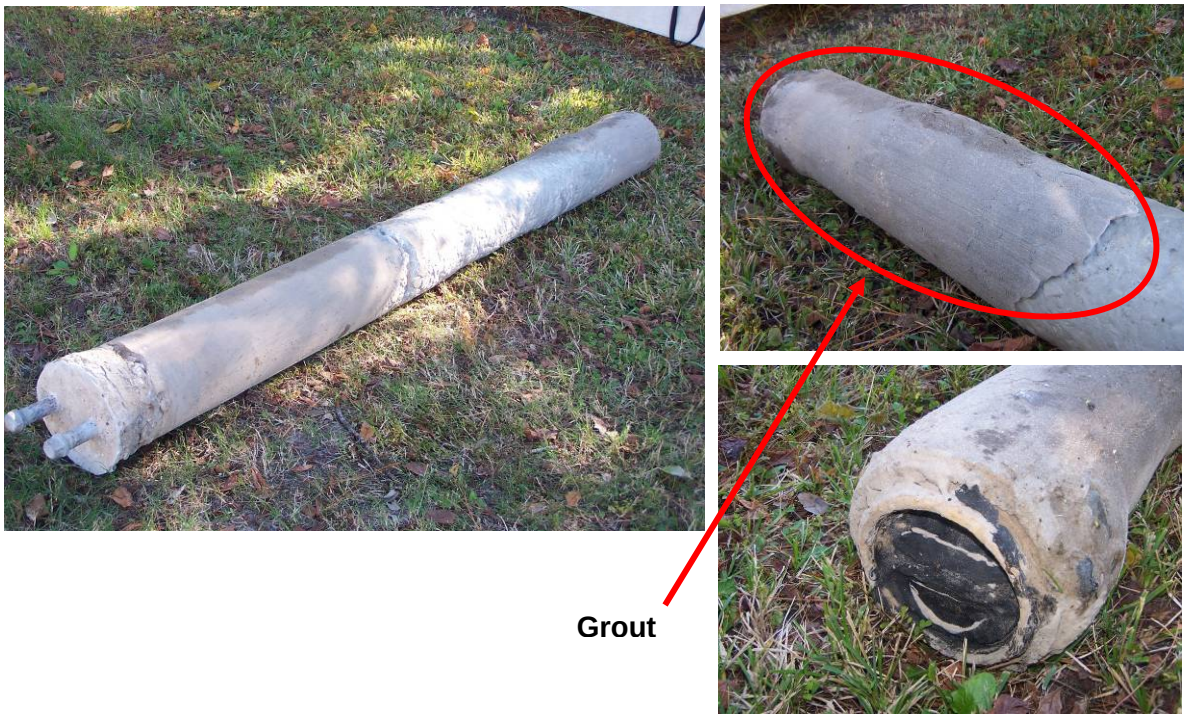

Figure 5-16 East shaft.

Figure 5-17 North shaft.

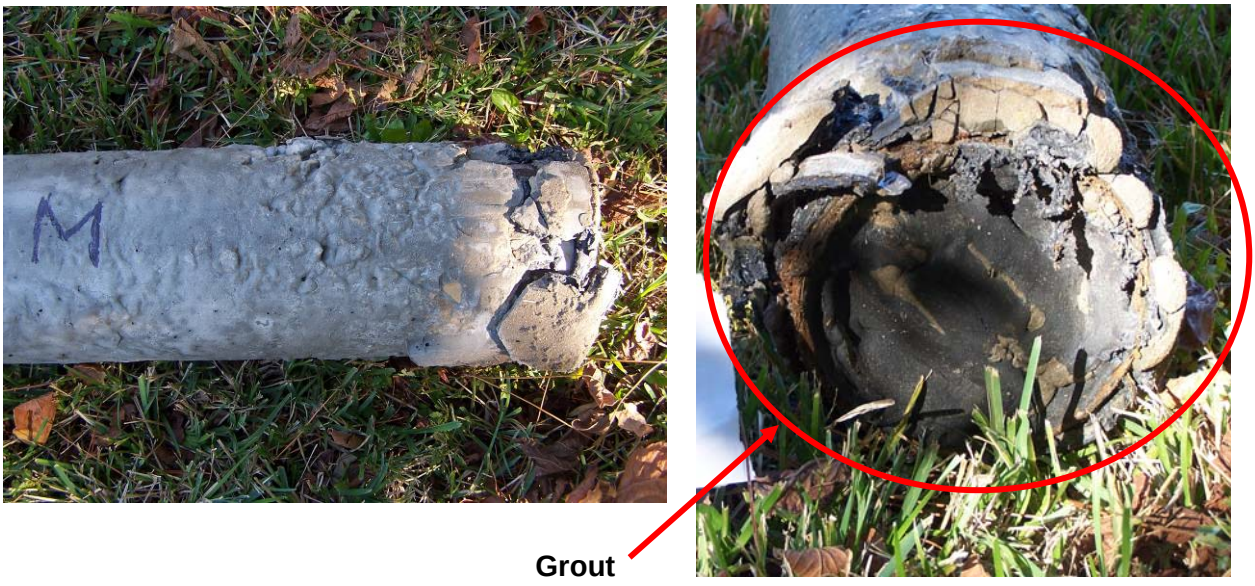

Figure 5-18 West shaft.

5.2.8 Measured Soil Stresses in the Vicinity of the Group

Variation of soil stresses in the vicinity of the group was measured with Geokon stress gages during multiple stages (tip grouting, load testing), and are shown in Figures 5-19 to 5-22. It can be seen from the plots that stresses around shaft tip increased during grouting and dropped immediately when the grouting was stopped. This is due to the grout valve at the shaft head being opened immediately after grouting (i.e., no locked-in grout pressure at the tip), and the fact that little, if any, grout bulb formed near the shafts.

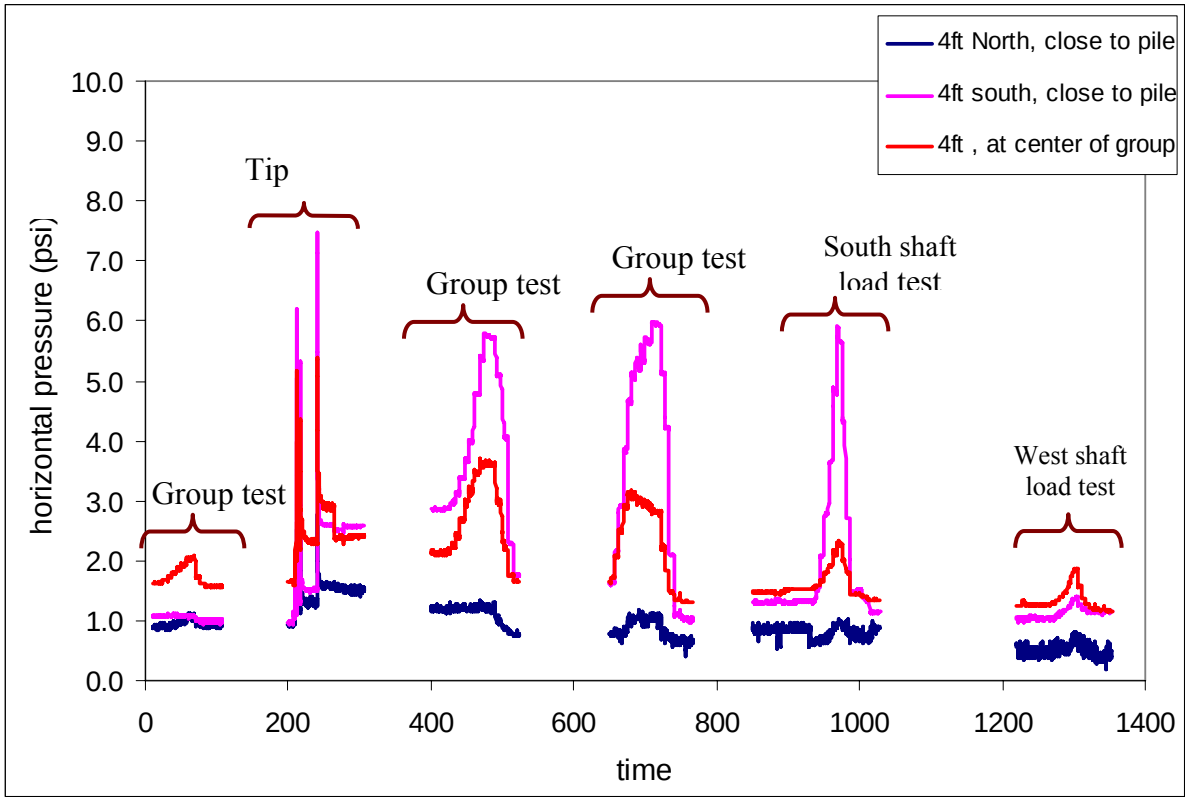

Figure 5-19 Variation of horizontal stress at 4-ft. depth.

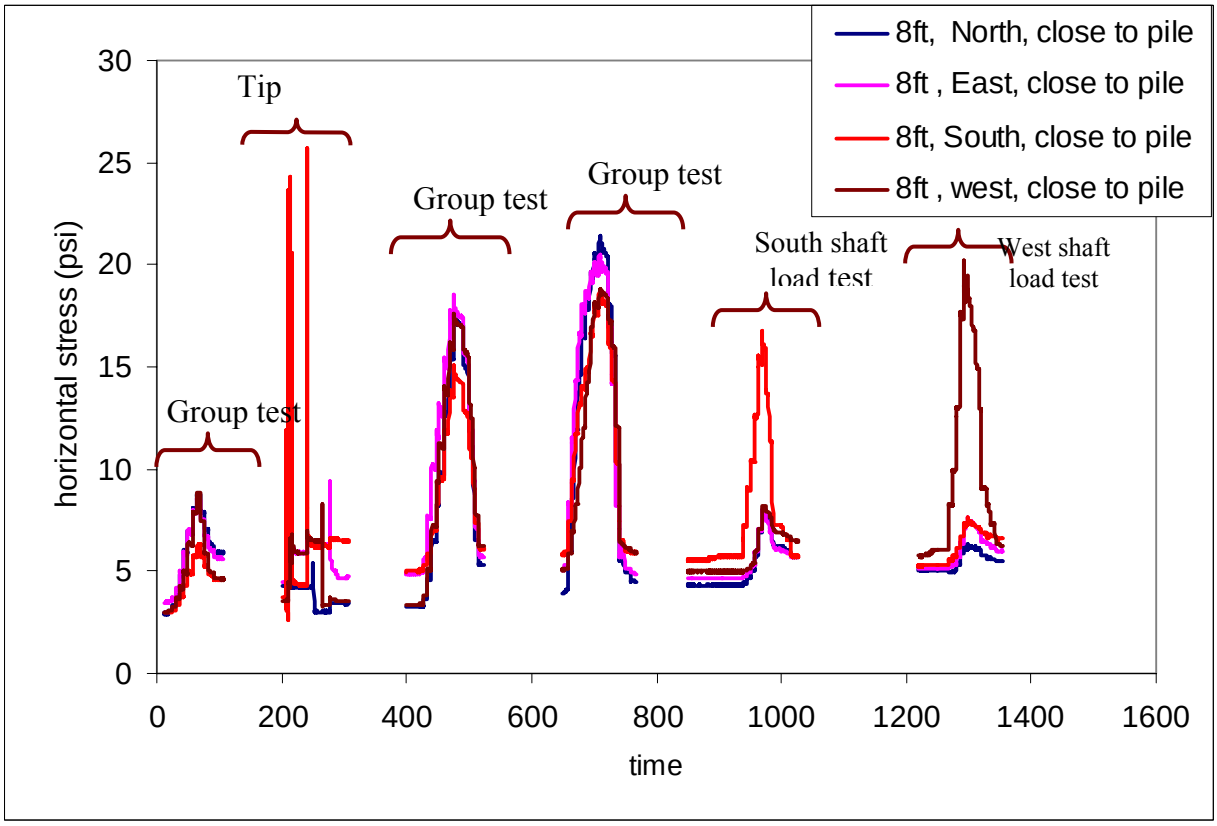

Figure 5-20 Variation of horizontal stress at 8-ft. depth.

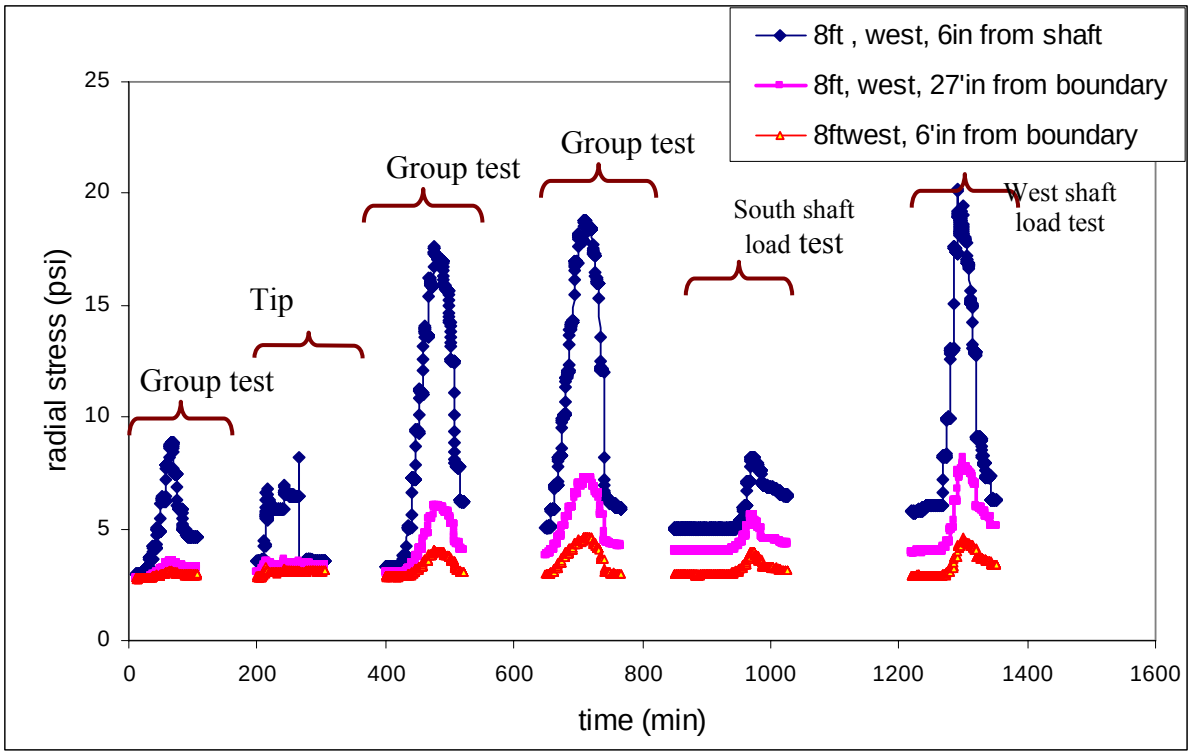

Figure 5-21 Comparison of horizontal stress variation at 8 ft.–West direction.

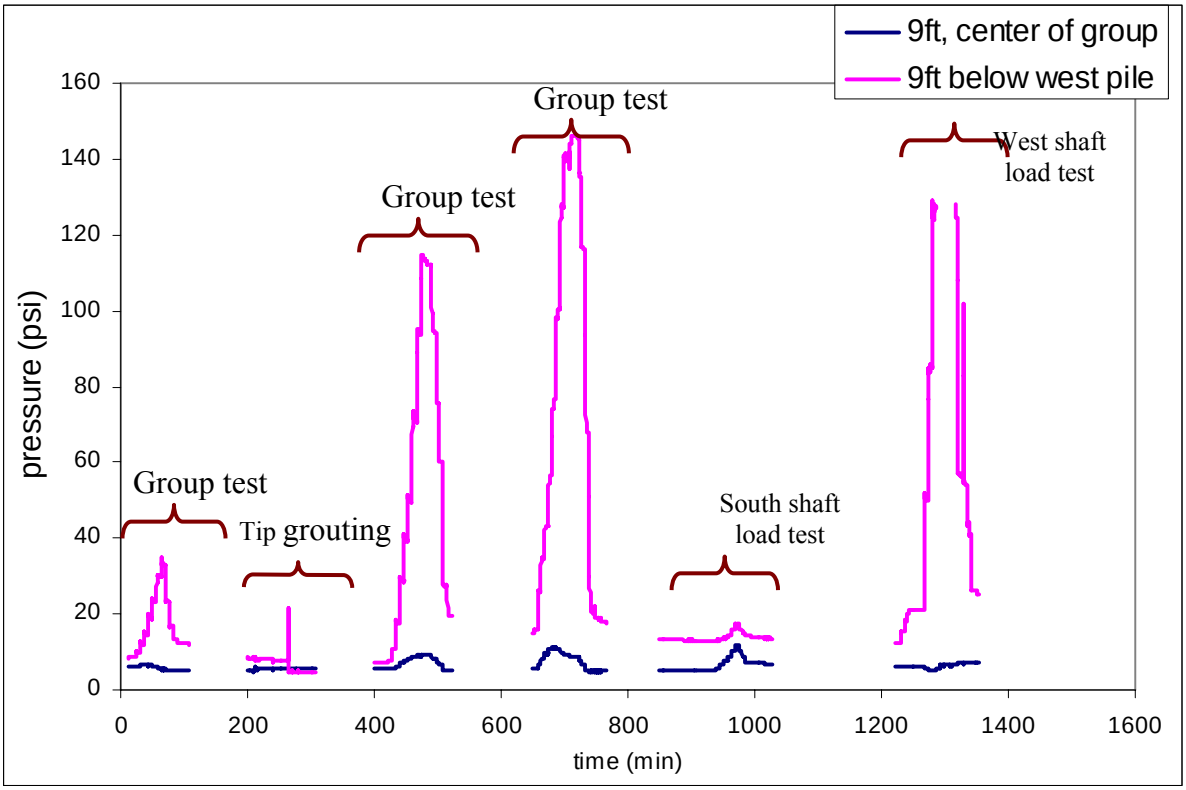

Figure 5-22 Variation of vertical stress at 9-ft. depth.

5.2.9 Analysis of Experimental Drilled Shaft Group Behavior

This section discusses the experimental behavior of tip-grouted drilled shafts based on the load-deformation data and soil stress measurement during different stages: 1) post side grouting; and 2) post tip grouting. Shown in Figure 5-23 is the load versus vertical displacement at the top of each shaft during group loading prior to tip grouting, and Figure 5-24 is the DeBeer's log-log plot of Figure 5-23. From the DeBeer's plot, it can be seen that the skin resistance of each shaft ranges from 3 kips to 3.7 kips, which reasonably agrees with the skin resistance (3.5 kips) determined using FDOT's FB-Deep software for SPT values of $N = 6$.

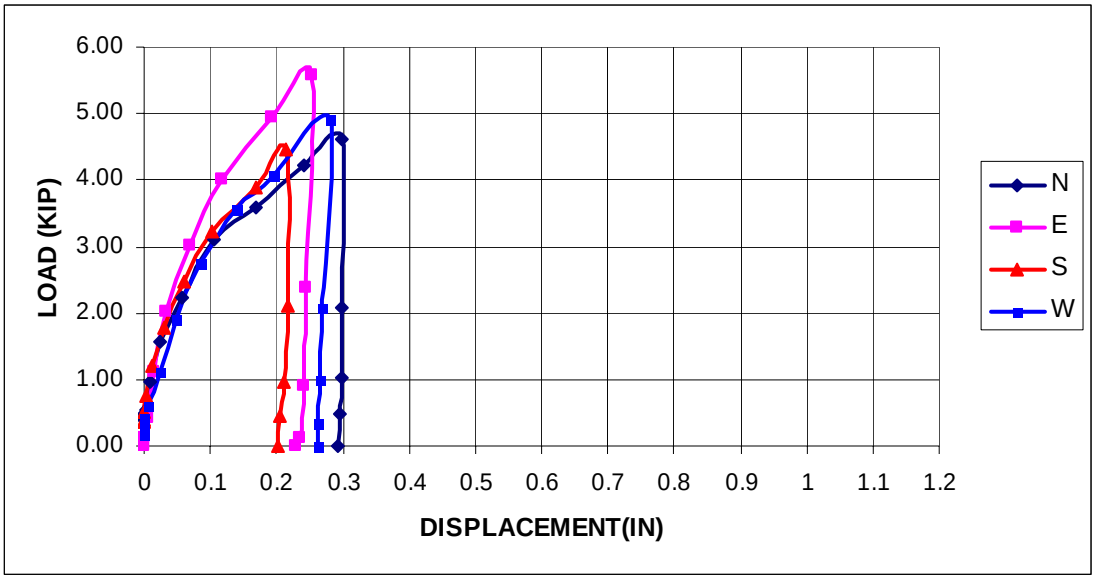

Figure 5-23 Load versus vertical displacement.

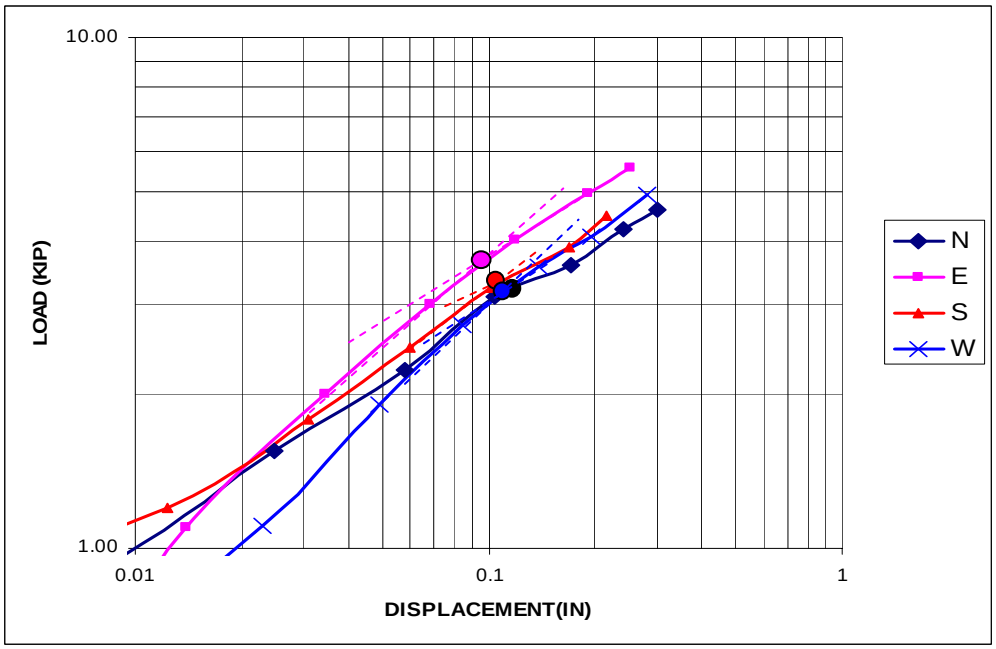

Figure 5-24 DeBeer's log-log plot.

Similarly, shown in Figure 5-25 is the load versus vertical displacement at the top of each shaft during the first load test after tip grouting (i.e., Group test 2a). The maximum displacement of soil at the center of the group was 0.278 inch, which is much less than the average displacement of shaft (0.68 inch) which suggests that the shafts behaved indepen-

dently during group loading. The displacement of the south shaft (0.45 inch) was less than the displacement of other shafts, and this is attributed to the larger volume of grout pumped (larger shear resistance).

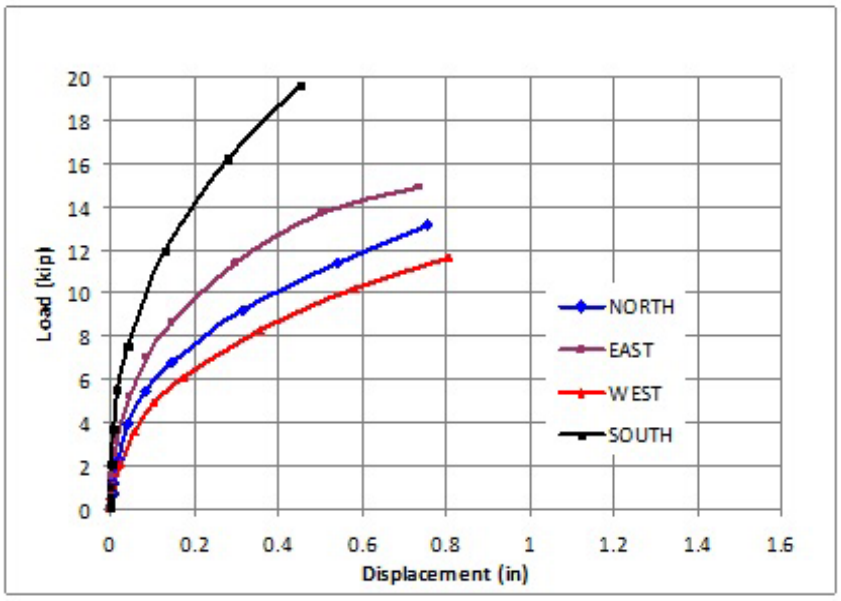

Figure 5-25 Load versus vertical displacement of shafts–Group test 2a.

As identified in Figure 5-25, group test 2a mobilized very little tip resistance for the south shaft, and hence, as identified in Section 5.2.6.2, another group test (2b) was performed with a rearrangement of the loading frame to mobilize more tip resistance of the south shaft. Figure 5-26 shows the combined (group test 2a and 2b) load versus vertical displacement at the top of each shaft. Note, the first cycle is group test 2a and the second cycle was group test 2b. The displacement of the west shaft was the minimum due to the smallest load acting on it. It can be seen from the Figure 5-26 that the load-displacement response obtained from group test 2b behaves as the reloading curve of the load displacement response from group test 2a. At a large displacement (above 1 inch), load-displacement responses of shafts are nearly parallel, suggesting that the rate of tip mobilization is nearly the same for all the shafts.

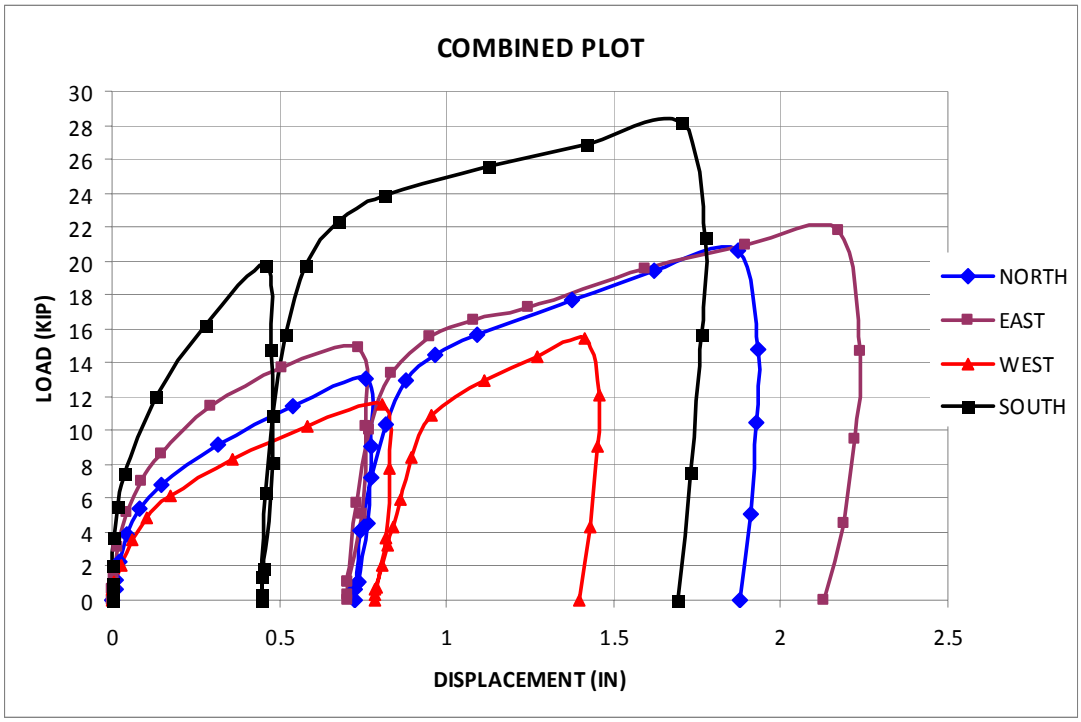

Figure 5-26 Combined load versus displacement plot (Group tests 2a and 2b).

Figure 5-27 shows the load-displacement response obtained from the single south shaft plotted with the load-displacement response of the shaft under group loading (group test 2a and 2b). Evident from the load-displacement response, the shaft response was similar in both scenarios. Shown in Figure 5-28 is the displacement of each shaft measured during the load testing of the south shaft only. Due to the negligible displacements of the other shafts while loading the south shaft, little, if any, group interaction was occurring. Note, if group interaction existed, loading on one shaft would cause notable displacement of other shafts in the group due to shear transfer through the soil (Figure 2-1). Similar behavior was observed, i.e., the displacement of other shafts was negligible (see Figure 5-29), when the west shaft was loaded separately. Moreover, Figure 5-30 indicates that the maximum stress induced below the west shaft, due to the loading on the south shaft, was only 4 psi, versus the double-digit stress increase observed for jet-grouted piles.

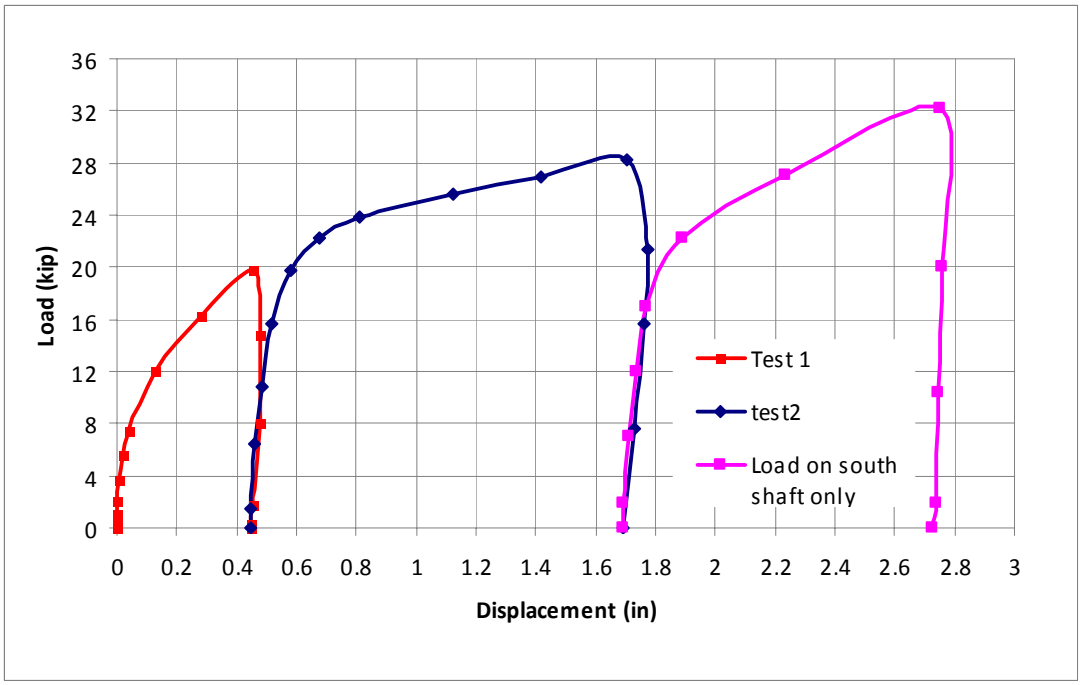

Figure 5-27 Combined load-displacement response (Group tests 2a, 2b, and loading on south shaft only).

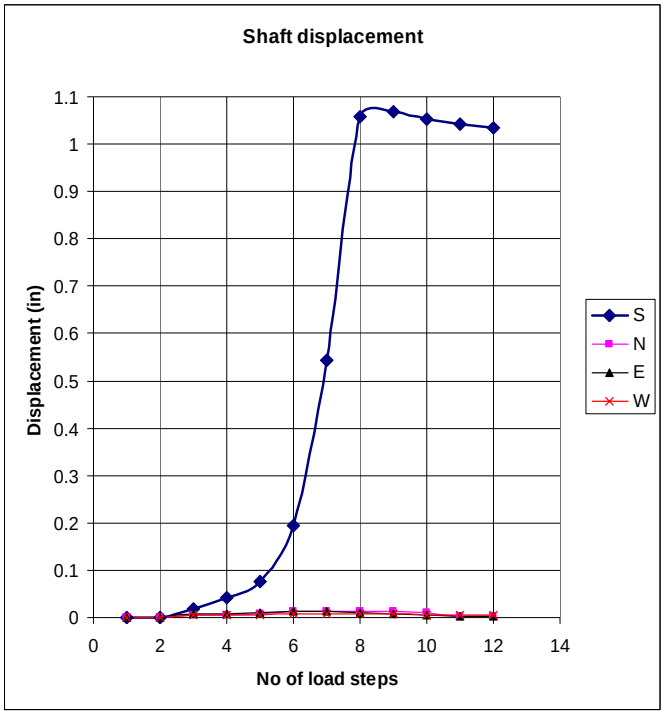

Figure 5-28 Displacement of each shaft during the load test on the south shaft.

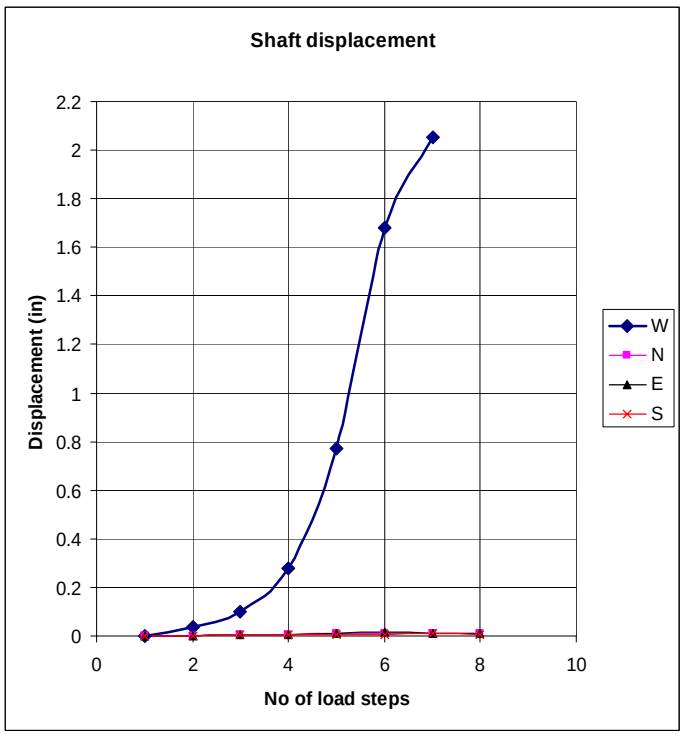

Figure 5-29 Displacement of shafts during loading on the west shaft alone.

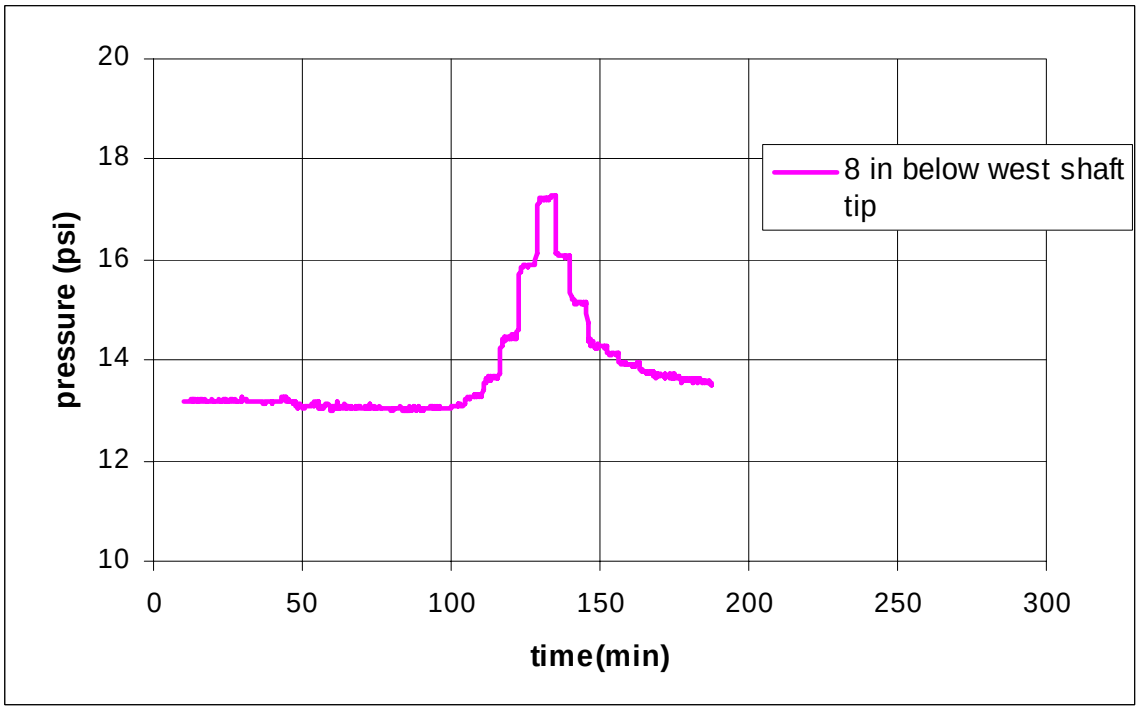

Figure 5-30 Vertical stress at 8 inches below the west shaft during loading on the south shaft.

Based on the observed stresses and displacements, experiments suggest that the group behavior of tip-grouted shaft or group efficiency is nearly equal to 1. Figure 5-31 depicts the load-displacement response obtained from the test on the west shaft alone plotted along with the load-displacement response of the shaft in the first two group tests done after tip grouting (group tests 2a and 2b). Like the load test on the south shaft, the load-displacement response proceeds as the reloading curve of the group tests 2a and 2b.

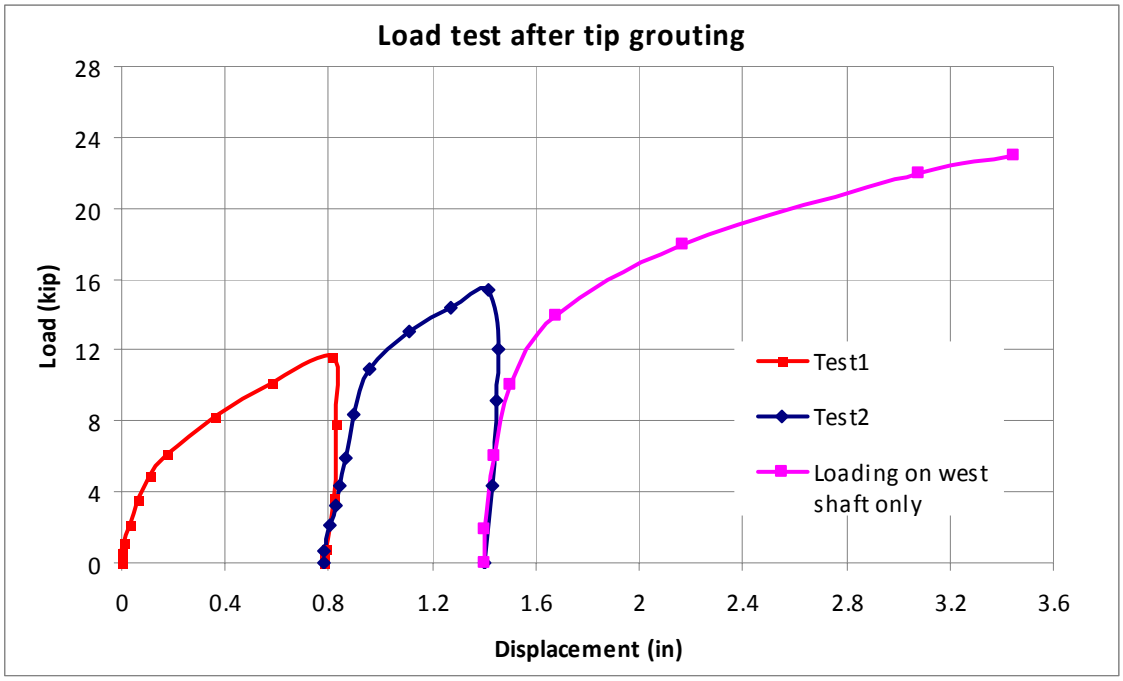

Figure 5-31 Combined load-displacement response (Group tests 2a, 2b, and loading on the west shaft only).

As identified in the last section, during tip grouting, the grout flowed along the shaft-soil interface (the weakest path in the present case) after filling the void space at shaft tip. The size of the vertical grout flow was dependent on the grout volume pumped. This differs significantly to jet-grouted piles, which have low upward grout movements due to high principal stress in the horizontal from side grouting of the piles. Drilled shafts have the lowest principal stress in the horizontal direction at the vertical soil-shaft plane and is a major

conduit for grout flow in the upward direction. In addition, since the grout is fluid, as it flows alongside the shaft it relieves any side friction as it propagates upward. A similar grout zone around the experimental shaft has been observed in the field on full-scale post-grouted drilled shafts reported by Mullins and Winters (NGES Auburn: Post grouting drilled shaft tips-Phase II, Fig. 4-79, 2004) (see Figure 5-32). After grout hydration, the vertical grout zone around the shaft increases the skin resistance of the shafts. The increase in skin resistance depends on the amount of grout pumped. However, this is not true in all cases. Because, the grout will always flow along the weakest path in the soil, it may not be the shaft-soil interface, e.g., in layered soil, the grout may flow along the layer interface. So, it is difficult to predict the improvement in skin friction due to tip grouting.

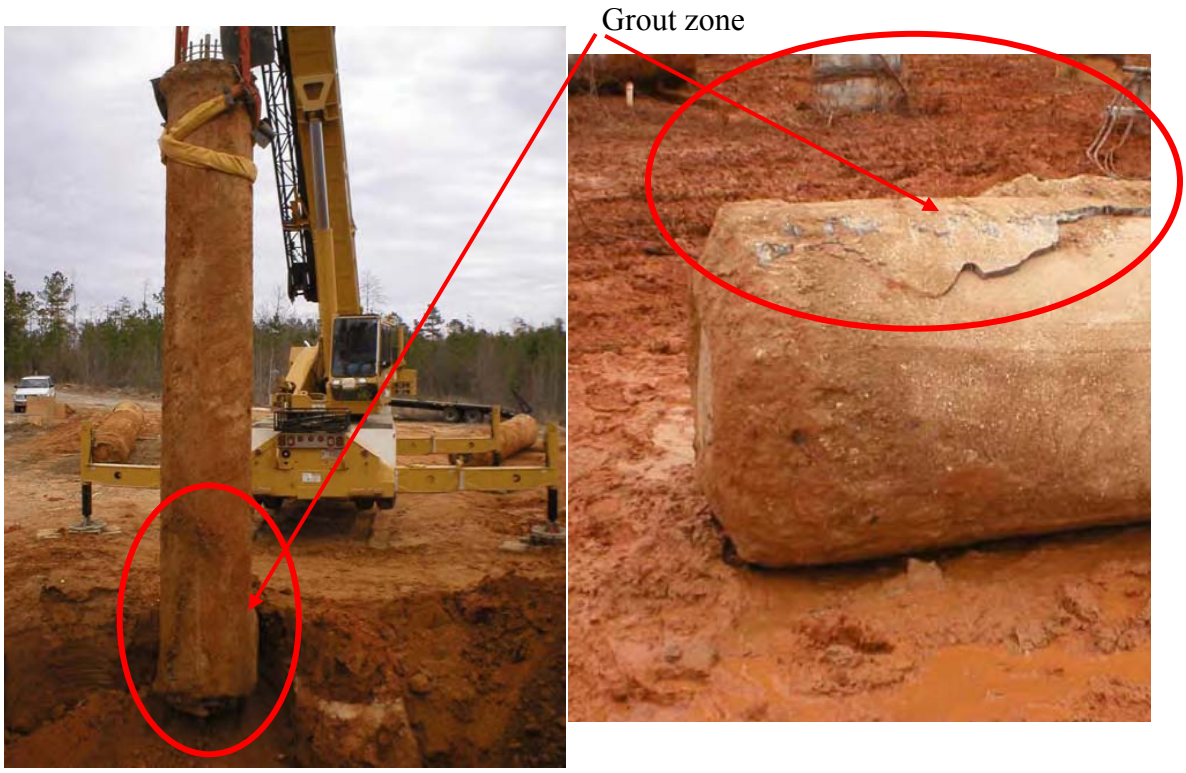

Figure 5-32 Post-grouted shaft–NGES Auburn (Mullin et al. 2004).

As no bulb was formed at the shaft tip, the improvement in tip resistance of the shaft is due to the preloading effect of grouting only. The grout compresses the soil in the zone

immediately below the shaft tip and improves its stiffness and not necessarily the soil's strength. The latter is represented by the observed low grout pressure during grouting. This is different than in the case of a jet-grouted pile, where tip grout pressures in the range of 220-240 psi were observed at the same shaft depths. It should be noted that the jet-grouted tip pressures were only available due to the much higher horizontal stresses (i.e., major principal stress) as a result of the side grouting of the piles. In contrast, the tip grout pressure (85 psi) observed during tip grouting of drilled shaft was only one-third of the value of the jet-grout pile because the major principal stress was vertical and the smaller horizontal stress was readily overcome by the shaft tip grout pressures.

The experiments also suggest that tip grouting of shafts preloads the soil, and results in increased tip stiffness, but not necessarily an increased tip resistance over un-grouted shaft tips. For example, the observed grout pressure (85 psi) times effective tip area (area of ring at tip = $\pi \times 6.5^2/4$) gives the preload applied at the tip (3 kips). The top down tests reveal that the initial 3 kips is mobilized under small deformations (i.e., higher stiffness); however, the capacity at large displacement may not be altered. This is shown in Figure 5-33 which shows the combined load displacement plot of the west shaft obtained from different load tests conducted before and after tip grouting with the tip grouted response added to the pre-grouted shaft response. It can be seen from the figure that the shape of the load displacement response of the pre- and post-grouted shafts are quite similar. From density measurement and cone testing at the 8-ft. depth, it is estimated that the SPT N values ranged between 5 and 7. Using Federal Highway Administration (FHWA) design, 0.6 $N \times$ Area, it is estimated that the shaft tip resistance is approximately 3.5 kips at settlement of 0.425 inch or 5% diameter of the shaft. However, due to preloading and improved stiffness, it is estimated that the available tip resistance is approximately twice this value (Reese and O'Neill tip mobilization)

at an additional 5% diameter settlement. If the latter was to be added to the original skin friction (Figure 5-31, 3.5 kips), a total resistance of 10.5 kips should be mobilized at a displacement of an additional 5% or 0.85 inch, which agrees with Figure 5-33.

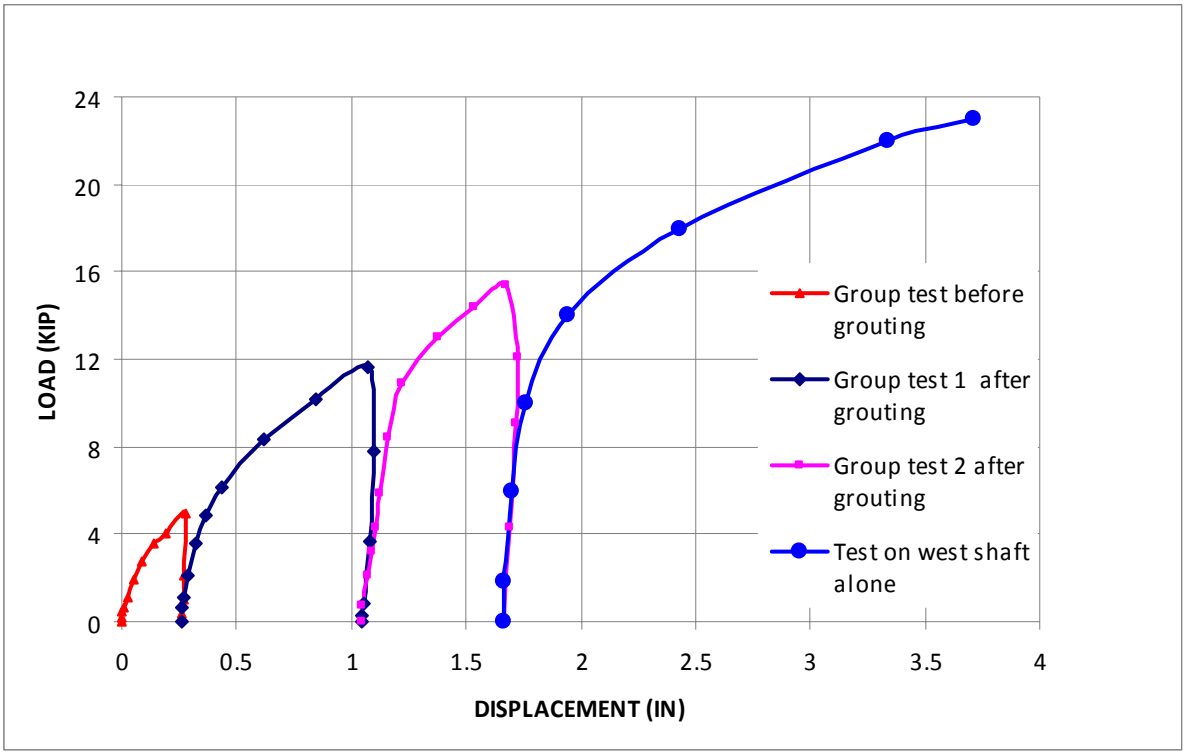

Figure 5-33 Load displacement curve of the west pile (from different load tests).

Unlike jet grout piles, care should be taken when using tip grout data for a drilled shaft to estimate either the pre- or post-grouted shaft's skin resistance. Specifically, the grout may flow upward along the shaft-soil interface (as in the present test) during tip grouting and a reduced skin resistance of shaft may result since the side grout would be in a fluid state. So, the grout pressure times tip area will not be equal the final skin resistance of shaft after the grout hydrates. A possible solution would be to regrout the shaft tip (i.e., stage-grout) and measure the increase in grout pressure which may be due to the hydrated grout alongside the shaft.

5.3 Testing of 8-inch Diameter × 13-ft. Long Stage Grout-Tipped Drilled Shaft Group

5.3.1 Fabricating the Rebar Cage and Tip Grout System for Drilled Shafts

Four drilled shafts of 8-inch diameter and 13-ft. long (L/D ratio ~ 20) were chosen for the second tip-grouted group shaft tests. This test was to assess the influence of embedment length and possible use of staged grouting to measure the final tip and side resistance of post-grouted shafts. Area of steel reinforcement for drilled shafts was calculated according to building code requirements for structural concrete (ACI 318-02). The rebar cage consisted of five #5 rebars as longitudinal reinforcement and #3 bars at 12-inch spacing for shear reinforcement. The tip grout delivery system was again assembled from 1-inch steel pipes and fittings with gum rubber sleeves. There were three sets of 3/8-inch diameter holes (4 holes at each location) on the bottom 1-inch steel pipe for grouting purposes. The grouting pipe passed through a steel plate of 1/2-inch thickness and a steel ring 6-inches long and 1/4-inch thickness was welded to the bottom of the rebar cage. The bottom of the steel ring was covered with Ultra-Soft polyurethane membrane (1/8-inch thick with a tensile strength of 150 psi and a stretch limit of 500%) similarly to the first shaft group test. Figure 5-34 shows the rebar cage and Figure 5-35 shows the grout exit locations with membrane covering for the drilled shafts. Note, the 6-inch ring was used to ensure a grout bulb formed below the shafts.

Figure 5-34 Rebar cage for the drilled shafts.

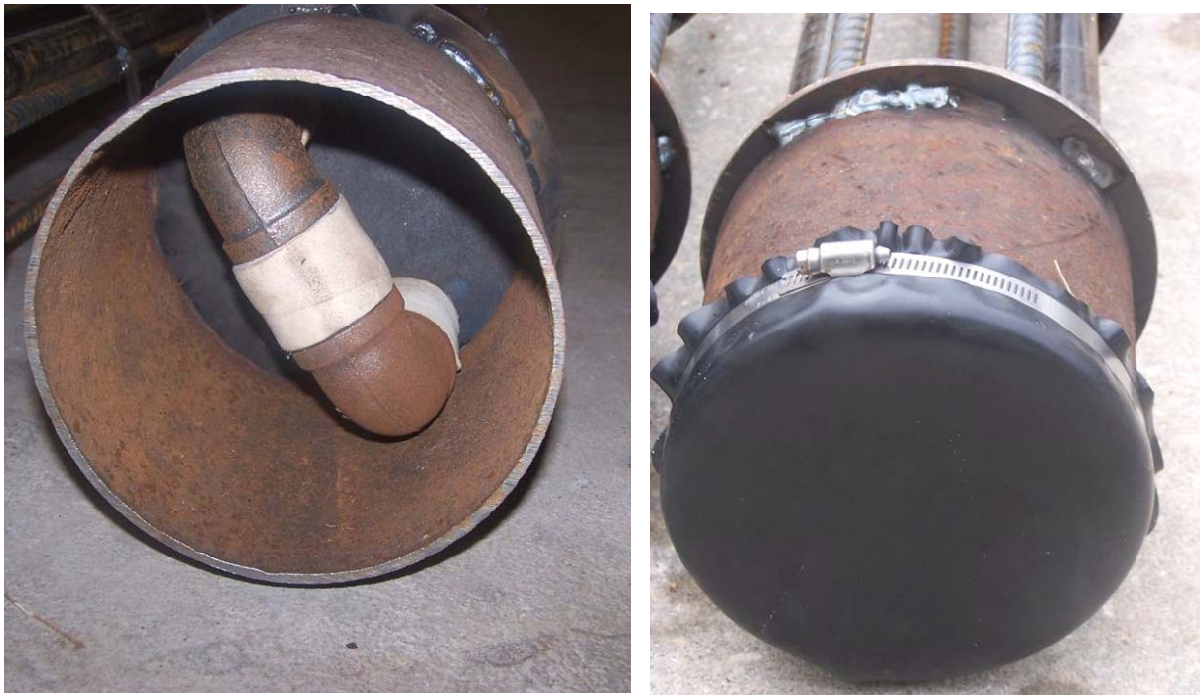

Figure 5-35 Grout exit and membrane covering.

5.3.2 Stress Gage Placement and Filling the Test Chamber with Soil

Four 13.5-inch (outer diameter, equal to the diameter of shaft) PVC pipes at 3D spacing were positioned (Figure 5-36) in the test chamber before soil placement to avoid drilling and other associated shaft construction issues. This also ensured the verticality of the shafts and aided the placement of the soil stress gages in close proximity to the shafts. The soil placed within the test chamber was the same and similar lift and compaction specifications were maintained. The moisture content of the soil was in the range of 7 to 9%.

Figure 5-36 PVC casing positioned in the test chamber.

In order to measure the soil stresses during grouting and load testing, a total of 16 stress gages were placed at different locations in the test chamber. Shown in Figure 5-37 is the layout of stress gages for the second set of tip-grouted drilled shafts. Stress gages were placed at five different elevations as shown in Figure 5-37. At a depth of 15-ft., one stress gage was placed at the center of the shaft group to measure vertical stress variation during

grouting as well as top down load testing. There were three stress gages at 14-ft. depth for vertical stress measurement; one below the center of the group, a second one below the east shaft and the third one below the west shaft. At 13.3-ft. from ground surface, there were six stress gages for horizontal stress measurement as shown in Figure 5-37. Similarly, four stress gages were at 11.3-ft. depth and two gages at 8-ft. depth for horizontal stress measurement.

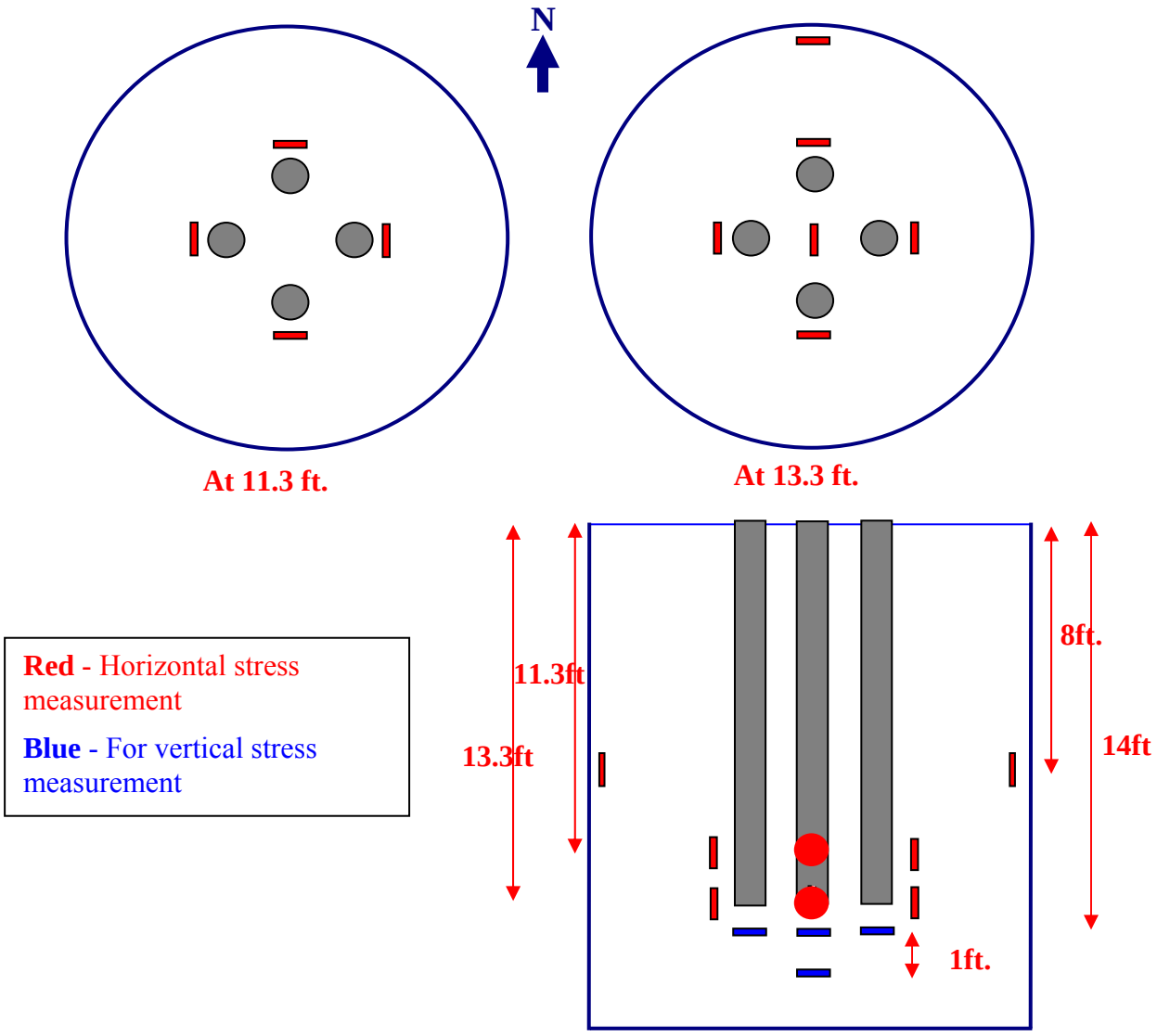

Figure 5-37 Stress gage layout.

In order to reduce the influence of the chamber boundary, it was decided to conduct tests at a D_r in the range of 40-45% as well as for comparison purposes to prior group testing. Soil was placed in 1.5-ft. lifts and compacted using a vibratory plate compactor. While filling the test chamber, a number of hand cone penetrometer tests were performed on each compacted soil layer. Cone tip resistances varied from 20 kg/cm^2 to 35 kg/cm^2 for all the lifts.

5.3.3 Insitu Casting of Drilled Shafts

After filling the test chamber, casting of the drilled shafts were initiated. First, the rebar cage with its grout distribution system was lowered into the PVC casing as shown in Figure 5-38. Next, the concrete was poured into the casing from the top down and then vibrated. Subsequently, the casing was pulled out using a fork lift under vibration and the top of shaft was leveled. Shown in Figure 5-39 is the shaft group after concreting.

Figure 5-38 Lowering the rebar cage into PVC casing.

Figure 5-39 Drilled shaft group after concreting.

5.3.4 Top Down Testing of Drilled Shaft Group Prior to Tip Grouting (Group Test 1)

Top down testing was conducted on the drilled shaft group after sufficient curing to estimate the side resistance. The test setup was same as the one used for the first drilled shaft group test. The test was performed in six load steps with a five-minute interval between increments, followed by an unloading phase. The test was continued until full mobilization of the skin resistance, which was ensured from the log-log plot of load versus displacement of shafts.

5.3.5 Staged Tip Grouting of the Drilled Shafts

After completion of the top down test on the shaft group, staged tip grouting of shafts was begun. To identify the grout flow pattern during the different stages of grouting, different colored grouts were used for each stage. In the first stage of grouting, 6 gallons of yellow colored grout was pumped into each shaft. After hydration of the first-stage grout, another 6 gallons of red colored grout (second-stage grouting) was pumped into each shaft. It was decided to carry out the third-stage grouting using black colored grout until the shafts showed an upward movement of about 1/4 inch. When the third-stage grouting was

attempted in the east and south shafts, grout pressures of 600 psi were recorded, however, no grout was pumped into the shafts. This was attributed to the formation of a solid grout plug at the shaft tip due to the first- and second-stage grouting. As the third-stage grouting was controlled by upward displacement (about 1/4 inch) of shaft, grouting of the west and north shafts discontinued after pumping of about 3 gallons of grout. Grout pressures and upward displacements of shafts were monitored during the different stages of grouting. The volume of grout pumped and the maximum sustained grout pressure observed during the various stages of grouting are given in Table 5-2. It can be seen from the values in the table that the grout pressures observed during the second-stage grouting was about 20 to 25% higher than the first-stage grouting pressures.

Table 5-2 Staged Tip Grouting Data

Shaft	First-Stage Grouting		Second-Stage Grouting		Third-Stage Grouting	
	Grout Pressure	Volume	Grout Pressure	Volume	Grout Pressure	Volume
North	170 psi	6 gal	200 psi	6 gal	200 psi	3 gal
East	190 psi	6 gal	240 psi	6 gal		---
South	200 psi	6 gal	270 psi	6 gal		---
West	180 psi	6 gal	220 psi	6 gal	200 psi	3 gal

5.3.6 Top Down Testing of the Stage Grouted Drilled Shaft Group

To assess the group capacity and group interaction, the following three different axial top down tests were performed on stage tip-grouted drilled shafts:

(1) Top down testing on the group;

(2) Top down testing on the east shaft; and

(3) Top down testing on the west shaft.

A description of each test is presented followed by a general analysis.

5.3.6.1 Top down testing of the group

The first axial top down testing on the stage tip-grouted drilled shaft occurred after approximately two weeks of the final tip grouting to allow hydration of the grout. The test was performed in nineteen load increments with a five-minute interval between increments which was followed by an unloading phase (4 equal load decrements). The displacement of shafts and soil deformation were monitored using digital dial gages. The test continued until an average displacement of about 1-inch was observed at the top of the shaft group. The maximum displacement of soil at the center of the group was 0.378 inch, which was much less than the average shaft displacement (1 inch) of the individual shafts within the group.

5.3.6.2 Loading on the west shaft alone

In order to estimate the interaction between shafts, loading on the west shaft alone was conducted. Displacements of other shafts and stress in the vicinity of the group were measured using digital dial gages and stress gages, respectively. The load test setup was the same as the one used in single shaft testing in the first group of drilled shafts (Figure 5-13).

5.3.6.3 Loading on the east shaft alone

For comparison purposes with the west shaft, a load test was performed on the east shaft. Again, stresses and displacements of the east shaft, as well all the other shafts within the group were monitored to assess group interaction. The results of the test are discussed in more detail in Section 5.3.9.

5.3.7 Excavation of 8.5-inch Diameter × 13-ft. Long Tip-Grouted Drilled Shafts

Excavation of 8.5-inch diameter × 13-ft. long tip-grouted drilled shafts was carried out after the group and individual top down load tests had been completed. Shafts were

excavated carefully to ensure that no breakage of the grout zone occurred during excavation. Figure 5-40 shows the excavation and removal of soil from the test chamber.

Figure 5-40 Removal of soil from the test chamber.

Shown in Figure 5-41 is the bottom of the east shaft and it can be seen from the figure that a grout bulb was formed at the side of shaft tip. Figure 5-42 shows the attributes of grout zones formed around the east shaft during the different stages of grouting. Evident from the figure, the initial grout (yellow) flowed alongside 6 ft. of the shaft (weakest path) during the first stage of the grouting as in the case of first grout-tip shaft group experiments. During the second stage of grouting, red grout tried to flow up alongside of the shaft and formed a bulb at the side but above the tip of the shaft. However, there was little, if any, contact between the red grout bulb and the side of the shaft, and hence, its contribution to the capacity of the tip-grouted shaft was negligible. As identified in Table 5-2, there was no stage three grouting, i.e., black grout, for the east shaft. Consequently, the increase in capacity of the east shaft due to tip grouting was attributed to: the preloading by the applied first-stage grouting; the increase in skin resistance of the shaft (due to the increased surface area and

radial stress due to grout flow alongside the shaft); and increased tip area at the bottom of the shaft.

Figure 5-41 Bottom of the east shaft exposed.

Figure 5-42 Grout zone–East shaft.

Shown in Figure 5-43 are the characteristics of the grout zone formed at the south shaft bottom. Again, it is clear from the figure that the yellow grout has flowed alongside of the shaft (around 4.5 ft.) after filling the void space at the shaft tip. The upward flow of yellow

grout has also formed a bulb at the shaft tip. During the second-stage grouting, the red grout tried to flow along the weakest path and it snaked around the tip bulb formed during the first-stage grouting. The increased capacity of the south shaft was due to the preloading of soil beneath the tip due to the applied first-stage grout; an increase in skin resistance of shaft (due to the increased surface area and radial stress due to the grout flow alongside the shaft); and the increased tip bulb area formed after the first stage.

Figure 5-43 Grout zone–South shaft.

Similarly, characteristics of the grout zone formed at the north shaft bottom are shown in Figure 5-44. Yellow grout flowed alongside (around 3.5 ft.) the shaft and also formed a small grout bulb at the shaft tip. During the second-stage grouting, the red grout flowed around the hardened yellow grout at one side of shaft tip. For the third-stage grouting, the black grout snaked around the red grout and flowed in a vertical upward direction. It was

observed for the north shaft that both the red and black grout had bonded well to the side of the shaft unlike the east shaft. Hence, the increased capacity of the north shaft was attributed to: the effect of preloading of soil by first-stage grouting; increase in skin friction; and an increased area of shaft tip used for other stages of the grouting.

Figure 5-44 Grout zone–North shaft.

Finally, Figure 5-45 shows the features of the grout zone formed at the west shaft bottom. Evident from the figure, a large continuous grout bulb formed at the shaft tip from all three stages of grouting. The yellow grout flowed alongside (around 3.5 ft.) of the shaft and also formed a small grout bulb at the shaft tip. During the second-stage grouting, the red

grout flowed around the hardened yellow grout and at one side of the shaft tip. During the third-stage grouting, the black grout snaked around the red grout from the second-stage grouting. It can also be seen that only the yellow grout (first-stage grouting) has flowed up alongside the shaft. In this case, the major contribution to the increased capacity of shaft is from the increased tip area (bigger tip bulb) and preloading effect.

Figure 5-45 Grout zone–West shaft.

From Figures 5-40 to 5-45, it is clear that the shafts with same diameter and length under same soil conditions have a different tip area after post grouting. The observed difference in axial capacity (discussed later) of these shafts after tip grouting is mainly attributed to this difference in post-grouted tip area. Moreover, the grout has flowed up

alongside the shaft mainly during the first-stage grouting for all shafts as observed in the first drilled shaft (8-ft. long) group tests. The upward flowing grout, after hydrating, increases the skin resistance, and thus, increases the axial capacity of the post-grouted shaft. However, this change in skin friction may not be assessed from first-stage tip grouting of shafts.

5.3.8 Measured Soil Stresses in the Vicinity of Group

Shown in Figures 5-46 to 5-48 are the soil stresses in the vicinity of the shaft measured during staged grouting as well as different load testing. It can be seen from the Figures 5-46 and 5-47 that the residual horizontal stress around the bottom side of the shaft increased to about four to six times the initial stress with staged grouting. The increase in soil stress was due to the upward flow of grout during tip grouting. First- and second-stage grouting caused a considerable increase in residual horizontal stress and the change in residual stress with third-stage grouting was not significant. The rate of increase in residual stress decreased

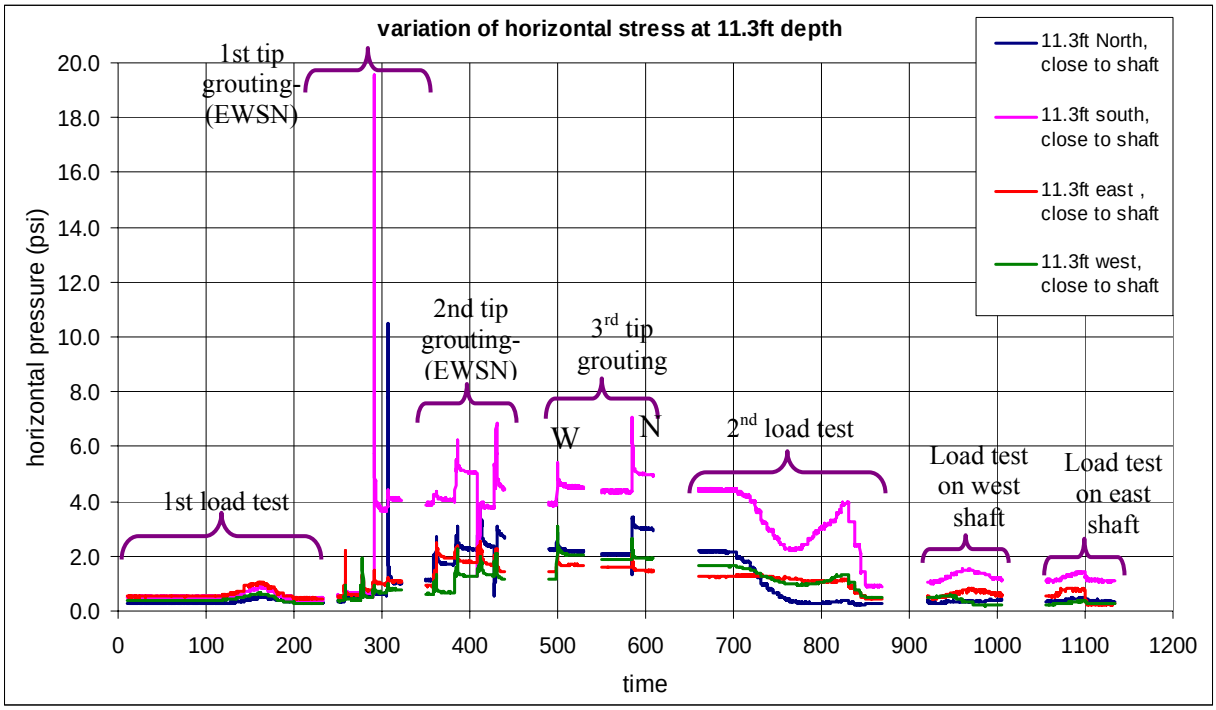

Figure 5-46 Variation of horizontal stress around the shaft at 11.3-ft. depth.

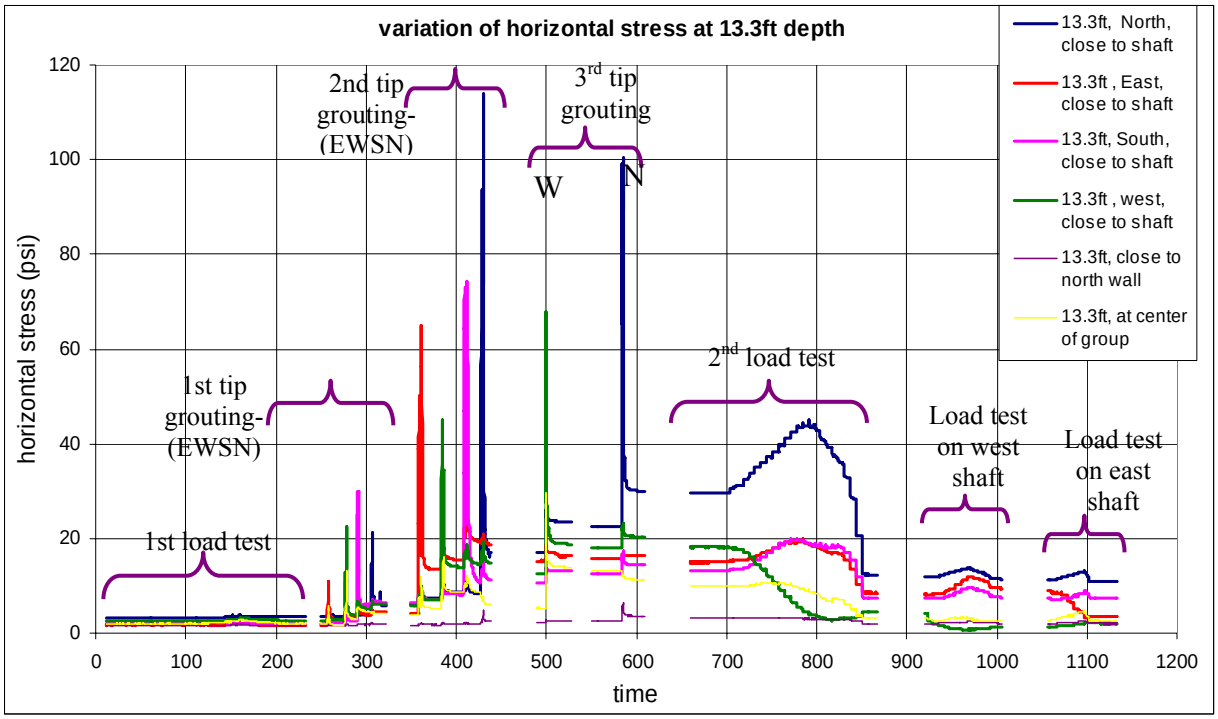

Figure 5-47 Variation of horizontal stress around shaft at 13.3-ft. depth.

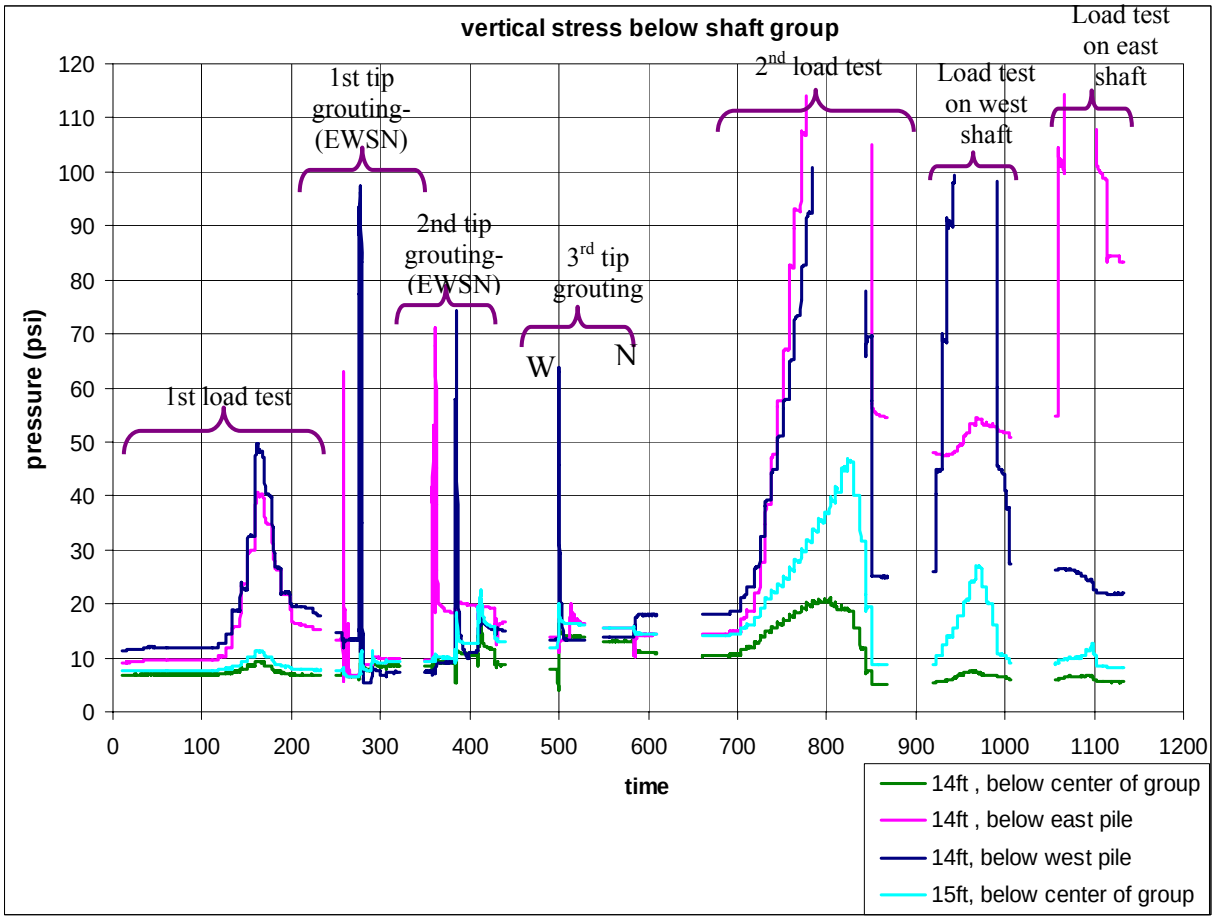

Figure 5-48 Variation of vertical stress beneath shaft group.

with each subsequent grouting. The increased residual horizontal stress resulted in a significant improvement in the skin resistance of the tip-grouted drilled shaft.

5.3.9 Analysis of Experimental Group Behavior

This section discusses the experimental behavior of the 8.5-inch diameter × 13-ft. long tip-grouted drilled shaft group based on the load-deformation data and soil stress measurement during the various stages of tip grouting and load testing.

Figure 5-49 shows the load versus vertical displacement at the top of each shaft during the load test prior to tip grouting, and Figure 5-50 is the DeBeer's log-log plot of the test. From the DeBeer's plot, it can be observed that the skin resistance of an individual shaft is in the range of 9.5 kips to 10.5 kips. The latter agrees with the skin resistance (10.5 kips) estimated using FDOT's FB-Deep software for an SPT values of $N = 6$.

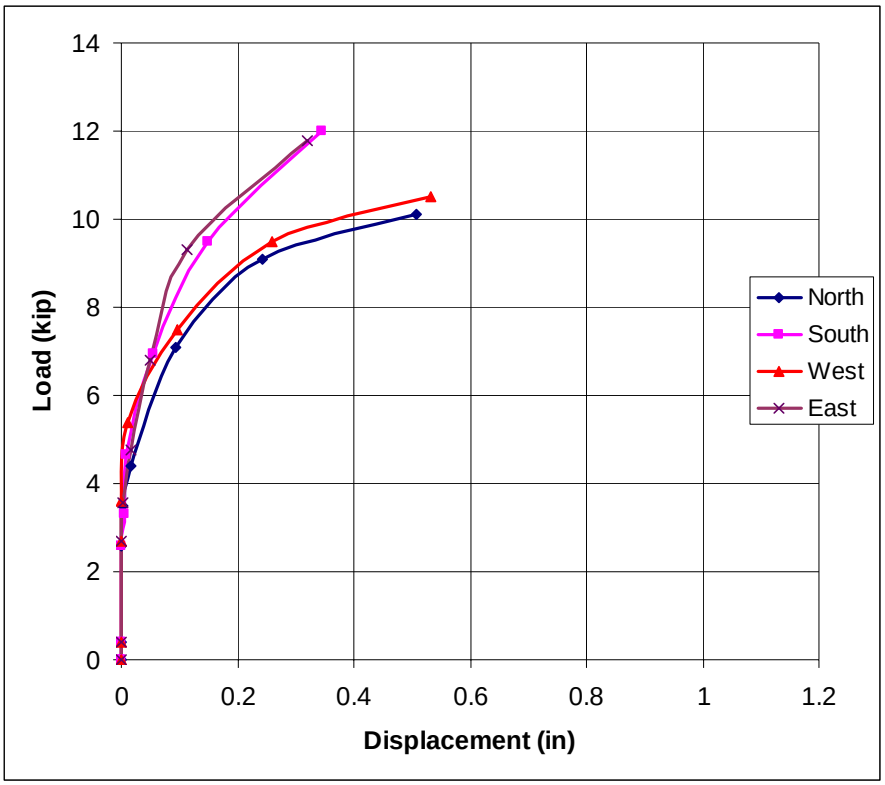

Figure 5-49 Load versus vertical displacement.

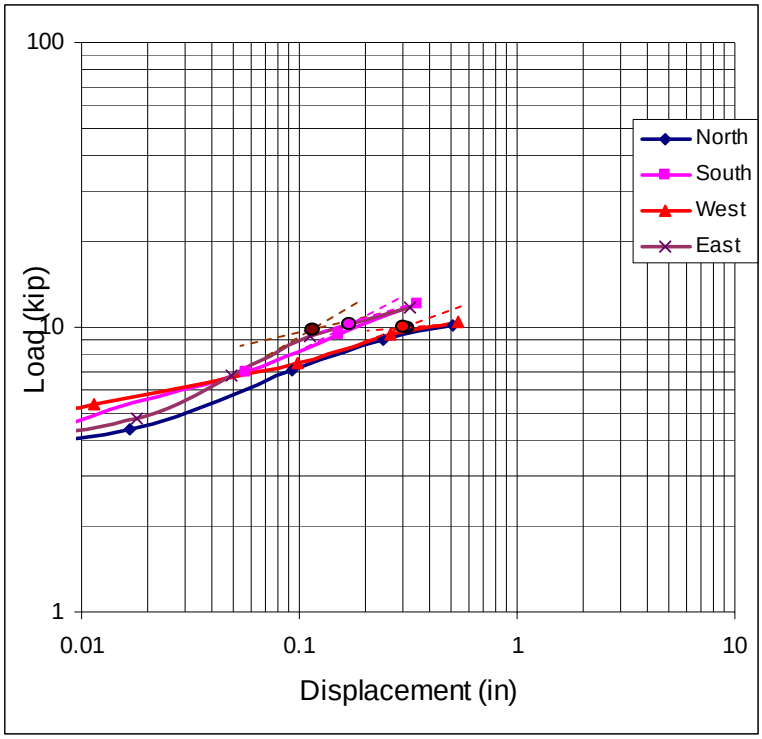

Figure 5-50 DeBeer's log-log plot.

Shown in Figure 5-51 is the load versus vertical displacement at the top of each shaft from the top down group test after tip grouting. Evident from the figure is that the load carried by shafts were significantly different (the west shaft carried the most load and the east shaft carried the least load) at the same displacement, and this was attributed to the difference in tip area (as observed in Section 5.3.7) of the shaft after grouting. As the maximum sustained grout pressure observed was more or less the same for all shafts, the effect of preloading (tip stress mobilization) should be similar. Note that the side resistance of the shafts may be slightly different depending on the grout coverage alongside each shaft. The maximum displacement of soil observed at the center of the group was 0.378 inch, which was much less than the average displacement of the individual shafts at 1 inch. This suggests that the shafts behaved individually during the load test (i.e., no/negligible group interaction).

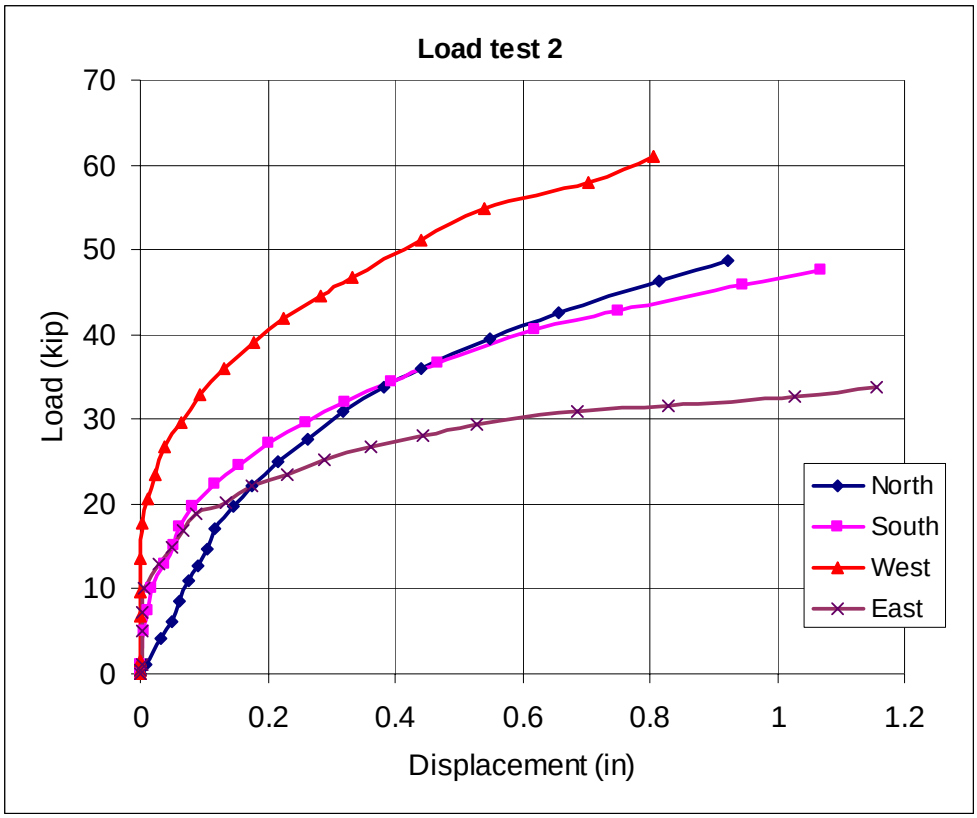

Figure 5-51 Load versus vertical displacement of tip-grouted shafts.

Figure 5-52 shows the load-displacement response of the west shaft when it was tested with the group and by itself. Again, the load-displacement response of the group and individually are quite similar, with differences attributed to displacement (mobilized tip). Similarly, Figure 5-53 shows the load-displacement response obtained from the test on the east shaft alone and together with the group. Again, the load-displacement response of the shaft from the group test matches the single results. Like the west shaft response, the load-displacement curve increases due to a higher mobilized tip due to large vertical movements.

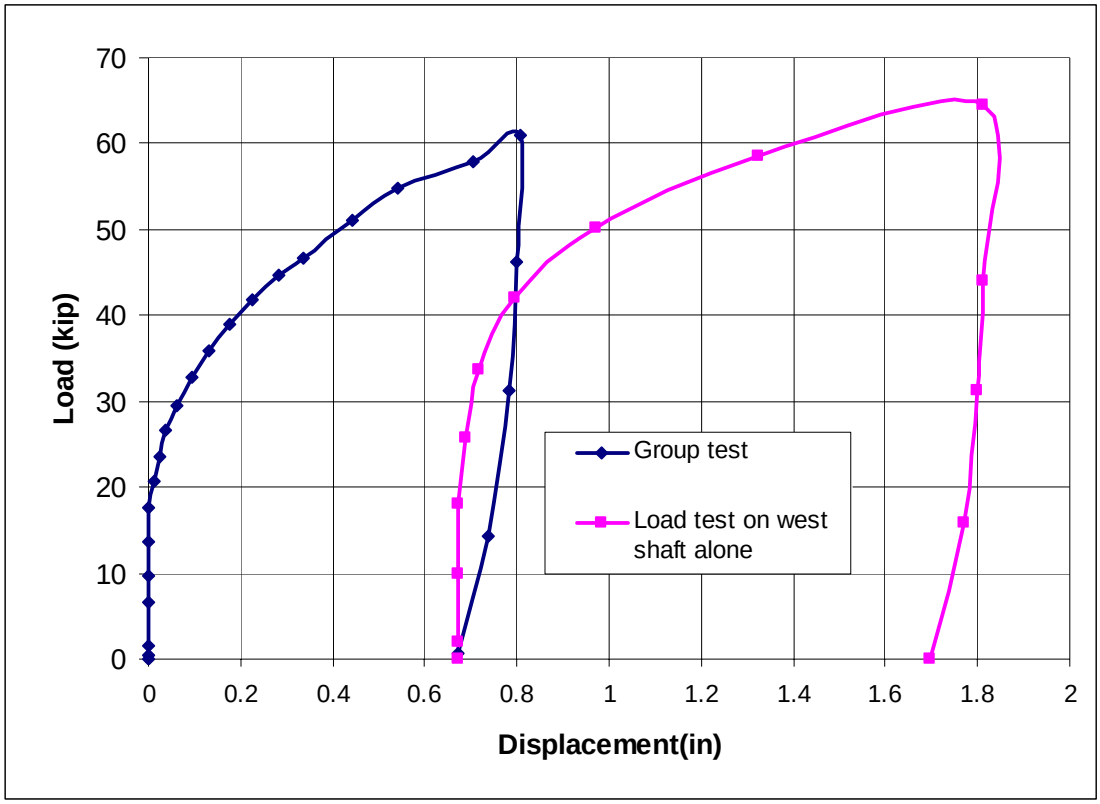

Figure 5-52 Combined load-displacement response of west shaft (from group test after grouting and loading on the west shaft only).

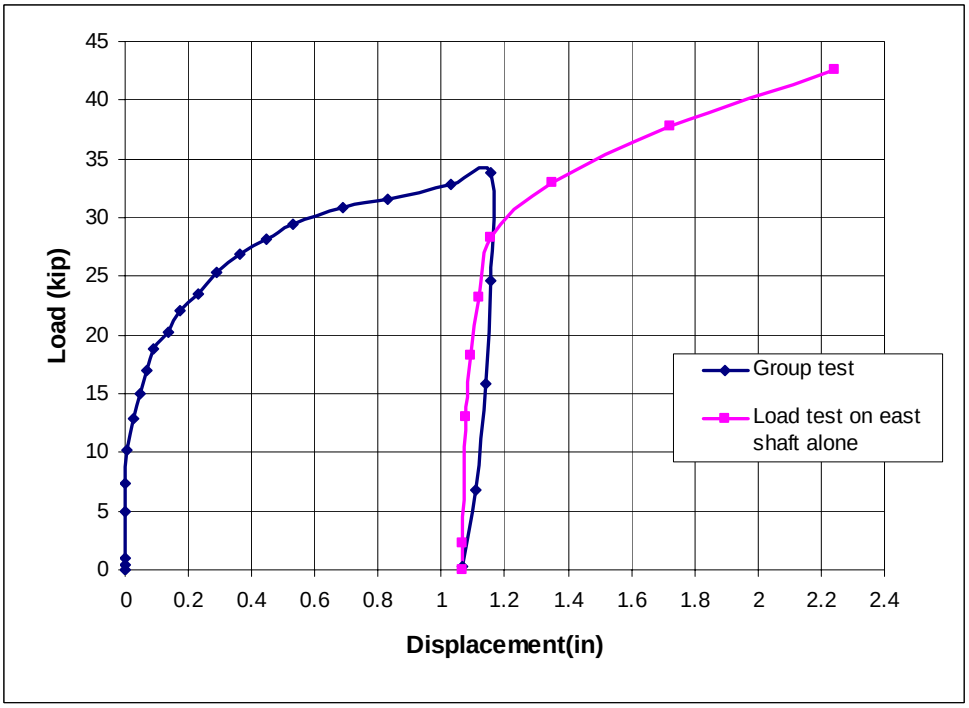

Figure 5-53 Combined load-displacement response of east shaft (from group test and loading on east shaft only).

Shown in Figure 5-54 is the measured displacement of the surrounding shafts when the load test was conducted on just the west shaft. It is apparent from the figure that the displacements of other shafts were negligible which reveals very little, if any, interaction between the shafts during loading. During the loading on the east shaft alone, similar behavior (see Figure 5-55) was observed in the adjacent shafts. In addition, it can be observed from the plot in Figure 5-56 that there was little, if any, increase in vertical stress below the east shaft during loading on the west shaft and vice versa. This implies that the axial group efficiency was nearly equal to 1.

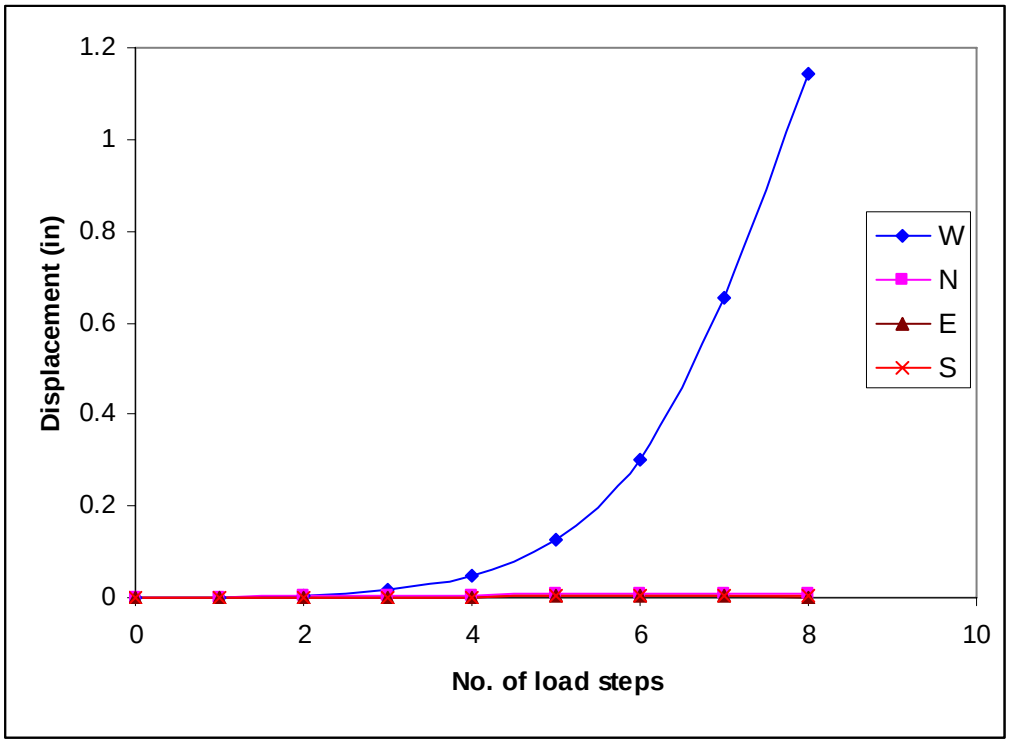

Figure 5-54 Displacement of the shaft during load test on the west shaft.

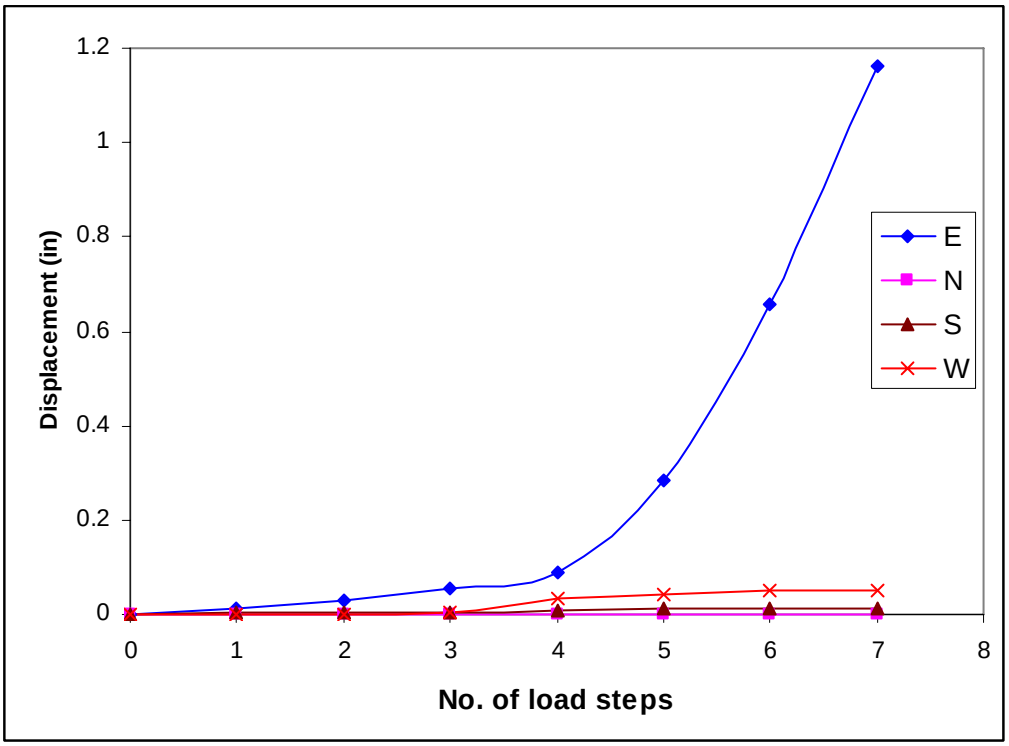

Figure 5-55 Displacement of the shafts during loading on the east shaft.

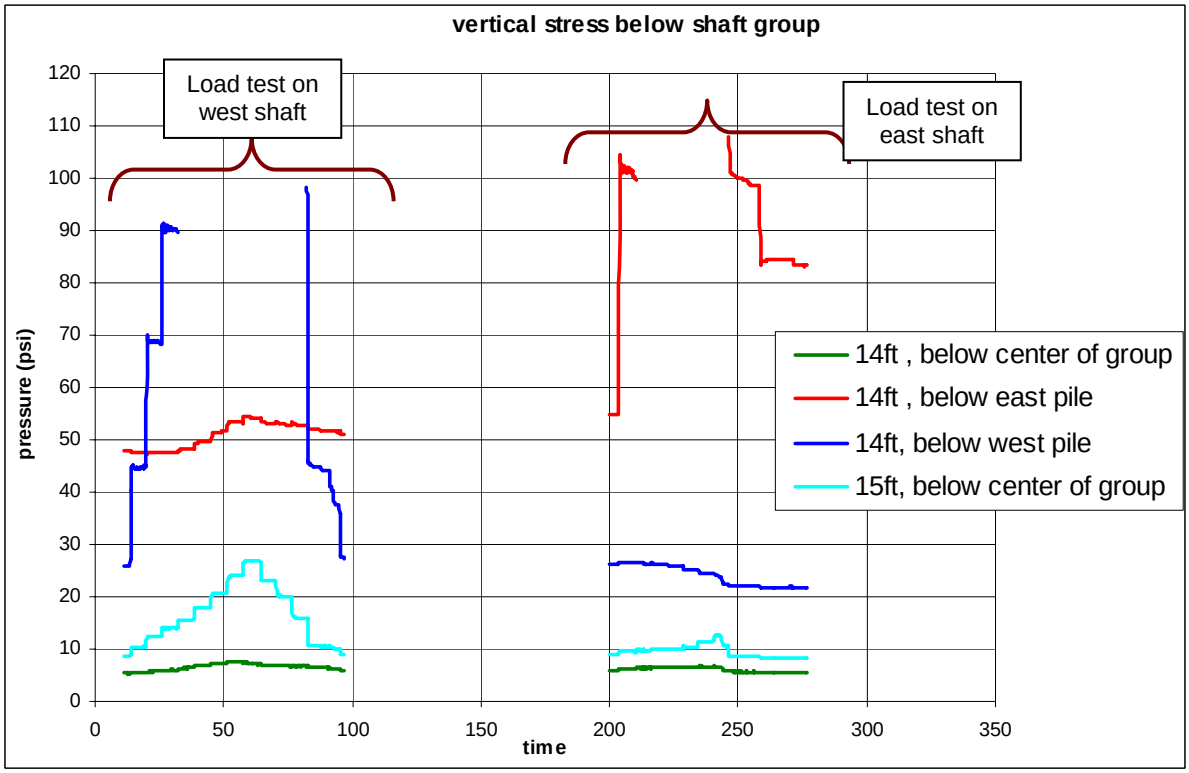

Figure 5-56 Vertical stress below the shaft group during load test on the west shaft and east shaft (*Note: Stress above 90-100 psi could not be obtained due to the capacity of stress gages being 100 psi*).

As mentioned in the analysis of the first drilled shaft group, care should be taken while using the grout pressure obtained from the first grouting to estimate the skin resistance of either the pre- or post- grouted shaft. Because the grout may flow upward along the shaft-soil interface, as observed in both experiments, a reduction in skin resistance was observed during tip grouting (i.e., grout is in a fluid state). Therefore, the grout pressure times effective tip area may not be equal to the skin resistance of the pre- or post-grouted shaft. However, it is realistic to use the sustained grout pressure measured during regrouting (second- or third-stage grouting) of shafts to estimate the skin resistance of a post-grouted shaft. Skin resistance of shafts estimated using grout pressures observed during the different staged groutings (skin resistance = grout pressure × tip area ($\pi \times 8.5^2/4$)) are given in Table 5-3.

Table 5-3 Skin Resistance Estimated Using Grout Pressure from Different Staged Grouting

Shaft	**First-Stage Grouting**		**Second-Stage Grouting**		**Third-Stage Grouting**	
	Grout Pressure	**Skin Resistance**	**Grout Pressure**	**Skin Resistance**	**Grout Pressure**	**Skin Resistance**
North	170 psi	9.6 kips	200	11.3 kips	200	11.3 kips
East	190 psi	10.8 kips	240	13.6 kips		---
South	200 psi	11.3 kips	270	15.3 kips		---
West	180 psi	10.2 kips	220	12.5 kips	200	11.3 kips

(*Note: Skin resistance is calculated using the measured grout pressure. However, actual grout pressure may be less than the measured grout pressure owing to the resistance offered by the grout pipe and rubber membrane*).

As can be seen in Table 5-3, the skin resistance estimated using the grout pressures measured during the first-staged grouting reasonably agreed with the initial skin resistance of the shafts before grouting. The skin resistance estimated using the regrouting data (second- and third-staged grouting) is about 20 to 30% higher than the initial skin resistance. This is

attributable to the increased surface area of the shaft and the increased horizontal stress around the shaft caused by the flow of grout alongside the shafts. The staged grouting of shafts helped in the following three ways: (1) increased the preloading effect (i.e., larger tip stress mobilization due to the increased grout pressure); (2) helped to form a grout bulb at the shaft tip (i.e., increased tip area), since the first-stage grouting increased the residual radial stress around the shaft, which in turn reduced the upward flow of grout during regrouting; and (3) the staged grouting data could be used to estimate the actual (final) skin resistance of a post- grouted shaft. Finally, from the load-displacement response and soil stress data, it can be concluded that the axial group efficiency of the tip-grouted shaft group was still approximately equal to 1 (i.e., no/little group interaction), even though some of the shafts had bigger grout bulbs at their tips.

CHAPTER 6
GROUP BEHAVIOR OF JET-GROUTED PILES AND GROUT-TIPPED DRILLED SHAFTS

6.1 Jet-Grouted Pile Group

6.1.1 Numerical Modeling of a Single Jet-Grouted Pile

To characterize the stresses near a jet-grouted pile, the installation and top down testing of a single jet-grouted pile was modeled using the two-dimensional finite element package, PLAXIS 2D. The pile and soil in the test chamber was modeled with the axisymmetric model with 15 noded triangular elements as shown in Figure 6-1. The sand in the test chamber was modeled with the Hardening Soil (HS) constitutive model (described by Schanz et al. 1999, coded in PLAXIS) and the pile was modeled as a linear elastic material. The Hardening Soil model resembles a Mohr-Coulomb model, but has additional features, such as a stress and strain dependent Young's modulus and a yield function that includes a cap to model irreversible plastic straining under primary compression. Material parameters used for sand and pile in the analysis are given in Table 6-1.

Table 6-1 Material Properties Used in PLAXIS

Parameter	Sand	Pile
Young's modulus, E (psi)	-	3.6×10^6
Deviatoric reference stiffness, E_{50}^{ref} (psi)	3030	-
Oedometer reference stiffness, E_{oed}^{ref} (psi)	3030	-
Unloading/reloading ref. stiffness, E_{ur}^{ref} (psi)	9090	-
Reference pressure, P^{ref} (psi)	4.6	-
Unsaturated unit weight, γ_{unsat} (pcf)	101	150
Saturated unit weight, γ_{sat} (pcf)	110	-
Friction angle, ϕ	31	-
Dilation angle, ψ	0	-
Poisson's ratio, υ	0.25	0.15
Power, m	0.5	-

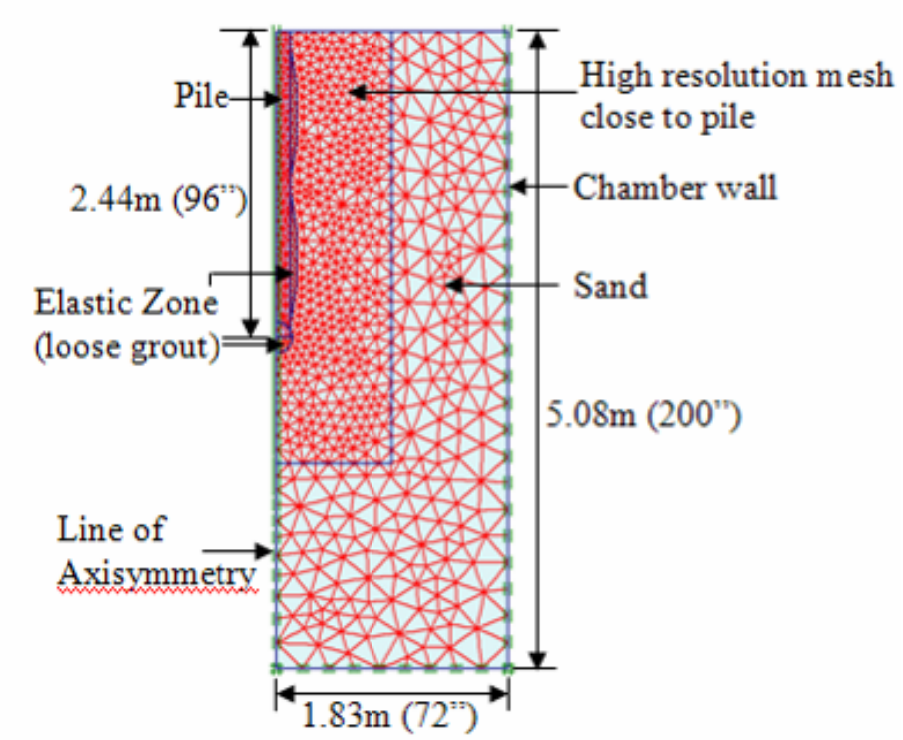

Figure 6-1 Finite element discretization.

For the simulation, the chamber wall was restricted from both radial and vertical displacements. The bottom boundary was also restricted; however, based on the distance to the pile, its affect was negligible. The square pre-cast jet pile was modeled as an equivalent circular pile with the same cross-sectional area. For the analysis, the pre-cast pile was embedded at the installation depth at the start of the calculation (i.e., the jetting process was not simulated), since PLAXIS 2D does not allow for simulation of the whole installation process. The membranes were initially characterized as a soft linearly elastic zone (E = 100 psi and υ = 0.25) as shown in Figure 6-1. The zones were located at the top and bottom of the pile, as well as the pile tip, which represent loose soil occupying the week zone formed around the shaft and tip during the jetting process. Next, the grouting process was simulated by applying positive volumetric strain (expansion) incrementally to each of the elastic zones. The sequence of simulation of grouting was the same as the actual grouting of the pile (i.e.,

first side grouting, then top down, and tip grouting). The expansion of each elastic zone was controlled by the final diameter of the respective grout bulb. From the experimental study, it was observed that the radial stress around pile increased during grouting and then immediately diminished after grouting to a residual value. This behavior was attributed to the elastic unloading after stopping the grout pump and the incompressible response of the grout. In the PLAXIS analysis, the unloading was simulated by applying volumetric contraction to the respective elastic zone after the application of the volumetric expansion representing grouting. The amount of applied volumetric contraction was controlled by the magnitude of measured residual stress around the pile, i.e., residual horizontal stresses measured in the chamber tests near the membranes. Next, each elastic zone's properties were replaced by elastic properties representative of hardened grout. Since the grouting process is a large strain problem, the Updated Mesh Option available in PLAXIS was used in the analysis. Figure 6-2 shows a typical deformed mesh after the simulation of both side and tip grouting. The maximum expansion pressure from finite element analysis for the top zone, bottom zone, and pile tip were 50 psi, 90 psi and 174 psi, respectively. This was in reasonable agreement with limit pressure (at 3 ft., 60 psi; at 6 ft., > 75 psi) measured from the PMT at the same respective depths. However, the side grout pressures observed during experimental study in FDOT project # BD545, RPWO#31 for the 8-inch and 6-inch square piles (80 psi–top zone; 120 psi–bottom zone) were more than the respective expansion pressure from PLAXIS analysis. The difference may be attributed to: (1) the resistance of semi-rigid membrane confining the grout zones, and (2) the rough interface between the membrane and the surrounding soil. It was believed the interface element should be attached to the sand with an interface friction angle equal to that of sand (i.e., no soil strength reduction) due to the rough

membrane. After the simulation of jet-grouted pile installation, the top down pile load test was simulated by the activation of a distributed load on top of the pile.

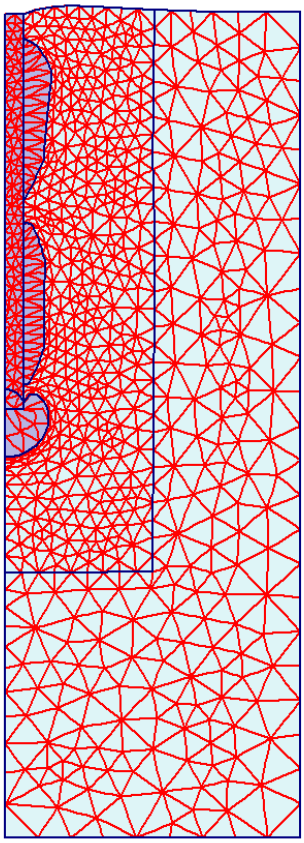

Figure 6-2 Finite element mesh after the simulation of jet-grouted pile installation.

Of interest are the principal stress states in the soil near the pile after grouting, as well as during top down load testing. As identified in FDOT BD545-31, the minor principal stress near the grouted pile was the vertical stress. Shown in Figure 6-3 are the original estimates of the vertical stress in terms of the soil's unit weight and coefficient (K_g) chart updated using the numerical analysis for different soil strengths along with measured experimental results (Figure 2-9). Knowing the vertical stress near the pile, the limiting unit side shear (Equation 2.19) may be computed.

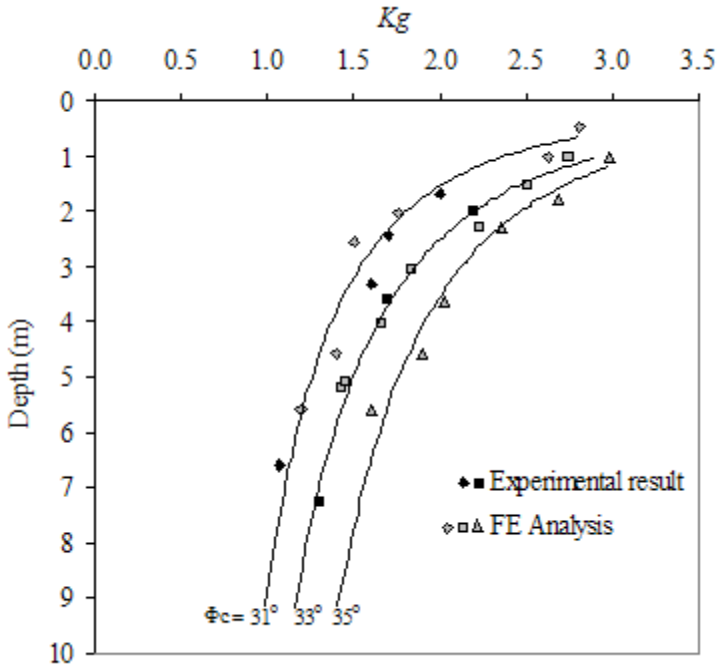

Figure 6-3 Estimate of grout vertical stress coefficient, K_g.

6.1.2 Expected Grout Pressures During Grouting of a Jet-Grouted Pile

As identified earlier, cavity expansion theory may be used to estimate grout pressure during side grouting and tip grouting of a jet-grouted pile. Side grouting of jet-grouted pile resembles the expansion of a cylindrical cavity and tip grouting resembles the expansion of a spherical cavity. Cylindrical cavity limit pressure, as well as spherical cavity limit pressure, are available (e.g., Yu and Houlsby 1991; Salgado et al. 2001) as a function of depth and soil properties.

Basically, cavity expansion processes are of two types: (1) expansion from a finite radius; and (2) expansion from a zero initial radius (i.e., cavity creation problem). Side grouting of a jet-grouted pile is the case of cavity expansion from a finite initial radius (radius of pile). In a cavity creation problem, the cavity is expanded from a zero initial radius and eventually reaches the limit pressure (e.g., pile driving operation). In the case of

cavity expansion from a finite radius, an increasing pressure is required for the cavity to continue expanding with a steady state condition attained only at very large expansion. That is, limit pressure is reached when the ratio of current cavity radius to initial radius approaches infinity. However, in the case of jet-grouted pile, a typical expansion ratio is two (i.e., the ratio of radius of side grout bulb to radius of pile), hence the pressure on the cavity wall developed during the grouting of jet-grout pile may be less than the limit pressure. In fact, side grouting of pile (with semi-rigid membrane) is not a pure cylindrical cavity expansion, but an expansion intermediate to cylindrical and spherical cavity expansion. Therefore, the limit pressure should be an intermediate value to the cylindrical and spherical cavity limit pressures. Moreover, a semi-rigid membrane around the grouting zone may exert resistance to expansion and may result in higher grout pressures than suggested by cavity expansion theory. Thus, three factors, namely expansion ratio, bulb shape, and membrane resistance, can make the observed side grout pressure different than the cylindrical cavity limit pressure. Table 6-2 shows a comparison of the measured pump pressures and the limit pressures estimated using Yu and Houlsby's closed form solution (for Mohr-Coulomb material with critical state friction angle, $\phi_c = 31°$; dilatation angle, $\psi = 0°$; and Poisson's ratio, $\upsilon = 0.25$) and Salgado's limit pressure chart (for $\phi_c = 31°$; relative density, $D_r = 50\%$) with direct measurements from the pressure meter test. Evident in the table, the measured side grout pressures at respective depth are greater than all of the predicted limit pressures, and the difference may be attributed to the resistance given by the semi-rigid membrane, as well as the shape of the expansion bulb (i.e., not cylindrical). However, the theoretical predicted side grout pressure may be considered a conservative estimate of expected grout pressures. In the case of tip grouting, both Yu et al. and Salgado's spherical cavity expansion theory are quite close to the measured results.

Table 6-2 Measured and Predicted Grout Pressures

	Side Grouting		Tip Grouting
	Top Zone 2.75 ft.	**Bottom Zone 6.25 ft.**	
Measured pressure (*average)* (psi)	80 psi	130 psi	230 psi
Yu and Houlsby's solution (1991) (psi)	56 psi	104 psi	210 psi
Salgado's chart (2001) (psi)	65 psi	110 psi	235 psi
PMT (psi)	60 psi	> 75 psi	--

6.1.3 Group Action of Jet-Grouted Pile Group

From the experimental study of the jet-grouted pile group at typical 3D spacing (3 × diameter of pre-cast pile section), it was observed that the displacements of piles were relatively uniform during the group test irrespective of the amount of load carried by each pile. It was also observed that the soil deformation at the center of the group was almost identical to the average displacement measured at the pile head as shown in Figure 6-4. Moreover, the deformation of the soil outside the footprint of the group within the test chamber (e.g., Figure 6-5) was also nearly uniform and it exhibited a quadratic variation from the group towards the chamber wall. The above three observations suggest that the pile group behaved as a block during axial loading.

The experimental and analytical analysis of jet-grouted piles suggested a significant increase in both densification of soil around the piles with an increase in the horizontal stress (σ_h) and shear modulus of soil in close proximity of the piles. Consequently, the pile has a much higher ultimate side resistance compared to traditional driven piles/drilled shafts. In the case of a jet-grouted pile installed in a group, the side grouting of adjacent piles increased the confining stress and shear modulus of the soil confined within the group. Consequently,

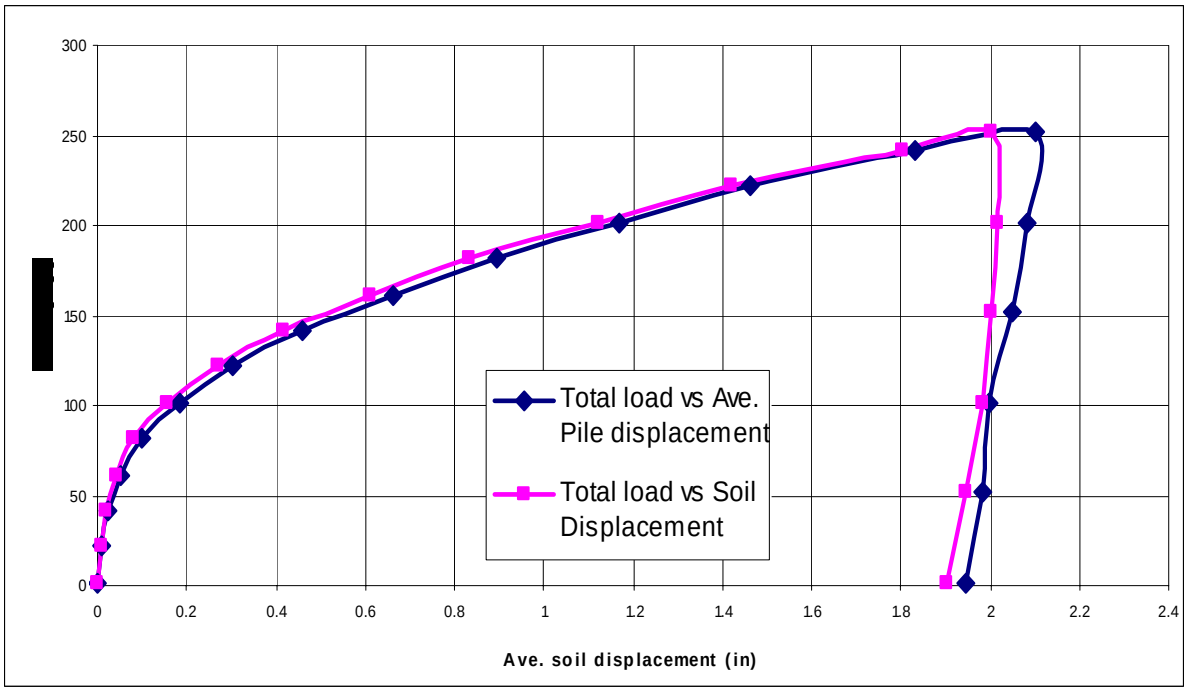

Figure 6-4 Total load versus average pile displacement and soil deformation (8-inch jet-grouted pile group).

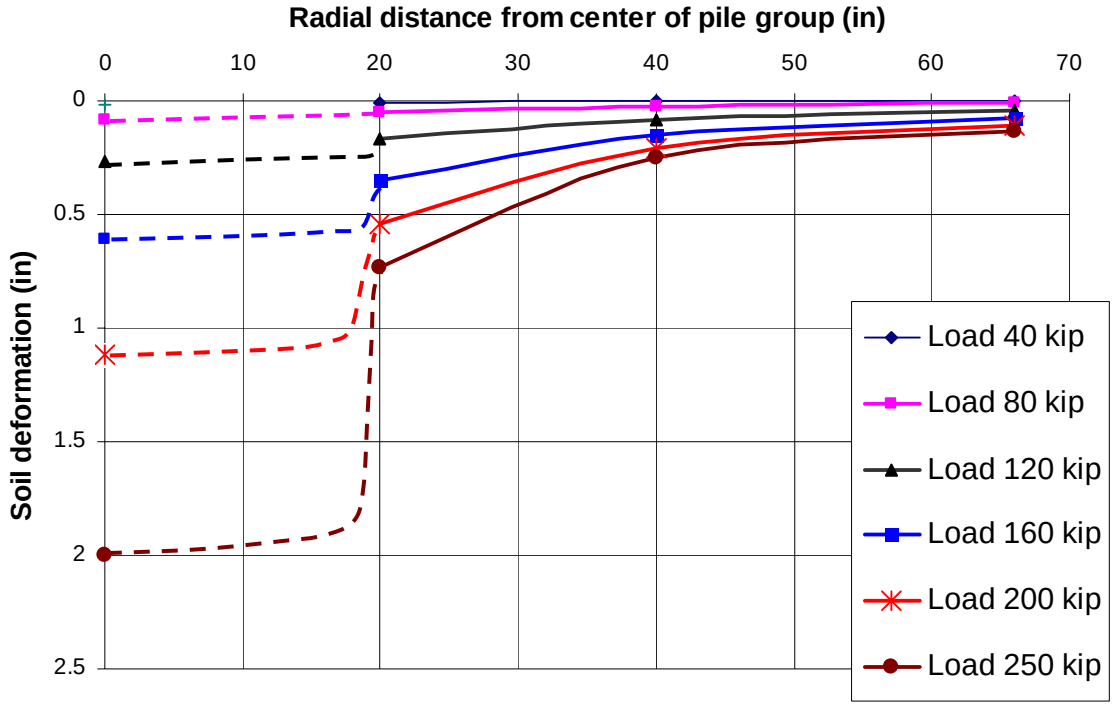

Figure 6-5 Soil deformation profile (8-inch jet-grouted pile group).

the soil within the footprint of the group underwent much smaller shear strains and the pile-soil-mass behaved as a rigid body. However, outside the footprint of the jet-grouted pile group, the horizontal radial stresses dissipated quadratically, and the soil's shear modulus also diminished quadratically. Therefore, the grouted pile group failed as a block (i.e., uniform movement) within the group, but quadratically outside the group under axial loading. The vertical side capacity of the group may be obtained by multiplying the shear stress on the surface of any single jet-grouted pile with the surface area of the block (i.e., block perimeter of the group × the length of the pile) which will be less than the side resistance of single jet-grouted pile × the number of piles in the group. In the case of the group tip resistance, grouting of the individual piles developed spherical cavity expansion stresses around each pile, as well as densification of soil (i.e., increased shear modulus) between the bulbs (primarily within the group foot print) through displacement of the soil in the radial direction. Consequently, when the group was loaded, the stresses from each pile transferred to the center of the group (i.e., superposition) resulting in higher stresses at the pile group center (see Figure 4-50) and block tip resistance (group foot print area × unit tip resistance) under axial top down loading developed. In the next section, an appropriate methodology proposed for the prediction of load displacement response of single jet-grouted piles/pile groups is discussed.

6.1.4 Development of T-Z Curve and Q-Z Curve for Single Jet-Grouted Pile/Jet-Grouted Pile Group

Load transfer methodology proposed by McVay et al. (1989) is used here to estimate load-displacement relation of jet-grouted pile/pile group. The load-transfer between pile and soil is actually based on two sets of load transfer functions. One set characterizes the load-transfer that takes place alongside the pile, which is commonly referred to as T-Z curves.

The other set characterizes the load transfers that occurs at the tip of the pile and is commonly referred to as Q-Z curves. Load transfer functions proposed by McVay et al. (FB-Multipier) are given as,

$$\textit{T-Z curve:} \qquad Z = \left(\frac{\tau_0 r_0}{G}\right).\left[\ln\left[\frac{r_m - \beta}{r_0 - \beta}\right] + \left[\frac{\beta.(r_m - r_0)}{(r_m - \beta)(r_0 - \beta)}\right]\right] \tag{6.1}$$

$$\textit{Q-Z curve:} \qquad Z = \frac{Q(1-\upsilon)}{4R_0 G\left(1 - Q\frac{R_f}{Q_f}\right)^2} \tag{6.2}$$

where r_0 = radius of pile;
r_m = radius of zone of influence;
τ_0 = shear stress on pile-soil interface;
G = Reloading shear modulus;
β = $r_0 \tau_0 . \frac{\mathrm{Rf}}{\tau_{\max}}$;
R_f = ratio of failure shear stress to its ultimate;
R_0 = radius of tip bulb;
υ = Poisson's ratio;
Q = mobilized tip resistance;
R_t = ratio of failure to ultimate tip resistance; and
Q_f = ultimate tip resistance.

Both load transfer functions are hyperbolic, and assume a reduction in soil modulus with strain in the radial direction. McVay's equation for unit skin friction of jet-grouted piles (Equation 2.19) is used to determine τ_{max} for T-Z curve. Ultimate tip resistance Q_f is obtained by multiplying the ultimate unit end bearing (q_b) with the area of tip. Correlation between spherical cavity limit pressure (p_{lim}) and ultimate end bearing pressure suggested by Randolph et al. (1994) is used here to estimate unit tip resistance q_b of the jet-grouted pile.

$$q_b = \left[1 + \tan\phi_c \tan\left(45 + \phi_c/2\right)\right] p_{lim} \tag{6.3}$$

The abovementioned methodology could be used for both single jet-grouted pile and jet-grouted pile group. In the case of a pile group, equivalent radius of block (i.e., equivalent

radius of group footprint) should be used in Equations 6.1 and 6.2. The surface area of the block should be used for estimating total side resistance of the group and the effective block footprint area should be used for estimating ultimate tip resistance (Q_f). Total axial load-displacement response of jet-grouted pile/group will be obtained from the combination of the T-Z response and Q-Z response of the pile/group.

Figure 6-6 shows a comparison of the predicted load-displacement curve for 8-inch square jet-grouted piles using the proposed methodology for the load test given in FDOT project # BD545 31, along with the finite-element prediction.

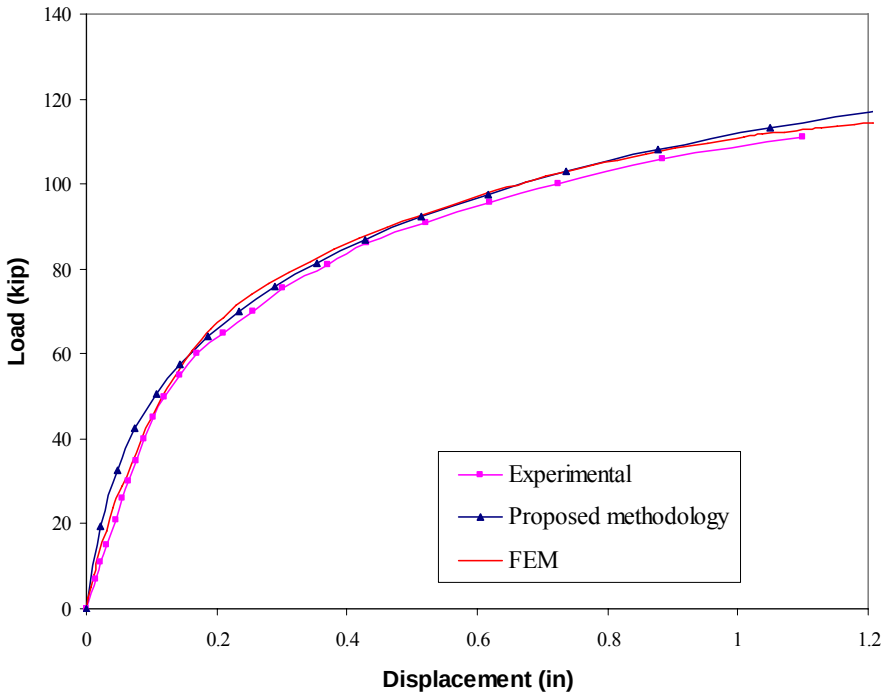

Figure 6-6 Comparison of load-displacement curves for 8-inch square × 8-ft. long (20-inch diameter bulb) jet-grouted pile.

Similarly, Figure 6-7 shows the results for the 6-inch square jet-grouted pile in FDOT report BD545-31. Evidently, the predicted load-displacement response for single jet-grouted piles using the proposed methodology was quite comparable with the measured load-displacement response and finite element prediction (Section 6.1).

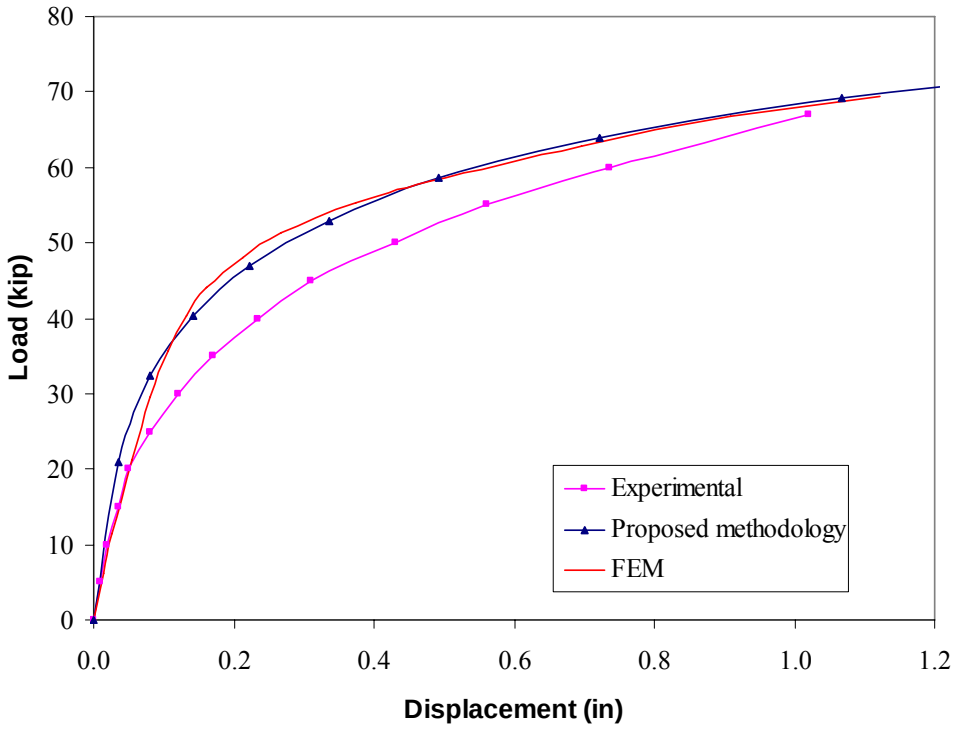

Figure 6-7 Comparison of load-displacement curves for 6-inch square × 8-ft. long (15-inch diameter bulb) jet-grouted pile.

Shown in Figures 6-8 and 6-9 are the predicted and measured load-displacement responses of the 8-inch square × 8-ft. long (16-inch side grout bulb) pile group and the 4.5-inch diameter × 8-ft. long (10-inch side grout bulb) pile group, respectively. Again, the group predictions were obtained using the block areas (side and tip) with Equations 6.1 through 6.3. Similar to the single jet-grouted pile response, the predicted group load-displacement curves of the four jet-grouted piles agreed reasonably well with the measured load-settlement response. Also shown in Figure 6-10 is DeBeer's estimate of side resistance based on linear slopes of the log-log plot of load versus displacement (both measured and predicted) of the pile 8-inch square × 8-ft. long group. It can be seen that the skin resistance

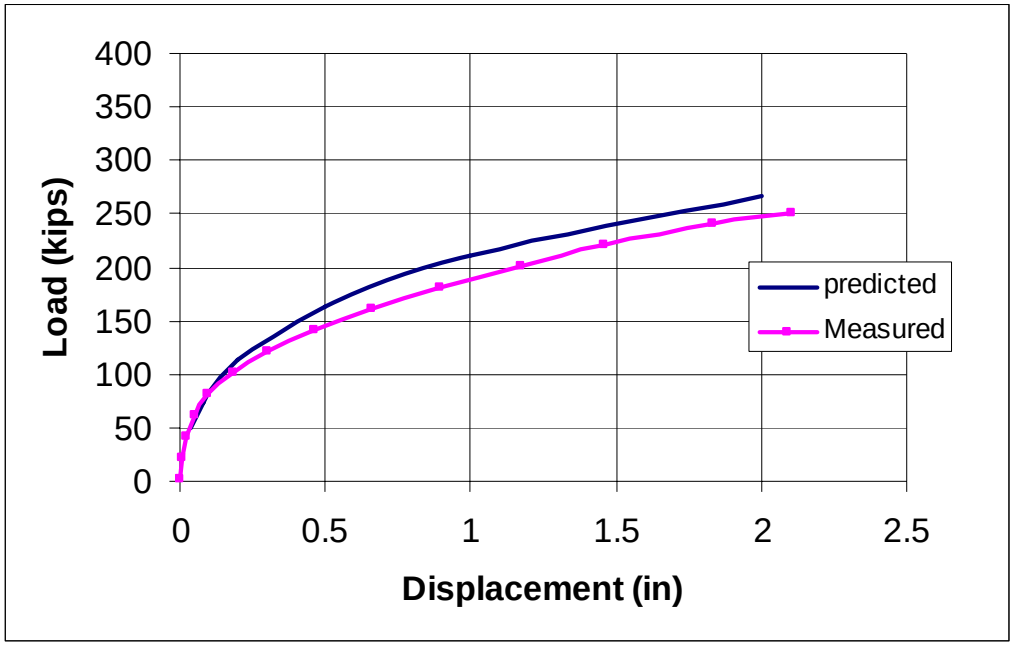

Figure 6-8 Comparison of predicted and measured load displacement response of 8-inch square × 8-ft. long jet-grouted pile group.

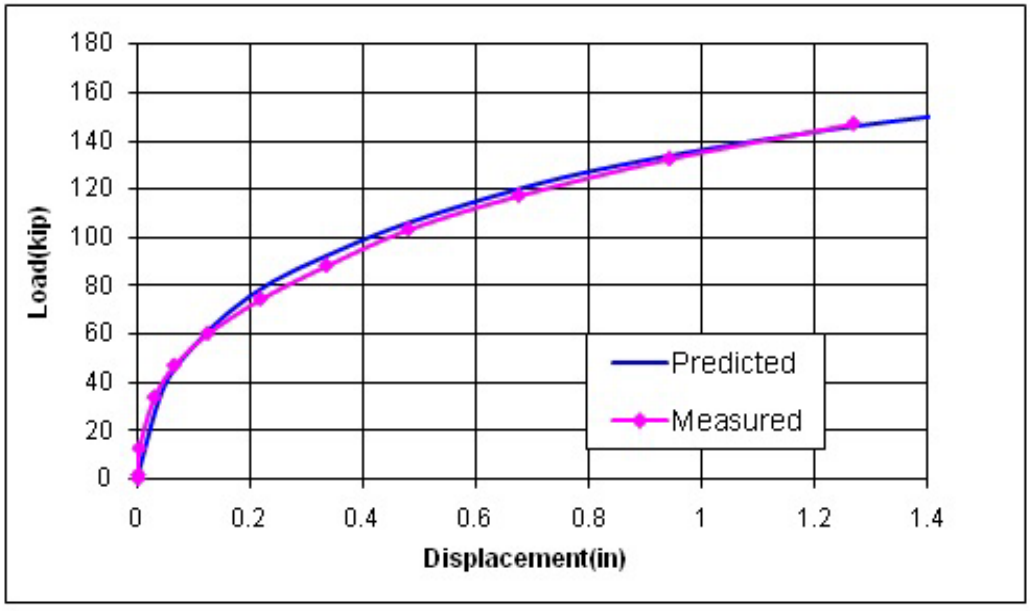

Figure 6-9 Comparison of predicted and measured load displacement response of 4.5-inch diameter × 8-ft. long jet-grouted pile group.

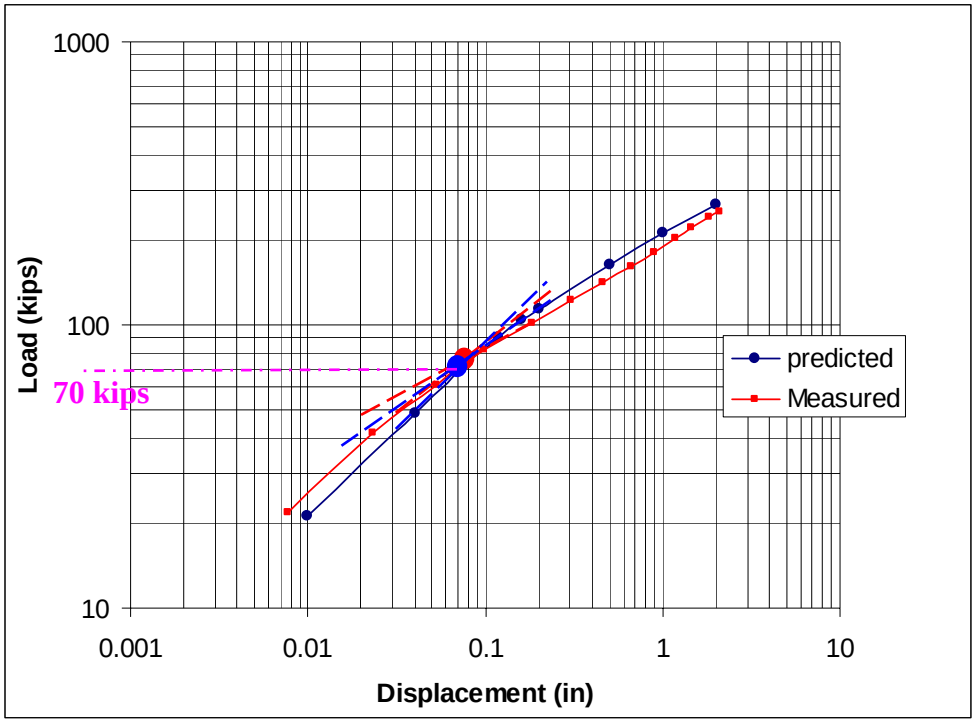

Figure 6-10 Log-log plot of load versus displacement response of 8-inch square × 8-ft. long jet-grouted pile group.

of the pile group estimated from DeBeer's plot is 70 kips (corresponding to the point of slope change), which was in good agreement with the predicted skin resistance shown in Table 4-2. Hence, the proposed design methodology can be used to predict the load-displacement response of single jet-grouted pile, as well as jet-grouted pile group with reasonable accuracy.

6.2 Grout-Tipped Drilled Shaft Group

6.2.1 Factors Affecting the Capacity of Grout-Tipped Drilled Shafts

Experimental study (Section 5.2.7) of grout-tipped drilled shafts revealed that during grouting, the grout flows up along the shaft-soil interface (weakest path) after filling the void space beneath the shaft tip. In contrast to the jet-grouted piles, the soil above the shaft tip has a very low radial stresses (relief due to drilling) compared to the vertical stresses at the shaft

tip, and hence, the grout was always observed to flow in an upward direction. In literature (Mullins and Dapp 2006), it was found that the skin resistance of shafts may be estimated by multiplying the measured tip grout pressure with shaft tip area. However, this approach may underestimate the actual skin resistance of shafts since the upward flowing grout may reduce (fluid grout carries no shear) the shaft's side friction during the grouting process. Moreover, the upward grout flow increases both radial stress around the shaft and surface area of shaft after hydration. This results in an increase in the skin resistance of the shafts as a function of the extent of grout zone around shaft. Therefore, a single grouting, the initial grout pressure times tip area may not be equal to the total skin resistance of shaft.

Since a single tip grouting may be difficult to predict the final skin resistance of a shaft, a possible alternative is to carry out multiple stage groutings and used the final monitored grout pressure to estimate skin resistance of the post-grouted shaft. It was observed from the experimental data that only small grout flows occurred during the later tip grouting (e.g., second and third stages). If the later stage higher grout pressures were assumed to act over the original tip area, higher skin resistance would be found, which is representative of increased capacity. For instance, an increase in skin resistance of 20 to 30% was observed when second-stage grout pressure was used to estimate skin resistance of post-grouted shafts. The latter was attributed to the hardened grout zone around the shafts from the initial tip grouting.

As identified in the literature, a post-grouted drilled shaft was developed to mobilize some of the unusable shaft tip resistance through soil preloading. Specifically, tip grouting compresses the soil immediately below the shaft tip increasing its stiffness, but not necessarily the soil's strength. The latter is suggested based on the observed low grout pressures during tip grouting versus the high tip grout pressures (220 to 250 psi) for the jet-

grouted piles at the same grouting depths. The higher grout pressures for the jet-grouted piles were only available after the higher horizontal stresses (i.e., major principal stress) were mobilized due to side grouting of the piles with the membranes. In contrast, the grout pressure observed during tip grouting of 8-ft. long drilled shafts was only one-third (85 psi) of that for the jet-grout piles because of the smaller horizontal stresses at the shaft tip which was readily overcome by the grout at the tip flowing upwards. Therefore, it is postulated that grouting of a drilled shaft tip just preloads the soil, and the grout pressure times the shaft tip area will be mobilized under small deformations during subsequent axial loading (i.e., higher stiffness); however, the ultimate tip resistance at large displacement may not be altered.

Excavation of post-grouted shafts revealed that the tip area of the shafts had increased due to tip grouting. For instance, the load-displacement response of multiple stage post-grouted drilled shafts (13-ft. long) revealed that the loads carried by the shafts were much higher even though the preloading pressures (i.e., grout pressure) were more or less the same. This difference in resistance was attributed to the different tip area of the post-grouted shafts. Therefore, drilled shafts with same initial diameter and length, in similar soil conditions, may exhibit different load resistance after post grouting depending on the grout volume pumped and number of grouting stages performed.

The experimental results suggest that the total capacity of a post-grouted shaft at permissible service displacement may depend on the three important factors: (1) increase in side resistance due to upward grout flow alongside of shaft; (2) preload or grout tip pressure; and (3) size of the grout tip bulb at the tip of the shaft. Unfortunately, it is not possible to predict the expected final tip area of the shaft, even though it has a significant impact on the shaft's total capacity, however, its assessment may be improved through stage grouting.

6.2.2 Group Behavior of Grout-Tipped Drilled Shafts

Axial top down testing of grout-tipped drilled shaft groups at typical 3D spacing (Chapter 5) revealed that displacement of soil at the center of the group was much less than the average displacement of shafts. During the top down testing of individual shafts in the group, it was observed that the displacement of other shafts was insignificant. Moreover, the increase in vertical stress measured beneath one shaft during the loading on another shaft was negligible. The above observations suggest that there was very little or no shear transfer between the shafts. Moreover, the experimental data suggest that there was little increase in radial stress and soil displacement around shaft tips during tip grouting which was attributed to low grout pressures as a result of the grout flowing up alongside the shafts. The negligible increase in confining stress and soil displacement was not enough to improve the soil stiffness between shafts, and consequently, high shear stain developed in soil around the shaft tip during axial group loading. The experimental data revealed that the group failed through individual failure of each shaft within the group. For instance, Figures 5-28 and 5-29 suggest little, if any, displacement transfer from single shaft to nearby neighboring shafts. Hence, the resistance of the group is suggested to be equal to the single grout-tipped shaft resistance × the number of shafts in the group. Or, the axial group efficiency of the grout-tipped drilled shafts at typical 3D spacing is equal to one (1).

6.2.3 Estimation of Group Resistance of Grout-Tipped Drilled Shaft Group

As discussed in the last section, group resistance of grout-tipped shafts can be determined by multiplying the single grout-tipped drilled shaft resistance with the number of shafts in the group. Therefore, to estimate group resistance the single grout-tipped drilled shaft resistance must be found first. However, the axial resistance of a grout-tipped drilled

shaft depends on the increase in side resistance due to upward grout flow, preloading pressure (grout pressure), and increased tip area of shaft as described in Section 6.2.2. Moreover, the increase in skin resistance and shaft tip area with tip grouting are subjective in nature and may not be possible to predict accurately. Hence, the minimum increase in resistance of grout-tipped drilled shafts over conventional shafts at permissible service displacement will be at a minimum due to preloading of soil with the applied grout pressure. Currently, there is only one design method (Mullin et al. 2001) available in the literature to predict the unit end bearing of grout-tipped drilled shaft. Mullin et al. (2001) developed the design methodology based on the field tests data of post-grouted drilled shafts. Figure 6-11 shows the comparison of unit end bearing of post-grouted drilled shafts determined from the test data of 8-ft. shafts and the unit end bearing predicted using Mullin's method (SPT N = 6). Both measured grout pressure (85 psi) and the expected grout pressure (60 psi) estimated using side resistance of shaft (i.e., expected grout pressure = side resistance/tip area) were used to estimate unit end bearing.

It can be seen in Figure 6-11 that the unit end bearing predicted using measured grout pressure and expected grout pressure estimated from the side resistance of shaft are quite different. Also evident from the figure, Mullin's method overestimated the unit end bearing of the post-grouted shaft. This difference may be attributed to the fact that Mullin et al. used top load-displacement response from field tests to develop the design chart along with empirical relationship for TCM (tip capacity multipier, Equation 2.17 and Figure 2-7). Moreover, the post grouting of shafts has a variable influence of shaft tip area, and the present experimental study showed the latter area has a great influence on the tip resistance of post-grouted shafts. In addition, the actual unit end bearing should be found from the tip load divided by final tip area of shaft.

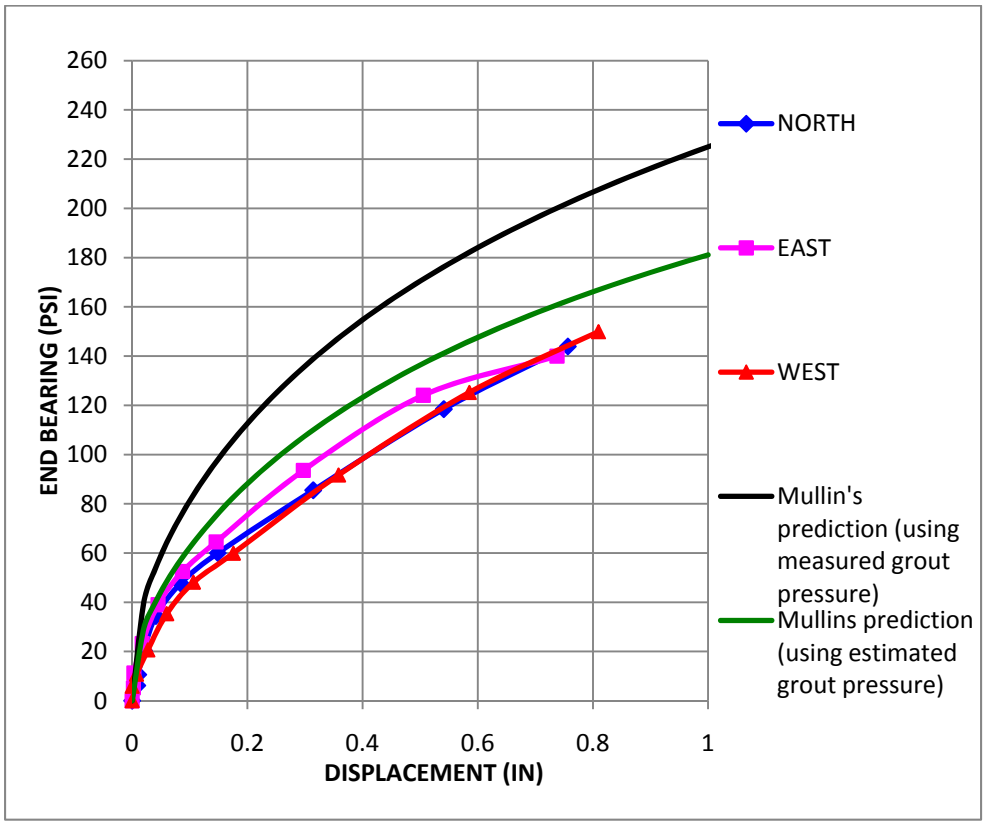

Figure 6-11 Comparison of unit end bearing (8-ft. long shafts).

Figure 6-12 shows the comparison of measured load displacement response of 8-ft. shafts and the load-displacement response predicted using the Mullin's method. In the figure, total resistance using Mullin's method for each displacement was determined by adding initial side resistance of shaft to tip resistance (equal to initial tip area × the unit end bearing, Figure 6-11).

In Figure 6-12, it can be observed that total load-displacement response predicted using Mullin's method agreed reasonably well with the measured load-displacement response of a few of the shafts even though it had overestimated unit end bearing (Figure 6-11) and over predicted the resistance of some shafts (west shaft). This is due to the fact that the measured load-displacement response represents the combined effect of preloading, increase in side resistance, and increase in tip area. But in some cases, the improved resistance will only be

due to preloading of the soil (e.g., west shaft), and in such cases, Mullin's method may overestimate the resistance of that post-grouted shaft.

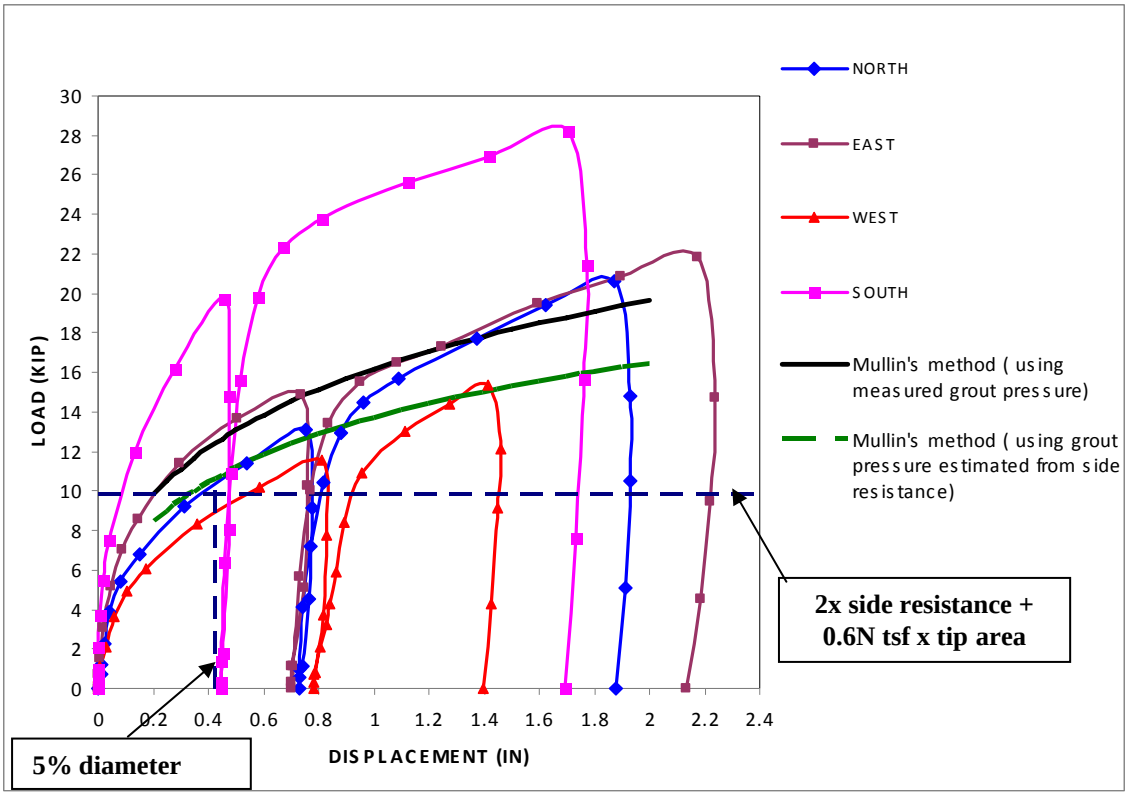

Figure 6-12 Comparison of load-displacement response (8-ft. long shafts).

As mentioned earlier, it is not possible to predict the increase in tip area and side resistance with tip grouting, especially during the design stage. But an improvement in resistance due to preloading of soil (increasing stiffness) beneath the shaft tip will occur. Moreover, the grout pressure produces a bidirectional force (i.e., upward and downward) at the shaft tip and the force applied to the soil beneath the shaft tip will be at least equal to the side resistance of shaft. Consequently, during axial loading both side resistance (F_s) and the unit end bearing corresponding to the force applied (equal to F_s) during grouting will develop. Thus, the minimum ultimate design resistance of post-grouted shafts (without considering the increase in tip area and side resistance) based on 5% displacement can be

estimated as the sum of side resistance of shaft (F_s), mobilized tip resistance (equal to F_s), and tip resistance of conventional shafts (i.e., total resistance at 5% displacement = $2.F_s$ + $0.6N$ tsf × tip area). The latter estimate is shown in Figure 6-12. It can be seen from the figure that this approach gives a good estimate of the minimum resistance of post-grouted drilled shafts. Further improvement in the resistance of post-grouted shafts was due to the increased tip area and side resistance of the shaft with tip grouting.

Shown in Figure 6-13 is the unit end bearing of the 13-ft. long east shaft estimated from the test data and the unit end bearing predicted using Mullin's method (for $N = 9$).

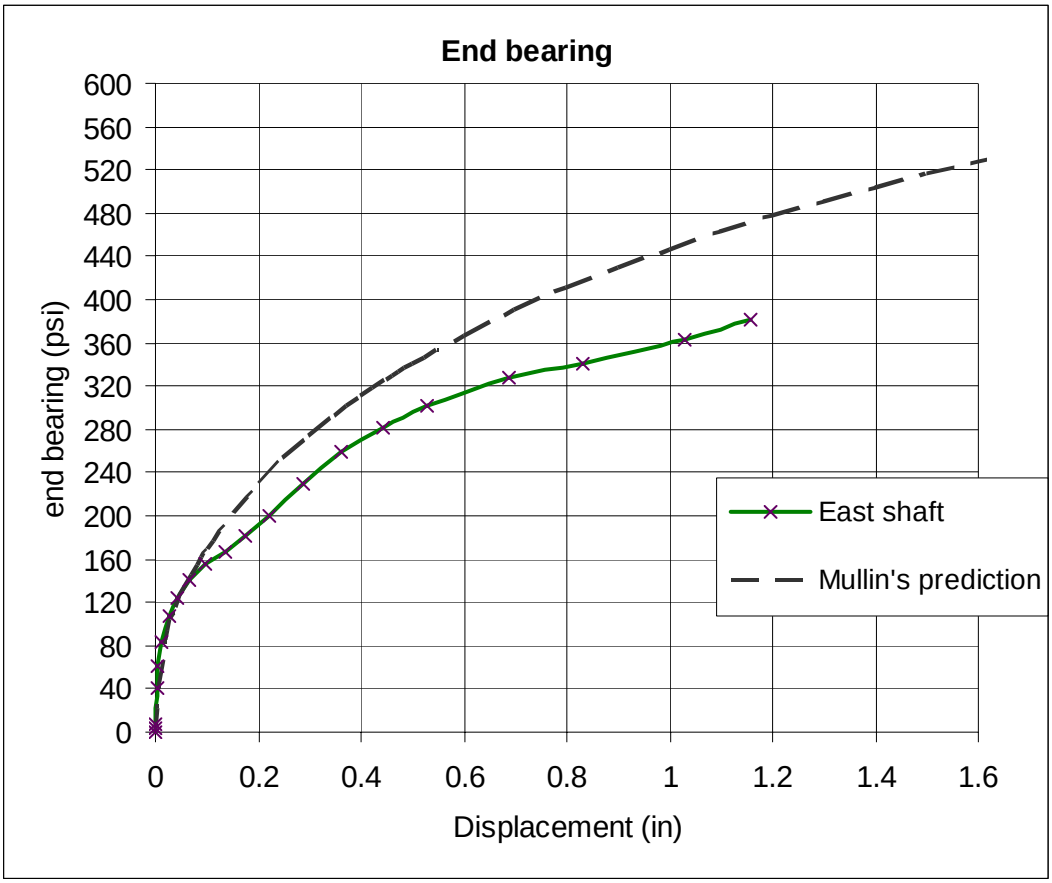

Figure 6-13 Comparison of unit end bearing (13-ft. long shaft).

It is clear from the figure that Mullin's method over predicted the unit end bearing of the shaft. However, Mullin's predicted load-displacement response (Figure 6-14) agrees quite

well with the total measured load displacement response of the east shaft. This is due to the increased side resistance of the east shaft (about 3 kips) due to grout flow around the shaft. Mullin's under prediction of resistance of the other shafts may be attributed to the large tip area of the shafts as a result of stage grouting. It can also be seen in Figure 6-14 that the proposed method (i.e., total resistance at 5% displacement = $2 \times F_s + 0.6N \times$ tip area) gives a reasonable estimate of the minimum ultimate design resistance of post-grouted drilled shafts.

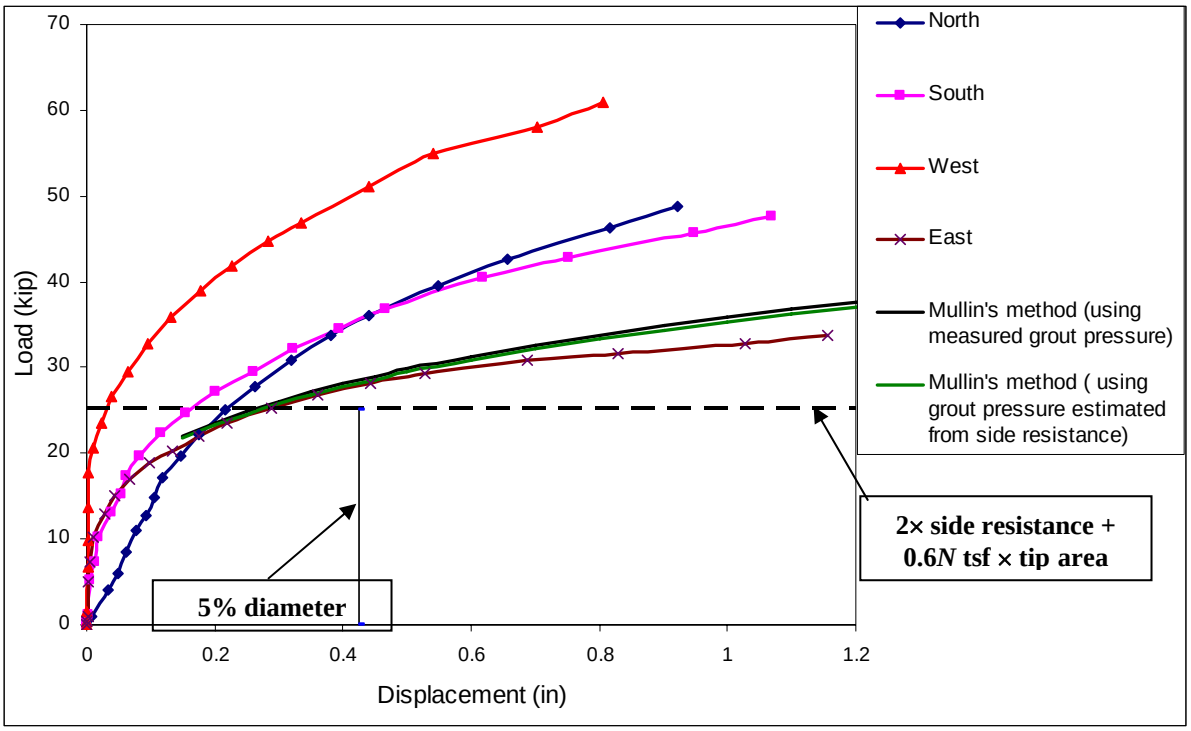

Figure 6-14 Comparison of load-displacement response (13-ft. long shaft).

6.2.4 Effectiveness of Staged Tip Grouting

Excavation of the first series of the grout-tipped drilled shaft group (8-ft. shafts) revealed that the grout had flowed upward alongside the shafts during tip grouting, which in turn reduced the side resistance of shaft during tip grouting due to negligible shear resistance of fluid grout. Consequently, the observed grout pressure may be less than the expected grout pressure, which will generally reduce the preloading effect. Moreover, the grout

pressure measured during initial grouting may not be representative of the pre- and post-grouted shaft's skin resistance.

One possible solution for improved assessment of the shaft's side and tip resistance was to regrout the shafts after sufficient time for hydration of the first grout volume. Subsequently, the shaft tip may be regrouted with the second grout pressure used to assess side friction and end bearing. Accordingly, during the second group investigation (13-ft. long shafts) staged grouting of the shaft tips were carried out. Increased grout pressures were observed during the second- and third-stage grouting of the shafts and was attributed to improved side resistance of the shaft due to the hydrated grout alongside the shaft from the first-stage grouting. Excavation of the post-grouted shafts, as well as the measured increased grout pressure, suggests that staged grouting of shafts helped in the following three ways: (1) increased the preloading effect (i.e., larger tip stress mobilization due to the increased grout pressure); (2) helped to form a grout bulb at the shaft tip (i.e., increased tip area), since the first grouting increases the residual radial stress around the shaft , which in turn prevented the upward flow of grout during regrouting; and (3) the staged grouting data could be used to estimate the actual (final) skin resistance of a post-grouted shaft.

CHAPTER 7
SUMMARY AND CONCLUSIONS

In Florida, bridge piers are either supported by pile or drilled shaft groups. The piles or shafts within a group are placed at the minimum possible spacing to reduce the reinforced concrete cap cost. However, axial group resistance may be significantly reduced when the piles are placed in close proximity to one another due to stress transfer occurring from one shaft to adjacent piles/shafts. In general practice, pile/shaft at three diameter (3D) c/c spacing will have a group efficiency factor of one (1.0). In the past few years, FDOT has been using post grouting technology to improve the tip resistance of the drilled shaft. Moreover, FDOT recently developed a new jet-grouted pile system (with side membrane) to improve both the side and tip resistance. Unfortunately, the efficiency factors for both post-grouted drilled shaft and jet-grouted pile in group placement were unknown.

The focus of this research was to investigate the group interaction of post-grouted drilled shafts and jet-grouted piles through the establishment of group efficiency factors and to develop appropriate analytical approaches for predicting load versus deformation response of post-grouted drilled shaft and jet-grouted pile groups. The study began with a group of 8-inch square by 8-ft. long jet-grouted piles (with 16-inch diameter side grout bulbs) in the FDOT test chamber at the University of Florida's Coastal Engineering lab. Pre-cast concrete piles with grout delivery systems and side membranes were first jetted into the soil in the test chamber, and subsequently, side grouting of the piles was carried out. Axial top down testing was then performed to estimate the side resistance of the group which was followed by tip grouting of each pile. After curing the tip grout, another top down test was performed to estimate the total resistance of the jet-grouted pile group. During the axial load test, the displacements of piles were relatively uniform and the soil deformation at the center of the

group was almost identical to the average displacement of piles. The latter suggests that the pile group failed as a block during axial loading. Moreover, the soil stress measurement beneath the pile group (Figure 7-1) showed an increase in vertical stress at the center of pile group, which was higher than the vertical stress increase recorded directly beneath the pile during axial group loading. This demonstrates the overlapping of stress bulbs from each pile, further supporting the block behavior of the pile group. Further justification is suggested from the soil deformation profile during the various stages of loading (Figure 7-2), which shows a uniform soil deformation within the group and a quadratic variation of deformation outside the boundary of the pile group.

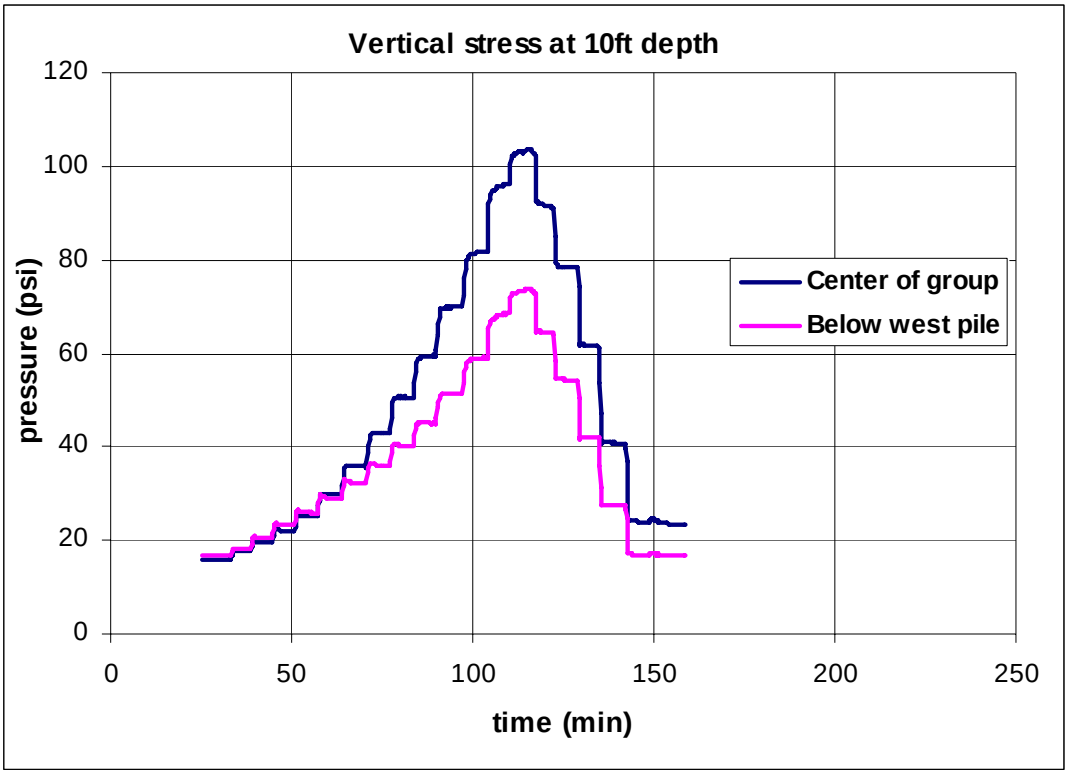

Figure 7-1 Variation of vertical stress beneath pile grout during top down testing.

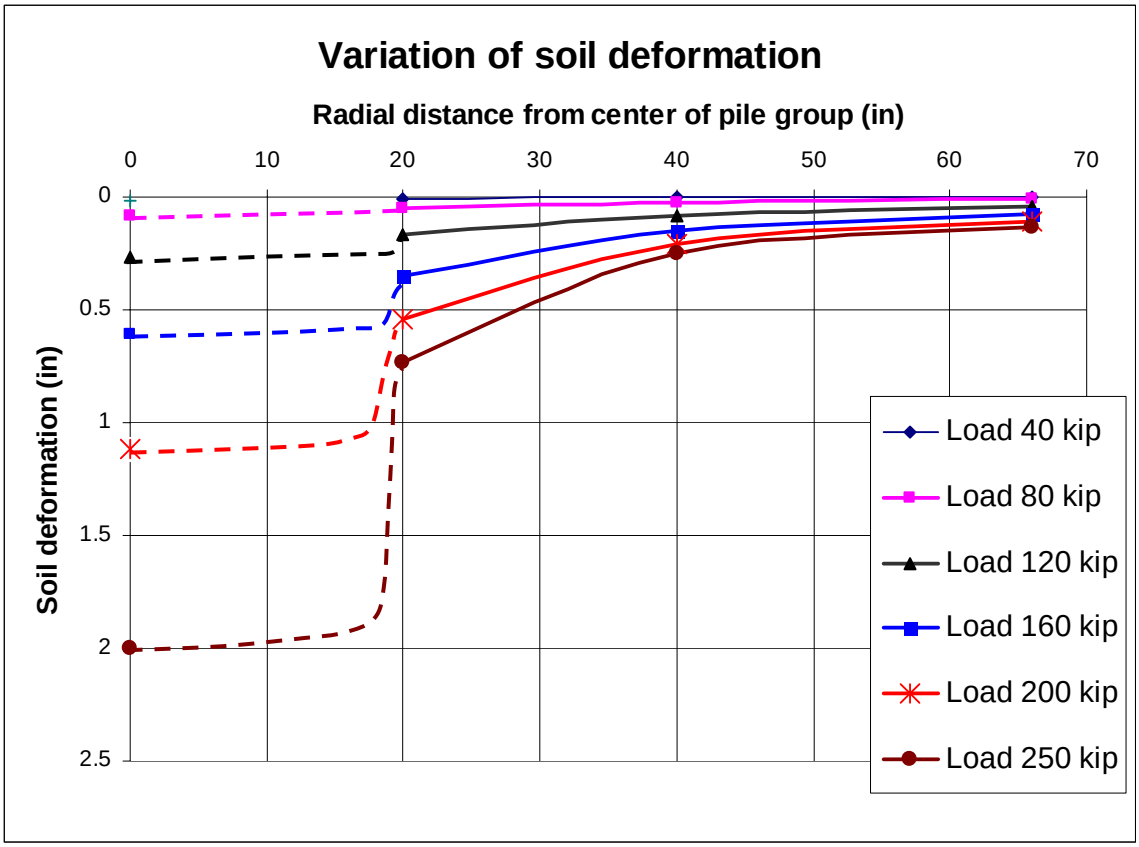

Figure 7-2 Soil deformation measurement during the group testing of 8-inch jet-grouted pile group.

In addition, the experimental data suggested that side grouting and tip grouting of adjacent piles within the group increased the confining stress and shear modulus of the soil mass within the group, resulting in a very low shear strain development in the soil mass within the group footprint area under axial loading. However, due to little confinement, a much higher shear strain pattern developed in the soil mass outside the footprint where shear modulus greatly diminished due to loss of lateral stress (no longer principal stress). Consequently, the grouted pile group should fail as a block during axial loading. Moreover, excavation of the jet-grouted pile group revealed that each pile in the group possessed good quality grout zones as shown in Figure 7-3.

Figure 7-3 Jet-grouted pile group after excavation.

Past cavity expansion research in sands (especially dense and medium dense sand) has shown significant chamber boundary influences in the case of penetrating objects (e.g., cones). Similarly, limited pressure during grouting, as well as frictional resistance of an individual pile may be influenced by the closeness of the chamber boundary. Hence, testing of smaller diameter jet-grouted piles (4.5-inch diameters × 8-ft. long and 10-inch diameter side grout bulb) group was performed to validate the results obtained from the first group test. Shown in Figure 7-4 are the small diameter jet-grouted piles with grout delivery systems. Similar to the first group, the measurement of load-displacement response of piles, soil deformation, and soil stress variation beneath the shaft during the axial loading of the

second jet-grouted pile group showed that the group behaved as a single block during axial loading.

Figure 7-4 Group of 4.5-inch diameter jet-grouted piles with grout delivery systems.

Numerical modeling of single jet-grouted piles (8-inch square × 8-ft. long and 6-inch square × 8-ft. long, FDOT project # BD545, 2009) was carried out using the finite element software PLAXIS-2D to investigate the soil stresses around the jet-grouted piles. The grouted vertical stress increase coefficient (K_g) plot proposed by McVay et al. based on experimental results (FDOT project # BD545, 2009) was updated using the numerical analysis results as shown in Figure 7-5. The T-Z curve and Q-Z curve for single jet-grouted pile/pile group was developed using the load transfer methodology proposed by McVay et al. (1989, FB-Multipier). The proposed T-Z curve and Q-Z curve were used to predict the load

displacement response of both single jet-grouted piles and grouped jet-grouted piles (Figure 7-6) and compared quite favorably with the measured load-displacement response.

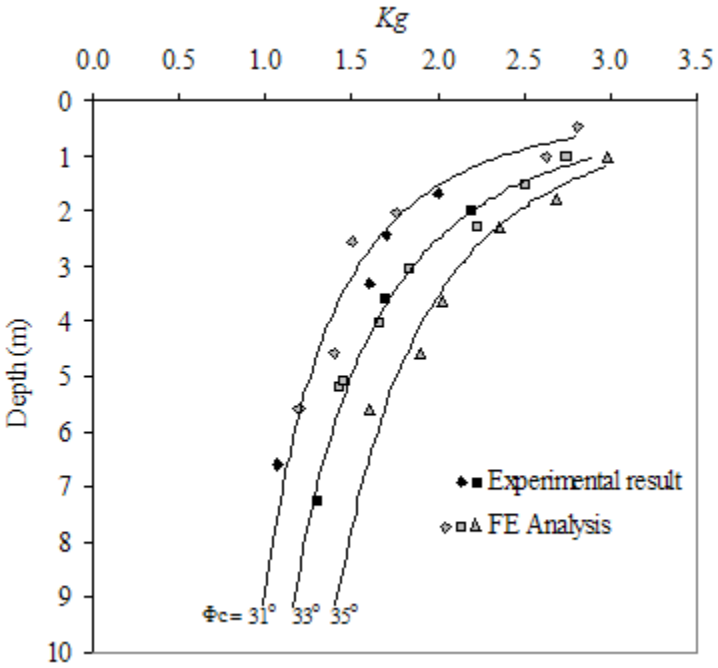

Figure 7-5 Updated grouted vertical stress increase coefficient, K_g.

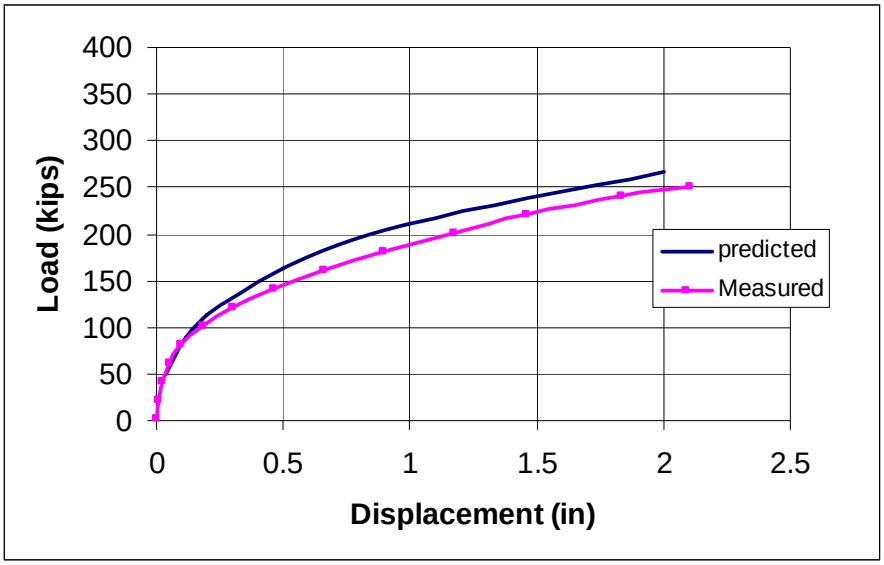

Figure 7-6 Comparison of predicted and measured load displacement response of 8-inch square × 8-ft. long jet-grouted pile group.

After the experimental investigation of jet-grouted pile groups, a study of grout-tipped drilled shaft groups was performed. The first group in the study was a group of four 8.5-inch diameter × 8-ft. long drilled shafts (L/D ~11) at 3D c/c spacing. The small diameter shafts were chosen to minimize the influence of the chamber boundary on the results. The objective of the first group test was to study various factors (e.g., preloading, tip bulb area etc.) influencing the axial resistance of grout-tipped drilled shaft. Also, since the shafts could be excavated, the study investigated the grout flow pattern on axial group efficiency at typical 3D spacing. After the insitu casting of all the shafts within the test chamber, an axial top down test was performed on the group to assess axial side resistance of the group. Subsequently, tip grouting (single stage) of each shaft was carried out. Another top down axial test of the shaft group was then performed along with individual shaft axial tests. The displacement of soil at the center of the group measured during group loading of the grout-tipped shafts was 0.278 inch and was much less than the average displacement of tops of each shaft displacement (0.68 inch). Moreover, the vertical soil stresses measured beneath the shaft group (Figure 7-7) during group loading showed little, if any, increase in vertical stress at the center of the group, unlike the jet-grouted pile group. Both displacements and stresses measured during group loading suggest that the shafts behaved individually and had no influence on another. To validate the latter, individual shafts were load tested, and the displacements of other shafts were monitored. For instance, shown in Figure 7-8 are the displacements of all the shafts when the west shaft was loaded. Evidently, there was little or no interaction between the west shaft and the other shafts in the group. The minimal group interaction was attributed to little, if any, change in soil stresses and stiffness within the footprint area of the group as a result of tip grouting. Hence, the resistance of the group is equal to the single grout-tipped shaft resistance × the number of shafts in the group.

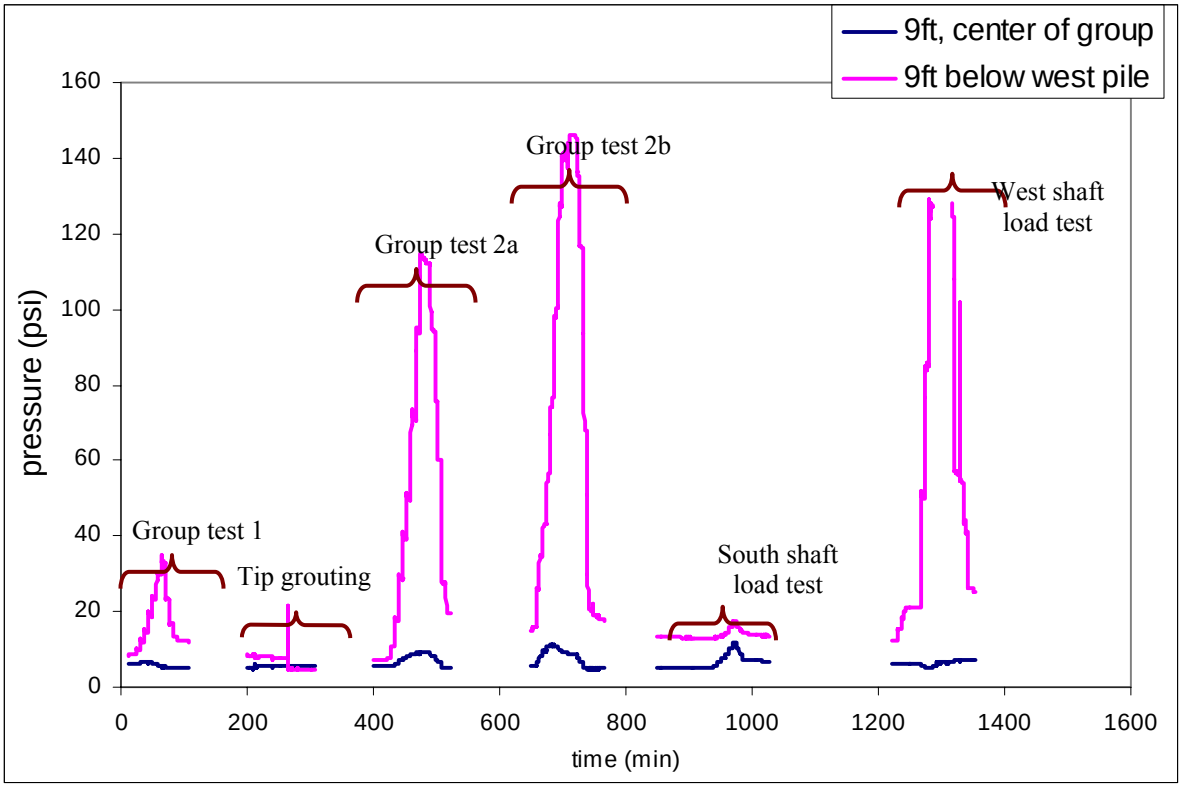

Figure 7-7 Variation of vertical stress beneath shaft group during group loading.

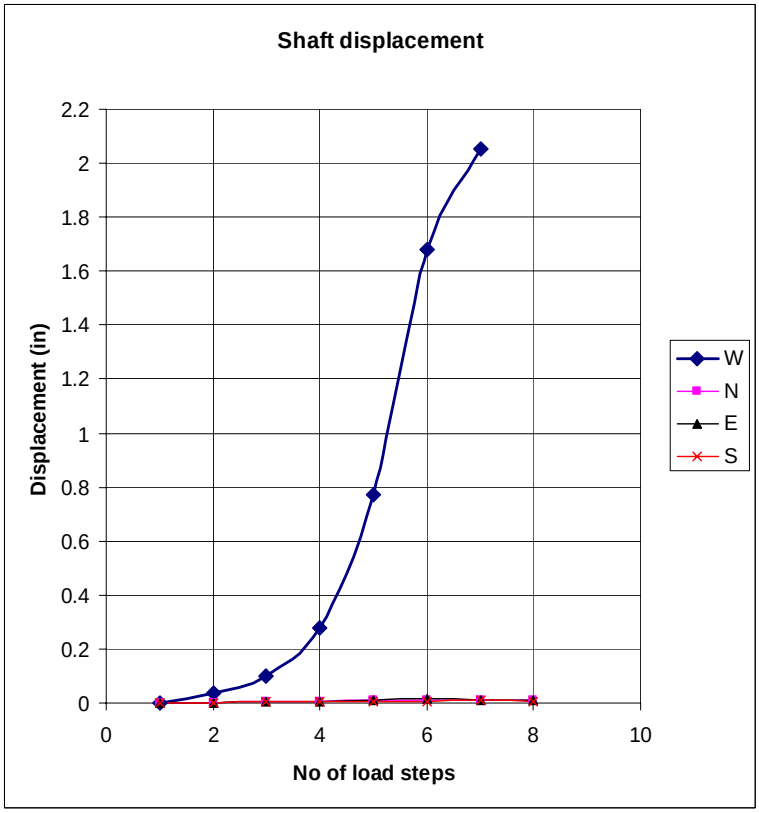

Figure 7-8 Displacement of shafts during loading on the west shaft alone.

For design, the axial group efficiency of the grout-tipped drilled shaft at typical 3D spacing may be set equal to one (1).

Excavation of the first group of post-grouted drilled shafts revealed that the grout had flowed up alongside the shaft-soil interface (weakest path) during tip grouting after initially filling the void space beneath the shaft tip (e.g., Figure 7-9). The upward flowing grout cover was also found to bond to the shaft and after hydration, an increase in skin resistance of shaft was measured. However, the magnitude of increase in skin resistance depends on the extent of grout zone around shaft, so it is hard to predict the improvement in skin friction when performing initial tip grouting. It was thought that a possible solution to assess increased shaft capacity (shaft and tip) was to carry out stage grouting.

Figure 7-9 Grout-tipped drilled shaft after excavation.

The second group chosen for study was a group of four 8.5-inch diameter × 13-ft. long drilled shaft (L/D ~18) at 3D c/c spacing. The intent of the second group test was to investigate the effectiveness of staged grouting on improving the resistance of grout-tipped shafts, as well as validate the earlier results, but at greater embedment depths. Accordingly, after insitu casting of drilled shafts, a top down axial test was again performed to assess shaft skin friction of the group. Staged tip grouting of the drilled shafts was then carried out using different colored grout for post investigation (i.e., excavation). After three different stages of tip grouting, a top down load testing of the group was performed along with individual loading of shafts within the group. Measured soil stresses, soil deformation, and load-displacement response of shafts demonstrated that the shafts, again, behaved individually during loading as observed in the first group study of post-grouted shaft. Excavation of shafts revealed that the grout from the first-stage grouting had again flowed upward alongside of the shaft (e.g., Figure 7-10), but a portion of the grout from the second- and third-stage grouting did accumulate around the shaft tip and increased the tip area. An increase in skin resistance of about 20 to 30% was observed when the regrouting pressure (second-stage) and original tip area were used to estimate the skin resistance of the post-grouted shaft. The increase in resistance was attributed to the hardened grout zone which had flowed up around shaft during first-stage grouting.

From the experimental study of post-grouted drilled shaft groups, it was concluded that the axial resistance of post-grouted shafts at FHWA failure criterion (5% diameter) depends on three factors: (1) preloading grout tip pressures; (2) increased skin resistance; and (3) increased tip area as a result of tip grouting. It was found that the increase in tip area and side resistance is subjective in nature (different for similar sized shafts in the same soil condition). However, it was found that the minimum improvement in the resistance of a

Figure 7-10 Excavated post-grouted shafts (Group test 2).

post-grouted shaft over a conventional shaft at failure displacements was equal to the mobilized tip load due to the application of grout pressure (i.e., preloading effect).

Comparison of measured and analytical methods found that Mullin's approach overestimated the measured unit end bearing of grout-tipped drilled shafts as shown in Figure 7-11. This may be attributed to the fact that Mullin's method did not take into account the influence of increase in tip area of the shaft with tip grouting. However, the total load-displacement response predicted using Mullin's method reasonably agreed with the measured response of some of the shafts and over predicted or under predicted the response of other shafts. The latter was attributed to the combined effect of preloading, increase in side resistance along the shaft, and increase in tip area of the shaft. Thus, significant variability in the capacity of post-grouted shafts at displacements at 5% diameter was observed. Due to the latter variability, a conservative design approach is recommended which considers the

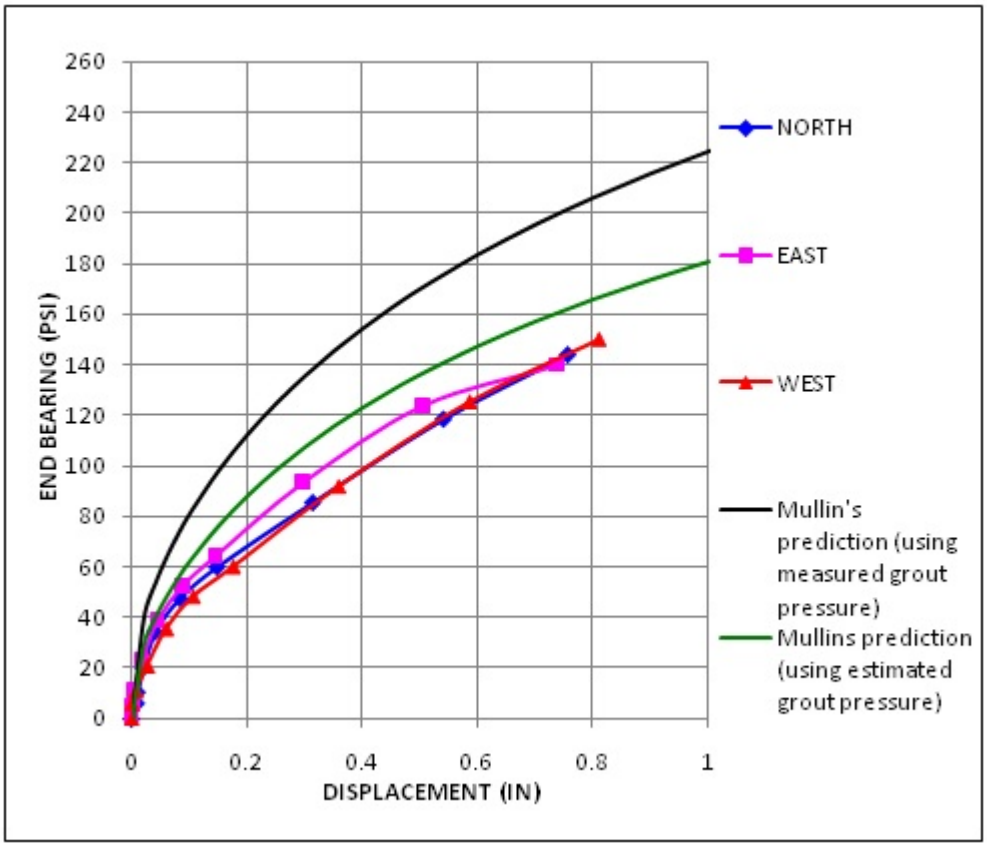

Figure 7-11 Comparison of measured and predicted unit end bearing (8-ft. long shafts).

improved shaft resistance due to tip grouting. The minimum increase in the tip resistance at a 5% settlement would be due to the preloading effect only. A minimum ultimate design resistance of post-grouted shafts (without considering the increase in tip area and side resistance) based on 5% displacement may be estimated as the sum of side resistance of shaft (*Fs*), mobilized tip load (equal to F_s), and tip resistance of conventional shaft (i.e., total resistance at 5% displacement = $2.F_s + 0.6N$ tsf × tip area) as shown in Figure 7-12.

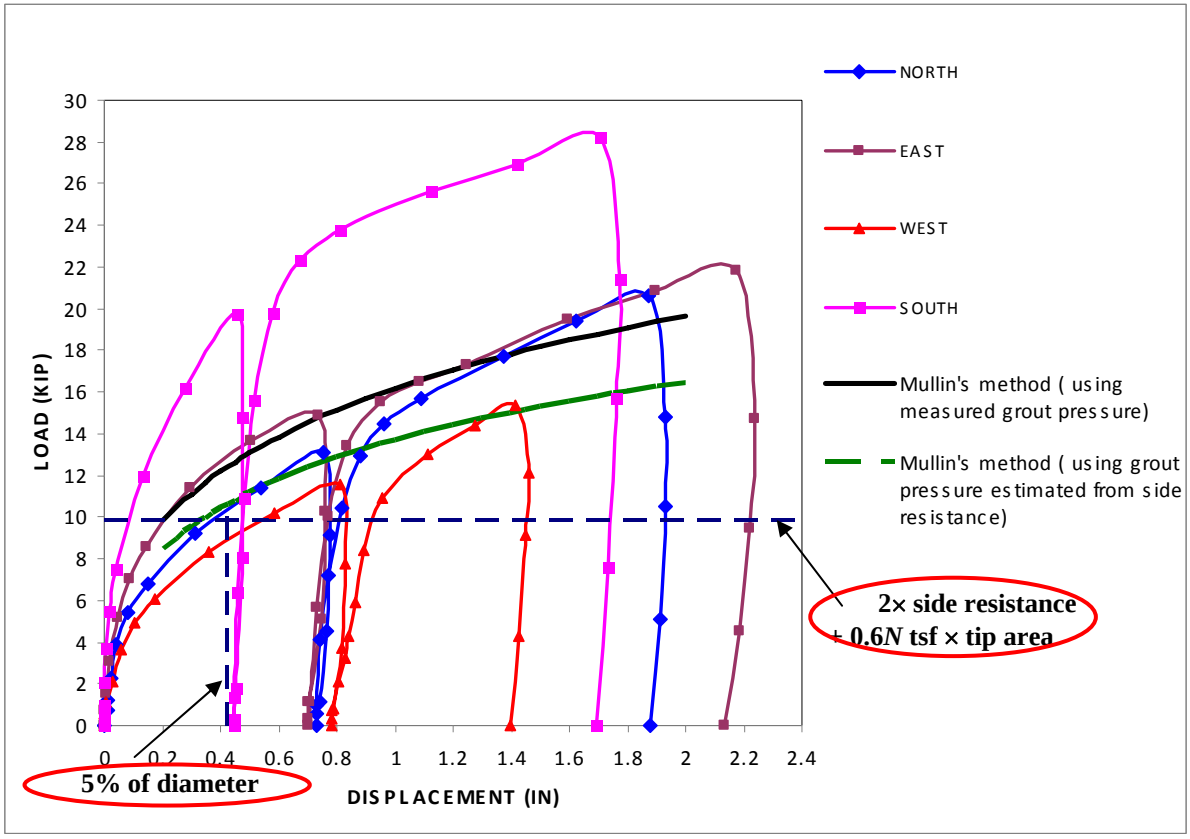

Figure 7-12 Comparison of predicted and measured total load capacity (8-ft. shaft).

Finally, it was found from the second group testing of grout-tipped drilled shafts that staged grouting improved group resistance by: (1) increasing the preloading effect (i.e., larger tip stress mobilization due to the increased grout pressure); and (2) assisting with the formation of a grout bulb at the shaft tip (i.e., increasing tip area), since first-stage grouting increased the residual radial stress around shaft (skin friction) and limited the upward flow of grout during regrouting. Also it was observed that the second- or later-stage grouting pressure could be used to estimate the final skin resistance of a post-grouted shaft.

REFERENCES

ACI Standard ACI 318-02. (2002). *Building Code Requirements for Structural Concrete,* Farmington Hills, Michigan.

Bishop, R. F., Hill, R., and Mott, N. F. (1945). "Theory of Indentation and Hardness Tests," *Proceedings of Phys. Soc*., Vol. 57, pp. 147.

Bruce, D. A. (1986). "Enhancing the Performance of Large Diameter Piles by Grouting," Parts 1 and 2, *Ground Engineering.*

Carter, J. P., Booker, J. R., and Yeung, S. K. (1986). "Cavity Expansion in Cohesive Frictional Soils," *Geotechnique*, Vol. 36, No. 3, pp. 349-358.

FHWA-IF-99-025. (1999). *Drilled Shafts: Construction Procedures and Design Methods,* Federal Highway Administration (FHWA), U.S. Department of Transportation.

Gibson, R.E., and Anderson, W. F. (1961). "In situ Measurement of Soil Properties with the Pressuremeter," *Civil Engineering Publ. Wks Rev*., Vol. 56, pp. 615-618.

Gouvenot, D., and Gabiax, F. D. (1975). "A New Foundation Technique Using Piles Sealed by Concrete Under Pressure," *Proceedings, Seventh Annual Offshore Technical Conference.*

Hill, R. (1950). *The Mathematical Theory of Plasticity*, Oxford University Press, London, pp. 97, 125.

Hughes, J. M. O., Worth, C. P., and Windle, D. (1977). "Pressuremeter Tests in Sands," *Geotechnique*, Vol. 27, No. 4, pp. 455-477.

Joer, H. A., Randolph, M. F., and Gunasena, U. (1998). "Experimental Modeling of the Shaft Capacity of Grouted Driven Piles," *Geotechnical Testing Journal*, Vol. 21, No.3, pp. 159–168.

McVay, M., Bloomquist, D., Forbes, H., and Johnson, J. (2009). "Precasted Concrete Pile Installation – Utilized Jetting and Pressure Grouting," FDOT Contract No. BD545, RPWO#31.

McVay, M. C., Townsend, F. C., Bloomquist, D. G., O'Brien, M. O., and Caliendo, J. A. (1989). "Numerical Analysis of Vertically Loaded Pile Groups," *Proceedings of the Foundation Engineering Congress*, American Society of Civil Engineers (ASCE), Northwestern University, Illinois.

Mullins, G., and Dapp, S. (2006). "Predicting End Bearing Capacity of Post-Grouted Drilled Shaft in Cohesionless Soils," *Journal of Geotechnical and Geoenvironmental Engineering*, ASCE.

Mullins, G., Dapp, S., Fredreric, E., and Wagner, R. (2001). "Pressure Grouting Drilled Shaft Tips – Phase I Final Report," Final Report submitted to Florida Department of Transportation.

Mullins, G., and Winters, D. (2004). "Pressure Grouting Drilled Shaft Tips – Phase II Final Report," Final Report submitted to Florida Department of Transportation.

Palmer, A. C. (1972). "Undrained Plain-Strain Expansion of Cylindrical Cavity in Clay: A Simple Interpretation of the Pressuremeter Test," *Geotechnique*, Vol. 22, No. 3, pp. 451-457.

Plumbridge, G. D., and Hill, S. J. (2001). "Performance of Shaft Grouted Piles and Barrettes," *Geotechnical Engineering- Meeting Society's Needs*, Vol. 1.

Randolph, M. H., Dolwin, J., and Beck, R. (1994). "Design of Driven Piles in Sand," *Geotechnique*, Vol. 44, No. 3, pp. 427–448.

Reese, L.C., and O'Neill, M. W. (1988). *Drilled Shafts: Construction and Design*, FHWA Publication No. HI-88-042.

Salgado, R., and Prezzi, A.M. (2007). "Computation of Cavity Expansion Pressure and Penetration Resistance in Sands," *International Journal of Geomechanics*, Vol. 7, No. 4, pp. 251-265.

Salgado, R., and Randolph, M. F. (2001). "Analysis of Cavity Expansion in Sand," *International Journal of Geomechanics*, ASCE, Vol. 1, No. 2, pp. 175–192.

Schanz, T., Vermeer, P. A., and Bonnier, P.G. (1999). "The Hardening Soil Model: Formulation and Verification", In: R. B. J. Brinkgrove, Editor, *Beyond 2000 in Computational Geotechnics*, Balkema, Rotterdam, pp. 280-290.

Sliwinski, Z. J., and Flemming, W. G. K. (1984). "The Integrity and Performance of Bored Piles," *Proceedings of the International Conference on Advances in Piling and Ground Treatment of Foundation*, Institution of Civil Engineers, London, UK.

Tsinker, G. P. (1988). "Pile Jetting," *J. Geotech. Eng*., Vol. 114, No. 3, pp. 326–336.

Vesic, A.S. (1972). "Expansion of Cavities in Infinite Soil Mass," *Proceedings, ASCE 98*, Soil Mechanics and Foundations Division, Sm3, pp. 265-290.

Yu, H. S., and Houlsby, G. T. (1991). "Finite Cavity Expansion in Dilatant Soils – Loading Analysis," *Geotechnique*, Vol. 41, No. 2, pp. 173–183.

APPENDIX A

Limit Pressure Charts (Salgado et al., 2001)

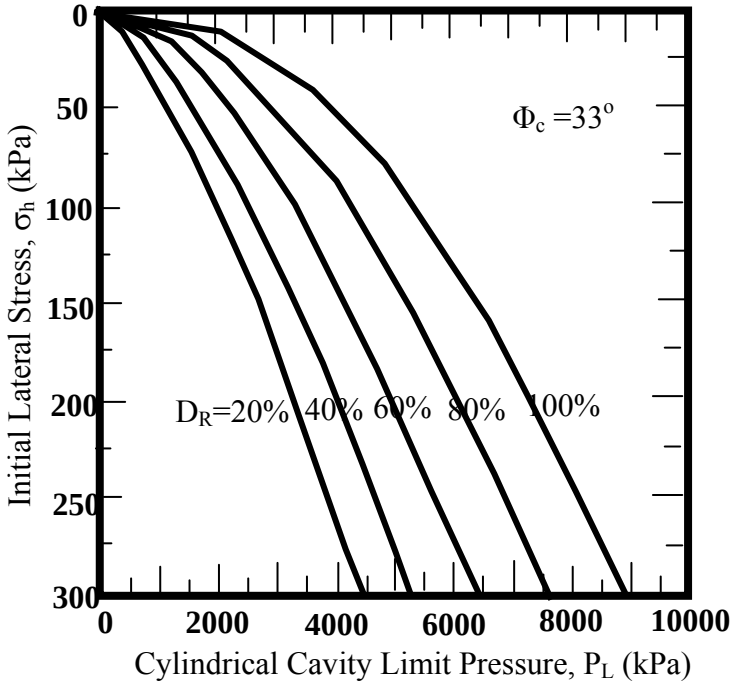

Figure A-1 Cylindrical cavity limit pressure versus initial lateral stress ($\Phi_c = 33°$).

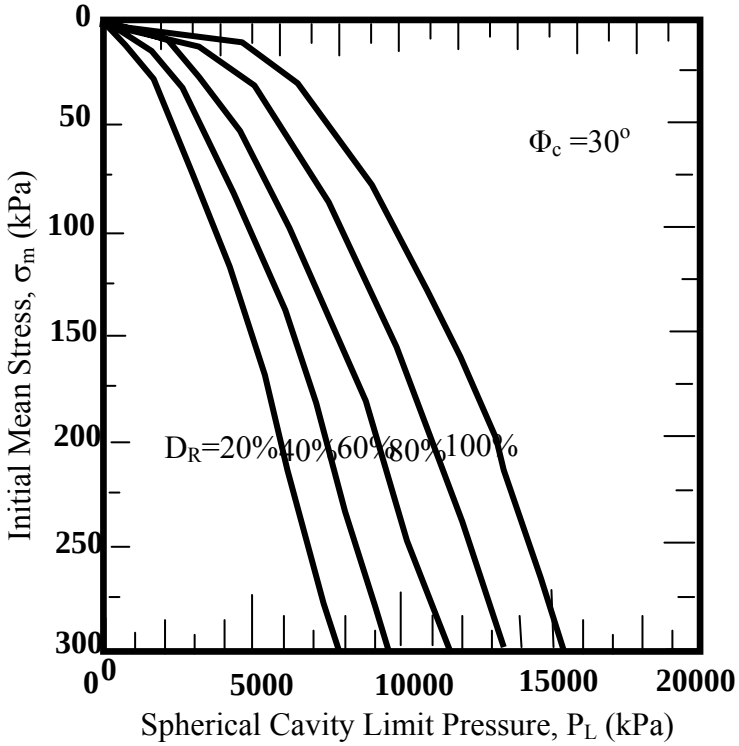

Figure A-2 Spherical cavity limit pressure versus initial mean stress ($\Phi_c = 30°$).

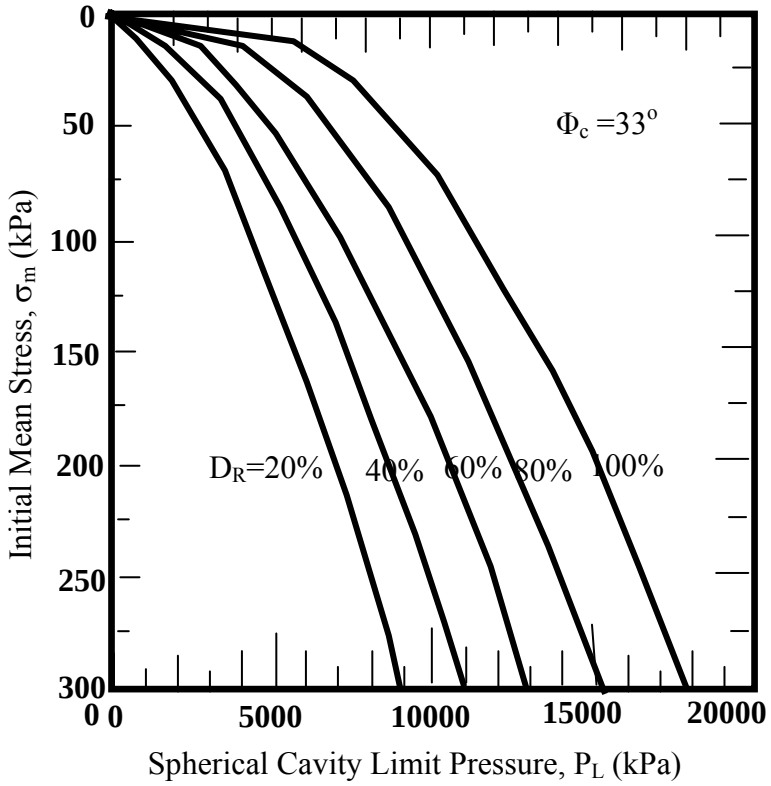

Figure A-3 Spherical cavity limit pressure versus initial mean stress ($\Phi_c = 33°$).